NTNU
Norwegian University of
Science and Technology

Unstable two phase flow in long vertical pipes

Morten Ravnås

Master of Science in Mechanical Engineering
Submission date: June 2018
Supervisor: Ole Jørgen Nydal, EPT
Co-supervisor: Zhilin Yang, EPT
Niranjan Reddy Challabotla, EPT

Norwegian University of Science and Technology
Department of Energy and Process Engineering

NTNU
Norges teknisk-naturvitenskapelige universitet

Institutt for energi- og prosessteknikk

EPT-M-2018- 69

MASTEROPPGAVE

for

Student Morten Ravnås

Våren 2018

Ustabil tofasestrøm i lange vertikale rør

Unstable two phase flow in long vertical pipes

Bakgrunn og målsetting

There are several types of flow instabilities which can cause operational problems for pipelines and risers transporting multiphase mixtures of oil and gas. Severe riser slugging has been well studied. This is a case where trapped upstream gas is compressed and causes periodic violent liquid flushing. Another type of instability is expansion generated flow oscillations in long risers or wells. This is a type of flow dynamics which needs to be demonstrated and documented better, both experimentally and by computational flow simulators.

Some dynamic flow simulations have been made before, and some small scale experiments in the EPT laboratory have in principle demonstrated the flow phenomena. The previous experiments were in rather short pipes (7m), in which the expansion effect is rather small. We can now do experiments in a longer vertical pipe (20m).

Ideally, we should have pressure as boundary conditions, not flow, in order for unsteady flow to occur. The inflow should be reduced with increasing tubing pressure. We will try to achieve this effect by running the centrifugal pumps at a suitable low frequency. Gas will be injected with a constant mass flow rate, and the flow oscillations will be recorded with video and with pressure sensors. The experimental results will be compared with available dynamic flow simulators.

Oppgaven bearbeides ut fra følgende punkter

1 Literature review of the flow instability
2 Laboratory preparations for the new vertical pipe
3 Experiments and simulations
4 Reporting

Senest 14 dager etter utlevering av oppgaven skal kandidaten levere/sende instituttet en detaljert fremdrift- og eventuelt forsøksplan for oppgaven til evaluering og eventuelt diskusjon med faglig ansvarlig/veiledere. Detaljer ved eventuell utførelse av dataprogrammer skal avtales nærmere i samråd med faglig ansvarlig.

Besvarelsen redigeres mest mulig som en forskningsrapport med et sammendrag både på norsk og engelsk, konklusjon, litteraturliste, innholdsfortegnelse etc. Ved utarbeidelsen av teksten skal kandidaten legge vekt på å gjøre teksten oversiktlig og velskrevet. Med henblikk på lesning av besvarelsen er det viktig at de nødvendige henvisninger for korresponderende steder i tekst, tabeller og figurer anføres på begge steder. Ved bedømmelsen legges det stor vekt på at resultatene er grundig bearbeidet, at de oppstilles tabellarisk og/eller grafisk på en oversiktlig måte, og at de er diskutert utførlig.

Alle benyttede kilder, også muntlige opplysninger, skal oppgis på fullstendig måte. For tidsskrifter og bøker oppgis forfatter, tittel, årgang, sidetall og eventuelt figurnummer.

Det forutsettes at kandidaten tar initiativ til og holder nødvendig kontakt med faglærer og veileder(e). Kandidaten skal rette seg etter de reglementer og retningslinjer som gjelder ved alle (andre) fagmiljøer som kandidaten har kontakt med gjennom sin utførelse av oppgaven, samt etter eventuelle pålegg fra Institutt for energi- og prosessteknikk.

Risikovurdering av kandidatens arbeid skal gjennomføres i henhold til instituttets prosedyrer. Risikovurderingen skal dokumenteres og inngå som del av besvarelsen. Hendelser relatert til kandidatens arbeid med uheldig innvirkning på helse, miljø eller sikkerhet, skal dokumenteres og inngå som en del av besvarelsen. Hvis dokumentasjonen på risikovurderingen utgjør veldig mange sider, leveres den fulle versjonen elektronisk til veileder og et utdrag inkluderes i besvarelsen.

I henhold til "Utfyllende regler til studieforskriften for teknologistudiet/sivilingeniørstudiet" ved NTNU § 20, forbeholder instituttet seg retten til å benytte alle resultater og data til undervisnings- og forskningsformål, samt til fremtidige publikasjoner.

Besvarelsen leveres digitalt i DAIM. Et faglig sammendrag med oppgavens tittel, kandidatens navn, veileders navn, årstall, instituttnavn, og NTNUs logo og navn, leveres til instituttet som en separat pdf-fil. Etter avtale leveres besvarelse og evt. annet materiale til veileder i digitalt format.

☒ Arbeid i laboratorium (vannkraftlaboratoriet, strømningsteknisk, varmeteknisk)
☐ Feltarbeid

NTNU, Institutt for energi- og prosessteknikk, 15. januar 2018

Ole Jorgen Nydal
Faglig ansvarlig/veileder

Medveileder(e): Post Doc Reddy Niranjan, Zhilin Yang

Abstract

Flow instabilities can cause operational problems when transporting multiphase mixtures of oil and gas in offshore risers and pipelines. Several types of flow instabilities have been studied and are well documented. This study will focus on Expansion Driven flow Instability (EDI) phenomena, which is relatively little known and hence this type of flow dynamic needs to be demonstrated and documented better. EDI is a phenomena where instabilities are induced by gas expansion in the riser itself. Small amount of accumulated trapped gas upstream the riser base could cause instabilities and cyclic behaviour when entering the riser due to the expansion driven flow acceleration given to the liquid column.

The purpose of this master thesis is to demonstrate and document EDI phenomena, through experiments and computational flow simulators. The experiments are conducted in the multiphase lab at the Norwegian University of Science and Technology (NTNU), where a new experimental test facility for long vertical pipes is installed. Experimental results are thereafter compared with simulation results from dynamic multiphase flow simulators (OLGA and Sluggit). Experiments are conducted for five different centrifugal pump frequencies, which is simulating a typical reservoir source at varying conditions. The fluids which are tested is air and water at atmospheric conditions. Air is injected into the system with constant flow rates, located upstream the riser base. For entrapment of air in the horizontal test-section a geometrical bump (jumper) is installed. The vertical pipe is 17,28m with a pipe inner diameter of 0,06m. To capture the EDI phenomena, pictures and videos are recorded using cameras, and data logged using pressure sensors and flow meters.

Oscillating behaviour are present for the three lowest pump frequencies, while the two remaining shows stable flow regime for all air flow rates injected. The trend is stable flow regime for high pump frequencies and high air flow rates.

OLGA is one of the multiphase flow simulator used during the study to verify the experiments. The numerical model is able to reproduce results which is close to some of the results observed in the experiment, with maximum 12% error, calculating the mean values. However, discrepancies are observed regarding the stability limits. These discrepancies may be attributed from geometrical simplifications and assumptions conducted in the model.

A 1D two-fluid model in the multiphase flow simulator Sluggit is developed. This model failed to capture the oscillation/instabilities observed for low injected air flow rates in the experiment. The Sluggit model showed on the other hand good agreement with the observed experimental results, in stable flow conditions.

An extension to the main experiment is conducted to map the flow patterns for higher air flow rates. Slug flow is observed for the highest superficial gas velocity (6,6m/s) tested.

Both experimental results and OLGA simulations demonstrated that Expansion Driven flow Instability phenomena occurs in the tested lab setup.

Sammendrag

Det finnes flere forskjellige typer ustabile strømnings fenomener som kan forårsake operasjonelle problemer når man transporterer flerfase blandinger av olje og gass i lange stigerør og rørledninger. Flere av disse ustabilitets fenomenene er allerede studert og godt dokumentert. Dette studiet vil fokusere på et lite kjent fenomen som kalles ekspansjons drevet strømning ustabilitet (EDI). Dette fenomenet må derfor demonstreres og dokumenteres bedre. EDI er et fenomen der ustabiliteten er indusert av gass ekspansjon i selve stigerøret. Små mengder av akkumulert gass oppstrøms innløpet til stigerøret kan forårsake ustabilitet og gi en syklisk oppførsel når gassen entrer innløpet, på grunn av den ekspansjons drevne strømnings akselerasjonen påført væskesøylen.

Målet med denne masteroppgaven er å demonstrere og dokumentere EDI fenomenet gjennom eksperimenter og numeriske strømnings modeller. Forsøkene utføres i flerfase-laboratoriet ved Norges teknisk-naturvitenskapelige universitet, der en ny eksperimentell testfasilitet for lange vertikale rør er installert. Eksperimentelle resultater er deretter sammenlignet med resultater fra de numeriske strømningsmodellene (OLGA and Sluggit).

Eksperimenter utføres for fem forskjellige sentrifugalpumpe-hastigheter, som simulerer et reservoar. Væsker testet er luft og vann under atmosfæriske forhold. Luft er injisert ved konstante strømnings rater, oppstrøms innløpet til stigerøret. En geometrisk hump (jumper) er installert med hensikt å akkumulere luft i den horisontale test seksjonen. Den vertikale røren er 17,28 m, med en indre diameter på 0,06 m. EDI fenomenet er dokumentert ved hjelp av bilder og video og i tillegg logget ved bruk av trykksensorer og mengdemålere.

Oscillerende oppførsel er tilstede for de tre laveste pumpefrekvensene, mens de to resterende viser et stabilt strømnings regime for alle de testede luft-rater. Trenden er stabilt regime for høye pumpefrekvenser og høye injiserte luft-rater.

OLGA er en av de numeriske flerfase strømnings simulatorene brukt for å verifisere eksperimentene. Denne modellen klarer å reprodusere resultater som ligger nær noen av de eksperimentelle resultatene, med maksimum 12% feil, beregnet over gjennomsnitts verdiene. Det er uansett observert ulikheter med tanke på stabilitets grensene. Disse ulikhetene kan være på grunn av geometriske forenklinger og andre antagelser som er gjort i modellen.

En 1D to-væske modell er utviklet i flerfase simulerings programmet Sluggit. Denne modellen klarte ikke reprodusere oscillasjon/ustabilitet som er observert for lave injiserte luft-rater i eksperimentet. Denne modellen viste derimot god overensstemmelse med de eksperimentelle resultat, i de stabile områdene.

En utvidelse av hovedeksperimentet er også utført for å kartlegge strømnings regimene for høyere luft-rater injisert. *Slugflow* er observert for den høyeste *superficial* gass hastigheten.

Både eksperimentelle og OLGA simulerings resultater viste at EDI oppstår for dette laboratorieoppsettet.

Preface

This is a Master's Thesis with focus on Expansion Driven flow Instabilities (EDI), given at NTNU as part of the study program Industrial Process Engineering. The thesis is carried out during the spring semester of 2018, with professor Ole Jørgen Nydal as supervisor.

The multiphase laboratory at Department of Energy and Process Engineering (EPT) have recently been extended by a new vertical pipe which now allows experiments on long vertical pipes. My job will therefore as a certified plumber and student include design, construction and testing of a new experimental test rig for EDI, as an extension of the Project work conducted by the author in the previous semester (Ravnås, 2017).

The test rig was finally ready for experiments in the middle of February, after many working hours spent in the lab. Thereafter the results were analyzed and compared to available dynamic flow simulators.

Trondheim, 2018-06-11

Morten Ravnås

Acknowledgment

I would first like to thank my supervisor professor Ole Jørgen Nydal for always having his office door open for Master's Thesis discussions.

For guidance in dynamic flow simulating I would like to thank professor Zhilin Yang and Post-doc Niranjan Reddy Challabotla.

For general understanding of the lab facilty and multiphase flow, thanks to PhD Candidate Cleide Vieira.

Finally, I would like to thank the entire lab staff, especially staff Engineer Martin Bustadmo for priceless help regarding practical work and technical solutions.

M.R.

Nomenclature

Symbols	Units	Description
A	$[m^2]$	Area
A_t	[-]	Actual value
F_t	[-]	Forecast value
g	$[m/s^2]$	Gravitational acceleration
h	[m]	Height of fluid column
H_s	[m]	Static depth
i	[-]	Index number
L	[m]	Riser length
$\dot{m}_g$	[kg/s]	Mass flow rate gas
$\dot{m}_l$	[kg/s]	Mass flow rate liquid
n	[-]	index number
P_{abs}	[Pa]	Absolute pressure
P_{atm}	[Pa]	Atmospheric pressure
P_{hyd}	[Pa]	Hydrostatic pressure
p_a	[Pa]	Available pressure
p_r	[Pa]	Required pressure
PE	[%]	Percent Error
q	$[m^3/s]$	Flow rate
S_r	[-]	Submergence ratio
U_b	[m/s]	Bubble velocity
U_{sg}	[m/s]	Superficial velocity of gas
U_{sl}	[m/s]	Superficial velocity of liquid
α	[-]	Void fraction
θ	[-]	under relaxation parameter
μ_g	$[Pa \cdot s]$	Dynamic viscosity for gas
μ_l	$[Pa \cdot s]$	Dynamic viscosity for liquid
ρ_g	$[kg/m^3]$	Gas density
ρ_l	$[kg/m^3]$	Liquid density
ρ_m	$[kg/m^3]$	Mixture density
$\sigma_{l/g}$	$[N/m]$	Surface tension between liquid and gas

Abbreviations

Acronyms	Description
Appx.	Appendix
AutoCAD® Plant 3D	Computer-aided design for piping
EDI	Expansion Driven flow Instabilities
EPT	Department of Energy and Process Engineering
EV Comp	Exposure Value Compensation
GUI	Graphical User Interface
ID	Identity
i.e	that is to say
LabVIEW®	Laboratory Virtual Instrument Engineering Workbench
LedaFlow®	Advanced Transient Multiphase Flow Simulator
MAPE	Mean Absolute Percentage Error
MATLAB®	MATrix LABoratory
MINDT	Minimum time-step
NTNU	Norwegian University of Science and Technology
OLGA®	OiL and GAs simulation tool
PVT	Pressure Volume Temperature
Sluggit®	Multiphase flow simulation tool
Tag	Identification label
vs	Versus

Contents

Masteroppgave i
Abstract iii
Sammendrag iv
Preface v
Acknowledgment vi
Nomenclature vii
Abbreviations viii
List of Tables xii

1 Introduction **1**
1.1 Background 1
1.2 Objectives 3
1.3 Approach 3
1.4 Outline 4

2 Literature review **5**
2.1 Multiphase flow instability mechanisms 5
2.2 Superficial velocity 10
2.3 Hydrostatic pressure 10
2.4 Flow regimes 10

3 Experimental setup and equipment **12**
3.1 Setup 12
3.1.1 Geometry 15
3.1.2 Fluid properties 15
3.2 Equipment 16
3.2.1 Centrifugal pump 16
3.2.2 Absolute pressure transducer 17
3.2.3 Flow meter 17
3.2.4 Camera 18

3.3 Experimental procedure . . . 18

4 Experimental results **19**
4.1 Test matrix . . . 19
4.2 Visual observations . . . 20
4.2.1 Oscillating . . . 20
4.2.2 Stable . . . 24
4.3 Pressure & water flow rate vs time . . . 26
4.4 Max/Min values vs superficial gas velocity . . . 27
4.5 Experimental overview plots . . . 30
4.6 Effect of varying pump frequency . . . 33
4.7 Effect of upstream flowline jumper . . . 33
4.8 Air injection . . . 34
4.9 Riser-base pressure . . . 36
4.10 Summary of experimental results . . . 36

5 Simulation **37**
5.1 OLGA . . . 37
5.1.1 Sensitivity . . . 38
5.1.2 Simulation result . . . 40
5.1.3 Summary of OLGA results . . . 44
5.2 Instability cycle . . . 44
5.3 Sluggit . . . 46

6 Flow regime transition **48**

7 Summary and recommendation for further work **53**

Bibliography **55**

Appendix **57**

A Results **57**
A.1 Pressure and water flow rate vs time . . . 57
A.1.1 Frequency=38Hz . . . 57
A.1.2 Frequency=38,5Hz . . . 61
A.1.3 Frequency=39Hz . . . 64
A.1.4 Frequency=39,5Hz . . . 67
A.1.5 Frequency=40Hz . . . 70

B Risk assessment excerpt **74**

C OLGA input file **76**

D Check list valves **81**

E Experimental procedure **84**

F Centrifugal pump **86**

G Experimental facilities **88**

G.1 Riser . . . 88
G.2 Separator . . . 89
G.3 Horizontal test-section . . . 91
G.3.1 Air injection . . . 91
G.3.2 Jumper . . . 92
G.3.3 Turns . . . 93
G.4 Connection to existing . . . 94
G.5 Drainage . . . 95
G.5.1 Horizontal drainage . . . 95
G.5.2 Vertical drainage . . . 96
G.6 Technical-room . . . 96

List of Tables

3.1 Experimental setup table 12
3.2 Geometry for each pipe-section 15
3.3 Fluid properties at 20°C and 1atm (Cimbala and Cengel, 2014) 15
3.4 Relation for centrifugal pump between capacity,frequency and speed, read directly from LabVIEW 17
3.5 Pressure sensor 17
3.6 Flow meter (air density at 20°C) (Chupin, 2003) 18

4.1 Test matrix 19

5.1 Sensitivity test for OLGA model 39

6.1 Extended test matrix for pump frequencies 38Hz and 40Hz 48

Chapter 1

Introduction

1.1 Background

One of the flow instability problems related to oil and gas industry is severe slugging in offshore risers. This phenomena is extensively investigated over the last few decades. Severe slugging is an upstream gas compressibility problem, where the gas eventually causes a blowout when the gas pressure equals the static head in the riser. This phenomena causes problems for a stable production and can damage equipment connected to the flow-line. A riser is the production pipe which is needed to transport the fluid from the reservoir to the surface (see Figure 1.1). Another similar case for a sufficiently long riser, is where the gas causes flow instability induced by gas expansion in the riser itself. This phenomena is named Expansion Driven flow Instabilities (EDI).

The need for long risers for field development in deep-water basins as well as an increasing number of low pressures reservoirs makes the study of EDI important. The deeper the reservoir is underneath the ocean surface and the longer the production riser implies that higher pressure required to lift the reservoir fluid. Also, for low pressure reservoirs, in-situ gas or artificial lift gas is widely used to be able to produce fluid to the surface. Both of the above-mentioned cases are prone to flow instabilities, and should therefore be well demonstrated and documented, by especially focusing on EDI.

Artificial gas lift is where compressed gas is injected towards the bottom of the riser. The gas can be injected both intermittently or continuously, with continues gas lift as the preferred method in most cases for subsea oil production (Clegg et al., 1993). Gas lift is one option considered in deep sea mining systems, where particles need to be transported to the surface. By injecting gas into the riser, the mixture density will be reduced, resulting in reduced pressure drop. EDI is therefore a phenomena which is likely to occur, if not taken into consideration when designing the setup.

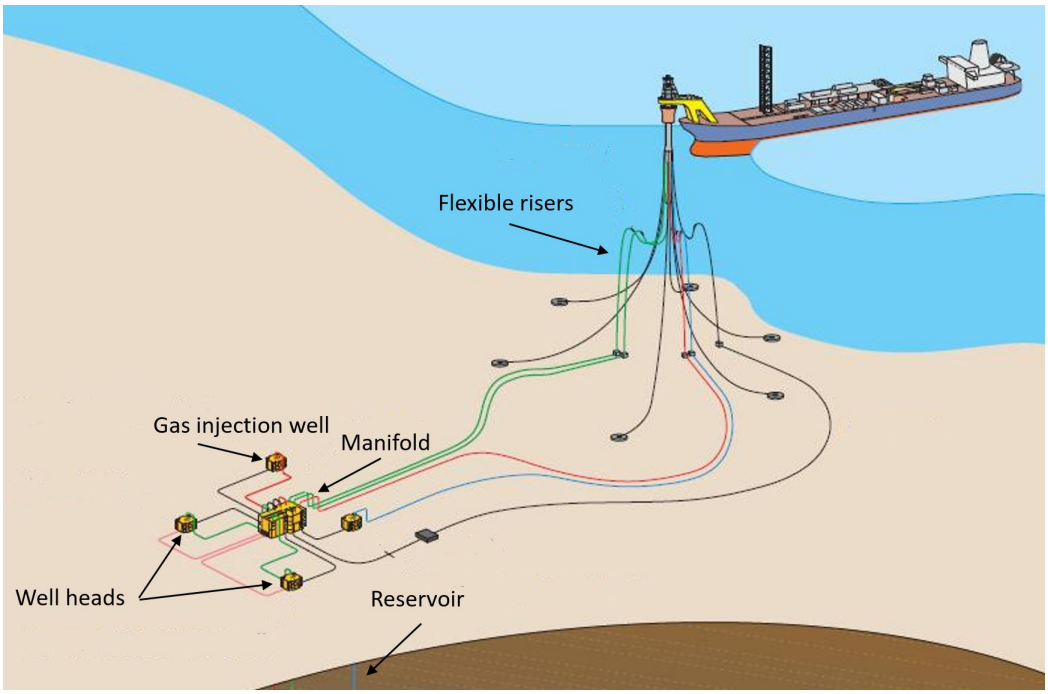

Figure 1.1: Illustration of a subsea production system (Offshore Energy Today)

For reservoirs at their declining stage or low-pressure reservoirs, two phase flow is predominant since the gas boils out of the liquid due to low pressure. Depending on the flow rate, inclination of flow-line and gas volume, the EDI may be prevalent.

Unlike severe slugging where it is stratified flow upstream the riser base, EDI in natural flowing fields may be present in both risers and wells. EDI is a result of inclination of the flow-line and varying flow rates of gas due to accumulation and expansion because of liquid blocking in lower bends. This may result in pushing the liquid backwards, creating a back pressure that could potentially *kill* the reservoir (Kjeldby, 2010). The EDI could have a great impact on a overall production in a field, and by predicting the flow conditions necessary for EDI, this scenario could be avoided.

The multiphase laboratory is located at energy and processing department at NTNU, and have recently been extended with a tower which now allows experiments on long vertical pipes (Figure 1.2). This gives new opportunities for studying vertical multiphase flows. Dynamic flows is one type of flow problems, and a test-section will be designed and constructed to study instabilities in air lifted systems, where EDI is the phenomena to be investigated more closely. The tower have interior height at approximately 20m, measured from the tower ceiling to the 1^{st} floor. It consists of a spiral staircase with a cylindrical void in the center. This void is now filled with a vertical multiphase flow setup, which is connected to the existing rig. This work is conducted by the author trough the specialization project conducted Autumn 2017 (Ravnås, 2017).

A few experiments and simulations have been conducted previously on Expansion Driven flow Instabilities. Kjeldby (2010) developed numerical simulations of EDI using OLGA and Sluggit, which are both multiphase flow simulation programs. This research has been continued trough Kjeldby et al. (2013) and Kjeldby et al. (2015) focusing on the simulation part. Kanu (2011) continued on the work done by Kjeldby (2010) by using the same flow parameters and geometry to verify the numerical simulations experimentally. The expansion effect was rather small, but did occur both experimentally and numerically for the setup. Kjeldby and Nydal (2012), conducted studies on EDI in two-phase flows in riser and wells, both numerically and experimentally. They emphasized the need for future studies conducting more systematic experiments in longer risers.

Figure 1.2: Installation of outer part of tower (Adressa)

This work is an extension of the work done by Kjeldby and Kanu. The main difference now is the new experimental rig, which gives new experimental opportunities on longer and larger pipes.

1.2 Objectives

The main objectives are to demonstrate and document EDI, both experimentally and by computational flow simulations.

1.3 Approach

- Literature study;
- Installation of gas injection further upstream and installation of a flexible horizontally geometry setup for the flow-line;
- Pressure sensors and camera installation;

- Conduct experiments with varying pump frequency and gas flow rate, in order to find condition at which EDI can occur. Pump is set to a suitable frequency to have minimum circulation of water when not injecting air;
- Measurements of riser base pressure and water/air flow rate for different setups;
- Develop pump-characteristics experimentally for the used pump frequencies;
- Perform a series of OLGA and Sluggit simulations with the same parameters as in the experiments;
- Process and present the experimental and simulated data using MATLAB;
- Compare experimental results to OLGA and Sluggit simulations;
- Record oscillations due to the EDI phenomena with camera installed along the vertical pipe;

1.4 Outline

- Chapter 1. Introduction: Structure already discussed in this chapter;
- Chapter 2. Literature review: Literature review on multiphase instability mechanisms in addition to basic multiphase theory;
- Chapter 3. Experimental setup and equipment: Includes the geometry and component descriptions, used in the experiment;
- Chapter 4. Experimental results: Includes test matrix, plots, results and discussion, ended with a summary;
- Chapter 5. Simulation: Presentation of the OLGA numerical model followed by a OLGA model sensitivity section. Results are presented and discussed. The instability cycle in EDI is visualized. Presentation of Sluggit model with corresponding results;
- Chapter 6. Flow regime transition: An extension for higher air flow rates is conducted for 38Hz and 40Hz. The purpose is to study the transition between slug and annular flow regime;
- Chapter 7. Summary and recommendation for further work: Concluding remarks are made for both experimental and numerical simulated results, ended with general remarks for improvements and further work;

Chapter 2

Literature review

2.1 Multiphase flow instability mechanisms

Instability mechanisms for two-phase flows can be divided into two sub categories, static and dynamic instabilities. When a unstable steady state is perturbed, this would initially get a positive feedback from the system. This can lead to a departure from the steady state, and would be classified as a static instability. For this category, the system can have a periodic behavior or the steady state conditions could change, depending on the boundary conditions for the system. If the flow on the other hand is subject to inertia and feedback as essential part of the process, it would be classified as dynamic instability. A perturbation here will give the system a negative feedback, and this could for various reasons not be enough for stabilization, but instead lead to a sustained flow oscillation (Hu, 2005).

Severe slugging in flowline-riser systems is often related to the upstream compressibility problem, where trapped gas upstream the riser base is compressed (Kjeldby et al., 2013). This can eventually cause blow out of the accumulated liquid in the riser. This type of severe slugging needs large upstream gas volume to be able to occur and would be categorized as a static instability phenomena.

For a case where the riser is sufficiently long, flow instability can be induced by gas expansion in the riser itself. Small amount of trapped gas can be enough to cause instabilities due to the expansion effect the accumulated gas will have in the riser column. Gas can for instance be trapped in a upstream jumper as seen in Figure 2.1. This phenomena is named Expansion Driven flow Instabilities (EDI). Jumpers are often added to prevent damage on the pipeline, due to elongation and compression, originated from thermal variations (Kjeldby et al., 2013). This geometry also prevents damage to the pipeline originated from flow-induced vibrations.

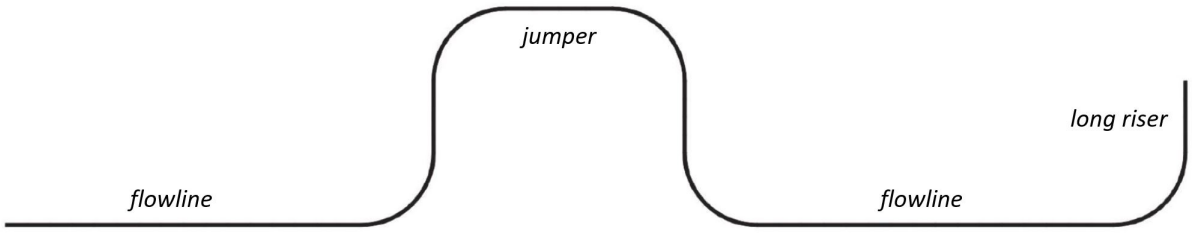

Figure 2.1: Flowline, jumper and riser (Kjeldby et al., 2013)

Another relevant geometry for Expansion Driven flow Instabilities is a slightly declining upstream flowline as seen in Figure 2.2. A stationary Taylor bubble might be developed here. This is possible if the case is continuous liquid production and the mixture component of the Taylor bubble velocity U_b equals the drift component to the bubble velocity, only with opposite sign. The stationary Taylor bubble can grow in length for both cases. Gas needs to be added trough a local gas source or from advected gas from the upstream flowline. When the gas accumulates, the nose of the Taylor bubble will eventually reach the riser base. At this moment the gas will start to expand up in the riser, and unstable production of liquid can occur while the accumulated gas is flushed out.

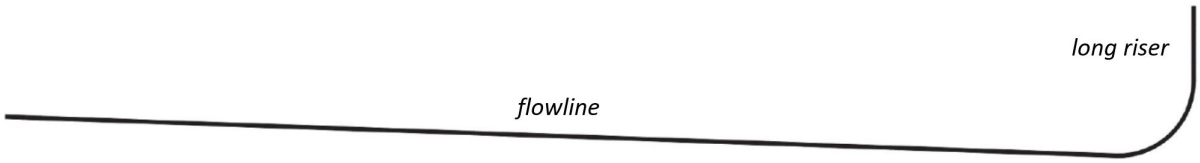

Figure 2.2: Declining flowline (Kjeldby et al., 2013)

A dynamic instability phenomena named density wave slugging can somewhat be likened to EDI, since both causes variation in liquid holdup. These two phenomena are often synonyms when referred to in the literature. The holdup will have an impact on the hydrostatic pressure and the mixture density across a long riser (Kanu, 2011).

Density wave instability phenomena is due to mixture density variations ρ_m given in Equation 2.1.

$$\rho_m = \rho_g \alpha + \rho_l (1 - \alpha) \tag{2.1}$$

Where ρ_g is gas density, ρ_l is liquid density and α is the void fraction.

This causes pressure drop perturbations in wells and risers originated from unstable gas-lift. Density waves causes large volumetric variations due to phase change. For wells at low reservoir pressure and low gas rate given from the gas-lift system, density wave instability phenomena are observed (Bin et al., 2003).

Artificial lift by gas-lift technique is one of the methods used in the industry to avoid severe slugging in deep water operations. This technique also gives new challenges regarding instabilities in density wave oscillations, tubing/casing heading and EDI. Xu et al. (1989) emphasized that operators of a well with continuous gas-lift experienced difficulties in maintaining the targeted production rate. To analyze a gas-lift system in a well, an equilibrium curve can be established by using two pressure-rate relationships for the gas-lift inlet. These relationships called in a more simplistic terminology, refers to upstream pressure as *available pressure* and to downstream pressure as *required pressure*. The two intersections points can been seen graphically in Figure 2.3.

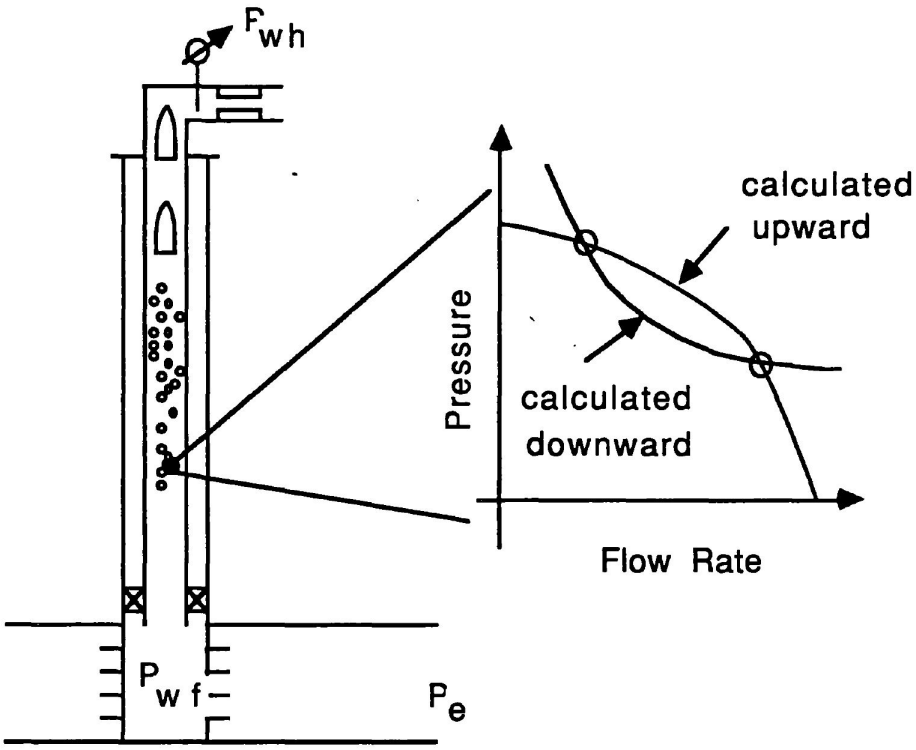

Figure 2.3: Determination of equilibrium conditions (Xu et al., 1989)

This curve cannot guarantee that the flow is stable even if the static stability criterion (Equation 2.2) is fulfilled.

$$\frac{\mathrm{d}p_a}{\mathrm{d}q} < \frac{\mathrm{d}p_r}{\mathrm{d}q} \tag{2.2}$$

Where p_a is available pressure, p_r is required pressure and q is flow rate.

This may be unstable if not satisfying the dynamic stability criterion. A flow could be dynamic unstable if inertia and feedback effect is an essential part of the process. If this is the case, the system would alternate above an average level in a periodic manner as seen in Figure 2.4, and in this scenario, density waves or EDI could be present.

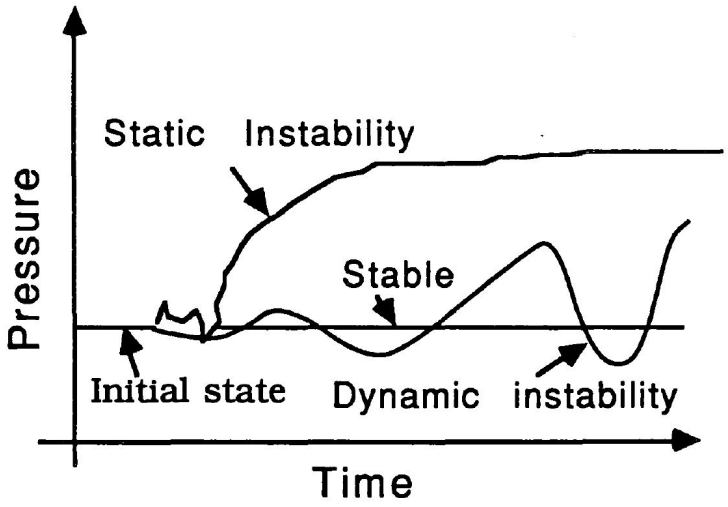

Figure 2.4: Illustration of stability concepts (Xu et al., 1989)

Since EDI often are related to pressure oscillations, the bubble formation and expansion are important factors. Mayor et al. (2008) simulated in addition to experiments, the gas phase expansion and gas hold-up in a free bubbling vertical slug flow. This study showed that the bubble expansion results in upward displacement of everything ahead of the bubble, proportional to the expansion of the bubble.

In Figure 2.5 the white rectangular shape illustrates bubble i, and zone A is the liquid flowing ahead of it. The bubbles behind bubble i induces a raise in the gas and liquid ahead of them, proportional to the sum of individual expansions. This results in a increased flow velocity ahead of bubble i, due to expansion of all bubbles flowing behind it.

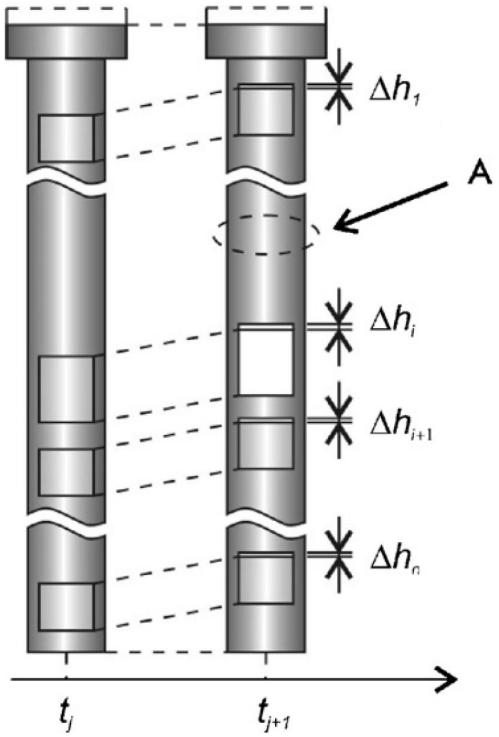

Figure 2.5: Two consecutive moments in the upward movement of bubbles (Mayor et al., 2008)

Poblano et al. (2002) investigated the effect on the tubing diameter for a gas-lift system. The result is showing a larger area of stable flow for tubing diameter at 0,09m, than for 0,18m (See Figure 2.6a & 2.6b). Care should therefore be taken when designing a gas-lift well with large diameter, especially if large variations in the injected gas flow rate is expected.

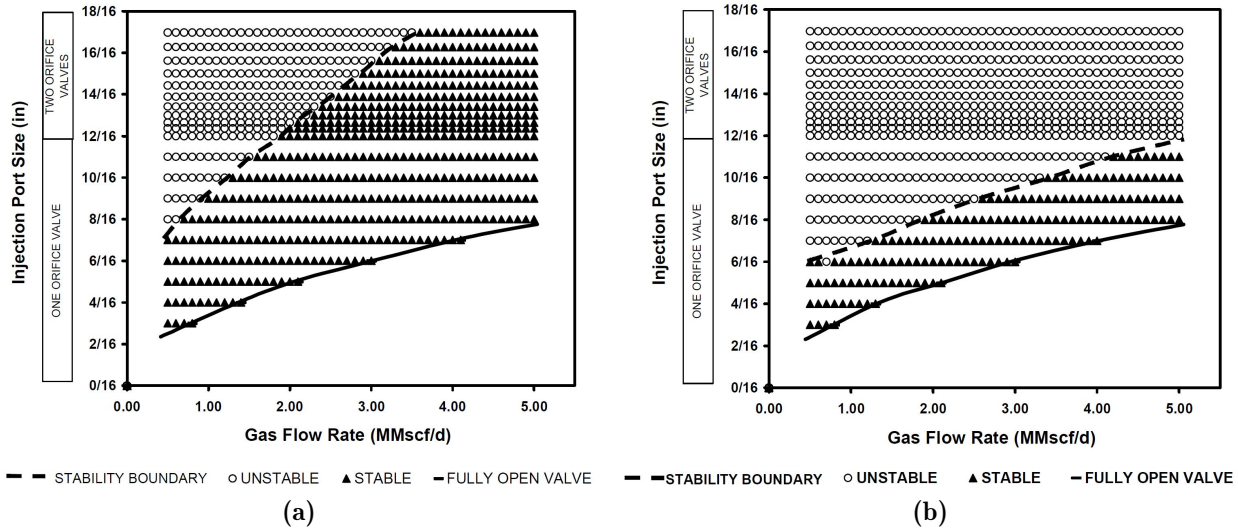

Figure 2.6: Stability map for tubing diameter (a) 0,09m (b) 0,18m (Poblano et al., 2002)

2.2 Superficial velocity

Superficial velocity is a hypothetical flow velocity, calculated in a way such that a given phase is flowing alone in the pipe represented with a cross sectional area.

Superficial velocity for gas U_{sg} is calculated from equation

$$U_{sg} = \frac{\dot{m}_g}{\rho_g A} \tag{2.3}$$

where $\dot{m}_g$ is the mass flow rate for gas, ρ_g is gas density and A is the inner cross sectional area of the pipe. The density which is used in the calculations for U_{sg} and U_{sl} are given in Table 3.3, and the reader should note that all of the calculation are for atmospheric conditions and 20°C.

Superficial velocity for liquid U_{sl} are calculated in the same way as U_{sg}. U_{sl} is represented in equation

$$U_{sl} = \frac{\dot{m}_l}{\rho_l A} \tag{2.4}$$

2.3 Hydrostatic pressure

Hydrostatic pressure P_{hyd} (Pa) is calculated from equation

$$P_{hyd} = \rho_m \cdot g \cdot h \tag{2.5}$$

where g is gravitational acceleration $(9,81 m/s^2)$ and ρ_m is the mixture density, defined in Equation 2.1. The height of the fluid column h given in meters (Shoham, 2006).

The absolute pressure will therefore be

$$P_{abs} = P_{hyd} + P_{atm} \tag{2.6}$$

where P_{atm} is atmospheric pressure and is set to 1,01bar which is for mean sea level.

2.4 Flow regimes

A flow regime describes the phase distribution of the multiphase mixture. The different flow regimes depends primarily on the superficial velocities, system geometry and the physical properties of the fluid mixture (Guet and Ooms, 2006).

The absent of a stratifying force (gravity) is the main difference between horizontal and vertical flow. Instead of stratified flow, a low flow rate for liquid and gas at high pressure will provide bubbly flow (Figure 2.7 (a)) regime, where buoyancy is the driving force.

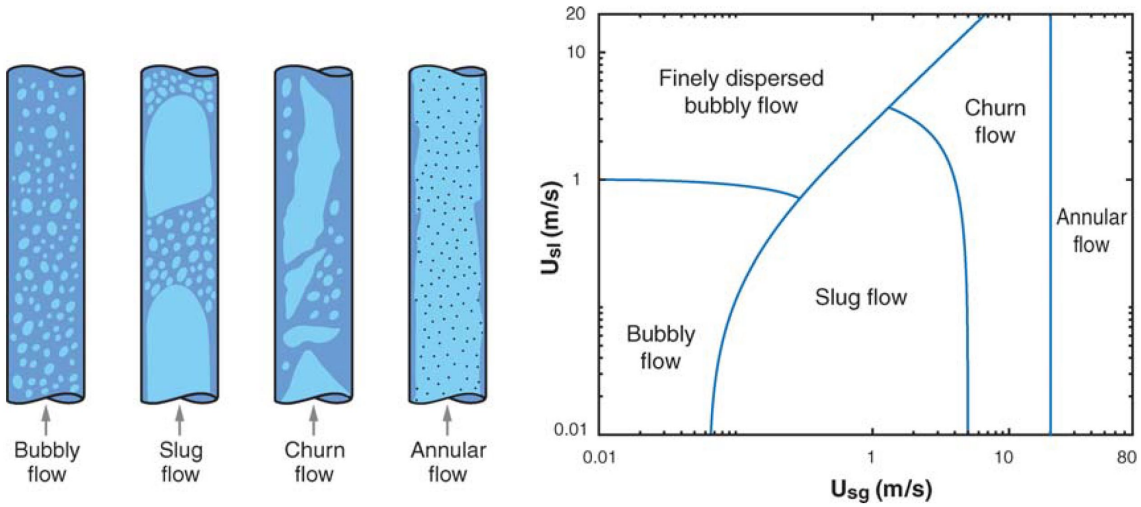

Figure 2.7: (a) Flow regime pattern for vertical flow; (b) Flow pattern map for a 72mm inner diameter vertical pipe flow of air and water (Guet and Ooms, 2006)

Intermittent, slug and churn flow can develop when increasing gas flow rate. Churn flow have a more frothy shaped appearance, and occurs often at higher gas flow rates than slug flow.

Annular flow occurs at even higher gas flow rates, and here the appearance is often a slow thin liquid film at the walls while droplets is located in the middle with high velocities.

The flow pattern map presented in Figure 2.7 (b) can be used as a qualitative flow pattern map, not as a general map, since the superficial velocity values depends largely on geometry, fluid properties and the system. This flow pattern map is based on Taitel et al. (1980) model, where the Churn-Annular flow transition is originated from equation

$$\frac{U_{sg}\sqrt{\rho_g}}{\left[\sigma_{l/g} g(\rho_l - \rho_g)\right]^{\frac{1}{4}}} = 3,1 \tag{2.7}$$

where $\sigma_{l/g}$ is the surface tension between liquid and gas. The other parameters are already discussed. According to this simple equation the churn-annular flow transition is independent of pipe diameter and liquid flow rate.

Chapter 3

Experimental setup and equipment

3.1 Setup

The laboratory experiments are carried out using the new experimental rig at EPT's multi-phase flow laboratory. Figure 3.1 shows the lower part of the experimental test-section where the ID labels are linked to Table 3.1 and Figure 3.2/3.3. A picture displaying the entire rig is not possible since the riser continues above the roof. The full geometry for the test-section is shown in Figure 3.2. The full lab setup can be seen in the Piping and Instrumentation Diagram in Figure 3.3, where the used flowlines for this experiment are highlighted in yellow.

Table 3.1: Experimental setup table

ID in Figure 3.1/3.2/3.3	Components
1	Air/Water separator, Tag F-001 (Appx.G.2)
2	Vertical Plexiglas pipe, internal diameter 0.06m (Appx.G.1)
3	Absolute pressure transducer, Tag PT 4.13 (Table 3.5)
4	Flexible hose laying on an adjustable cabel-ladder, internal diameter 0.06m (Appx.G.3)
5	Adjustable geometry device (Appx.G.3.2)
6	Air injection (Appx.G.3.1)
7	Absolute pressure transducer, Tag PT 4.14 (Table 3.5)
8	Centrifugal pump, Tag P-002 (Appx.F and Appx.G.6)

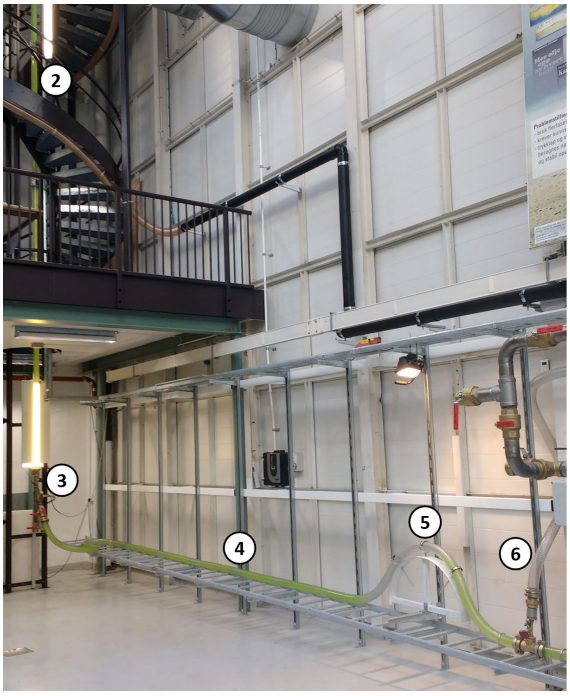

Figure 3.1: Lower part of experimental test-section

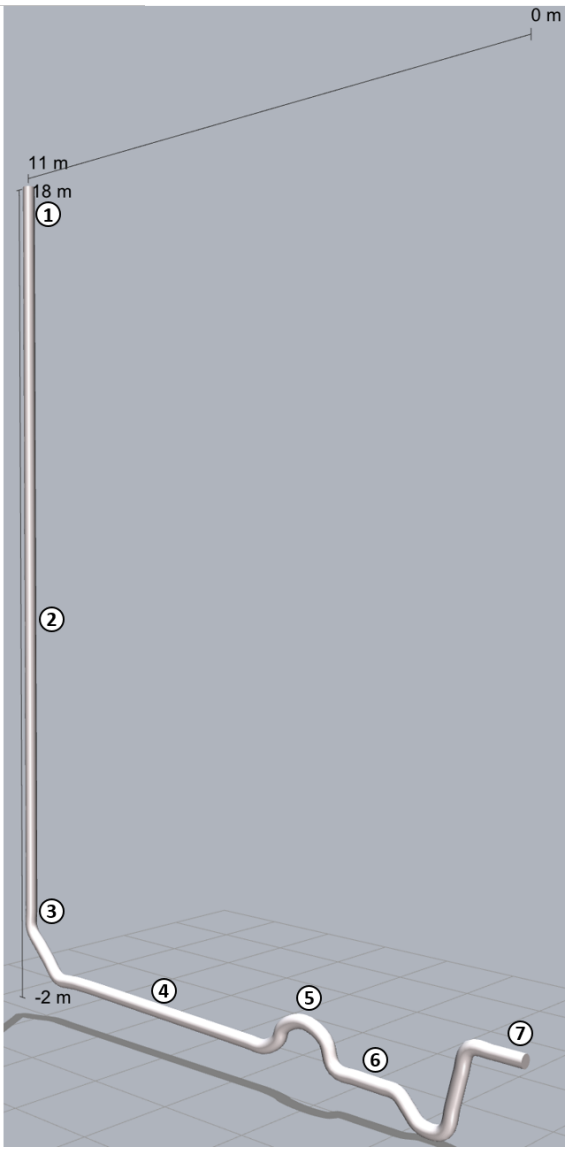

Figure 3.2: Experimental geometry developed in LedaFlow

Water is used as production fluid and air as lift fluid. These are separated at the top of the vertical pipe by a separator (ID 1 Table 3.1). The vertical pipe (ID 2) consists of transparent plexiglas connecting the separator and the riser base. Two absolute pressure transducers (ID 3/7) are mounted at the riser base and close to the inlet of the flexible hose, respectively. This flexible hose (ID 4) is mounted to a adjustable cabel-ladder. ID 5 is a adjustable geometry device formed as a half-circle. The radius can be adjusted to a certain level, and the purpose for this device is to create a *jumper* presented in Figure 2.1, to allow the entrapment of air before riser inlet. ID 6 is where air is injected into the system. In Figure 3.3, the centrifugal pump is marked with ID 8. More information for the respective ID tags can be found in Table 3.1 following its respective reference.

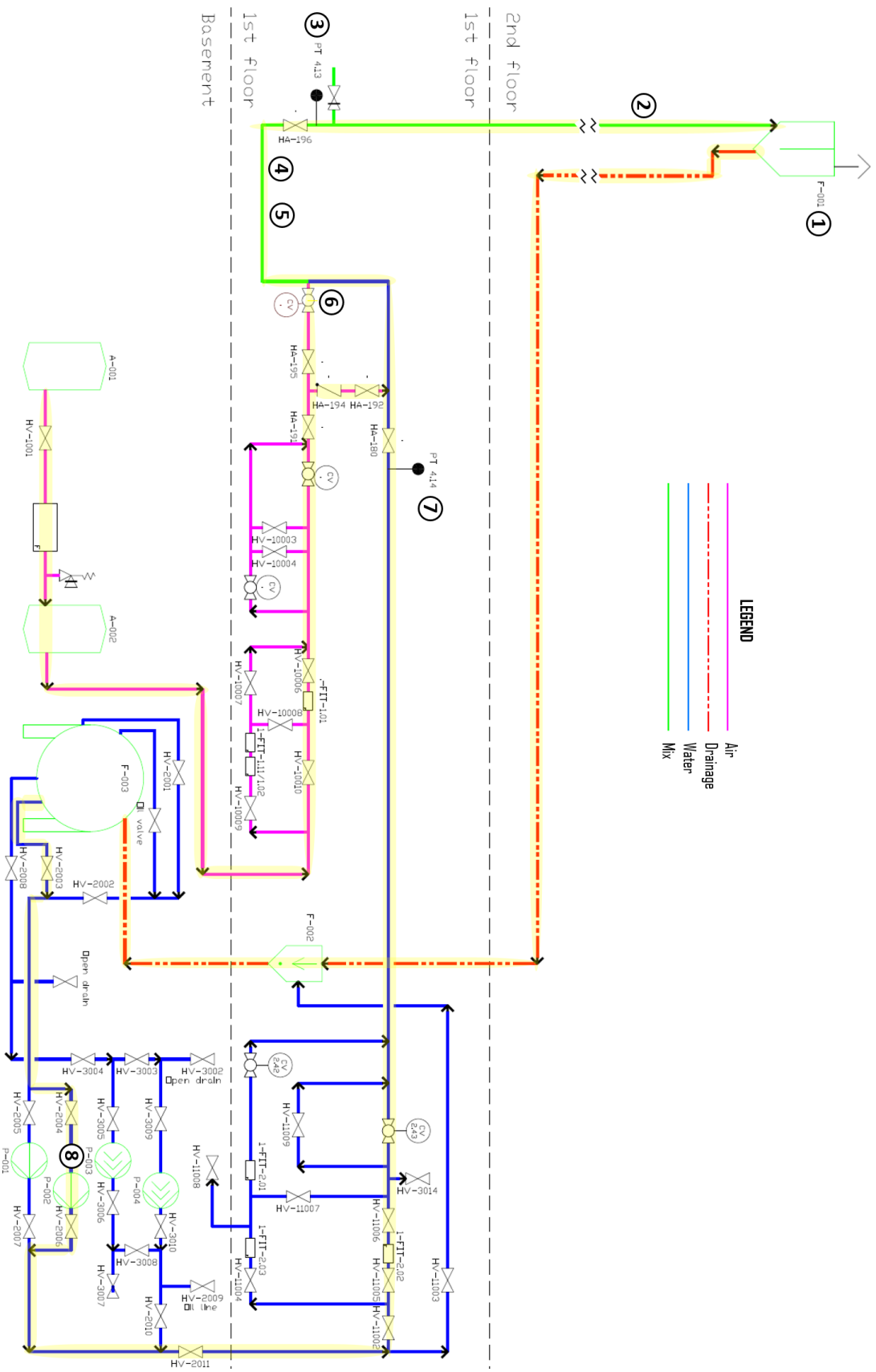

Figure 3.3: Piping and Instrumentation Diagram, where used flowlines are highlighted in yellow (AutoCAD Plant 3D)

3.1.1 Geometry

The geometry for this experiment is illustrated in Figure 3.2, which is the same geometry used in the simulations. The geometry is here folded out and presented in a 2-dimensional format. This is a simplification which does not include the u-turns presented in appx. Figure G.7. Table 3.2 have the exact geometry for the pipe-sections presented in Figure 3.2.

Table 3.2: Geometry for each pipe-section

Pipe	Length [m]	Elevation [m]	Inner Diameter [m]
1	2	0	0,060
2	1.4	-1,25	0,060
3	0,3	0	0,060
4	0.5	0,35	0,060
5	1,25	0,032	0,060
6	0,40	0,38	0,060
7	0,40	0,16	0,060
8	0,40	-0,16	0,060
9	0,20	-0,19	0,060
10	0,7	-0,14	0,060
11	5,2	0,13	0,060
12	0,4	0	0,060
13	0,5	-0,033	0,060
14	1,2	0,83	0,060
15	17,28	17,28	0,060

3.1.2 Fluid properties

This experiment is conducted using varying injected air flow rates, ranging from 0 to $6{,}96{\cdot}10^{-3} kg/s$. The maximum recorded pressure is 2,75bar and the temperature in the lab is approximately 20°C, assuming isothermal conditions for this experiment. The pressure in the lab is also at atmospheric conditions. Fluid properties for this experiment are presented in Table 3.3.

Table 3.3: Fluid properties at 20°C and 1atm (Cimbala and Cengel, 2014)

Fluid	Property	Symbol	Value	Unit
Water	Density	ρ_l	998	$[kg/m^3]$
Water	Viscosity	μ_l	$1,002 \cdot 10^{-3}$	$[Pa \cdot s]$
Air	Density	ρ_g	1,204	$[kg/m^3]$
Air	Viscosity	μ_g	$1,825 \cdot 10^{-5}$	$[Pa \cdot s]$
Water/Air	Surface tension	$\sigma_{l/g}$	$7,28 \cdot 10^{-2}$	$[N/m]$

3.2 Equipment

3.2.1 Centrifugal pump

The experimental rig consists of several options for pumps. For this experiment, the large centrifugal pump (Tag P-002 Figure 3.3) is used, with model number *100-35*, described in Appx.F, where the pump-characteristics from the manufacturer can be found. Additional pump-characteristics is experimentally developed for the frequencies used in the experiment (see Figure 3.4). Pressure and water flow rate is measured using the pressure sensor at the inlet (Tag PT 4.14) and the flow meter (Tag FIT 2.02), respectively. This experiment is conducted without the jumper (ID 5 Table 3.1). The flexible hose is now laying flat on the slightly inclined cabel-ladder. The small air trap in Pipe 13 (see Table 3.2) is also flattened to avoid instabilities. The reader should note that this geometry is only used when developing the new pump curves.

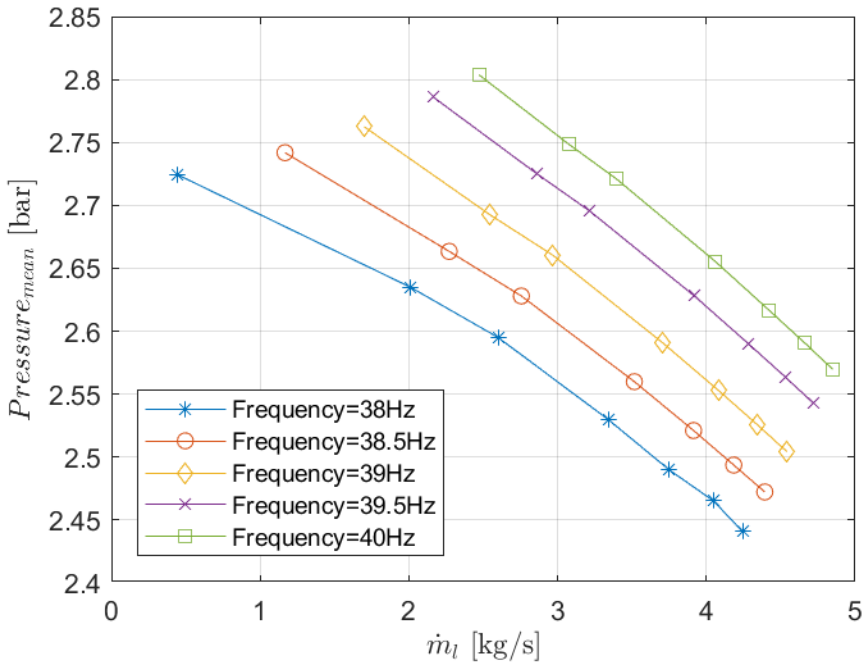

Figure 3.4: Implemented centrifugal pump curves in OLGA

The pump supply water from the main oil-water separator (Tag F-003 Figure 3.3) to the system, located in the technical-room (see Appx.G.6).

The centrifugal pump in this experiment is used to simulate a reservoir. As in a reservoir, the inflow is reduced by increased tubing pressure. This effect is achieved by running the centrifugal pump at a suitable frequency. The frequencies for this case is chosen since they are suitable for the experimental rig. Lower frequencies than 38Hz have been tested,

which makes the liquid (water) unable to overflow the riser outlet without artificial gas-lift. Adding artificial gas-lift results in air accumulation upstream the water flowline, which could potentially be a hazard for the measuring equipment installed.

The relation between capacity, frequency and speed can be seen in Table 3.4, where the values are read directly from LabVIEW. LabVIEW is a system-design platform for a visual programming language, and is here used to control the experimental rig.

Table 3.4: Relation for centrifugal pump between capacity,frequency and speed, read directly from LabVIEW

Capacity [%]	Frequency [Hz]	Speed [rpm]
78	38	2190
79	38,5	2216
80	39	2242
81	39,5	2269
82	40	2295

Variations in-between the chosen frequencies (see Table 3.4) varies the speed of the impeller in the pump, which again creates velocity and pressure. Increasing the capacity and therefore the frequencies gives higher speed to the impeller, and therefore increases the centrifugal force, increasing the velocity and pressure the pump can deliver.

3.2.2 Absolute pressure transducer

Two absolute pressure transducer are installed to among other things monitor the oscillations in the experiment. Tag PT 4.13 (see Table 3.5) is located at the riser base, i.e at the inlet of Pipe 15 (see Table 3.2). Tag PT 4.14 is located at the inlet of Pipe 1.

Table 3.5: Pressure sensor

Fluid	Model	Type	Tag	Range [bar]	Accuracy [%]
Gases, Vapours, Liquids	Aplisens PCE-28	Absolute pressure transmitter	PT 4.13/4.14	0-4	0,16

3.2.3 Flow meter

Flow rates are measured for single phase air and water using the pre-installed flow meters listed in Table 3.6. They are both located further upstream than the test-section. The location can be found in the P & ID (Figure 3.3) marked with its respective Tag.

Table 3.6: Flow meter (air density at 20°C) (Chupin, 2003)

Fluid	Model	Type	Tag	Range [kg/s]	Accuracy [%]
Air	Micromotion-CMF025 Elite	Coriolis	FIT 1.01	$3,33 \cdot 10^{-5}$-0,022	0,5
Water	Fisher Porter COPA XM Series 3000	Electromagnetic	FIT 2.02	0,83-10	0,5

3.2.4 Camera

The action-camera used to capture and record the visual is a *GoPro HERO 6 Black*. The main settings used to record the riser base is 1080 resolution, 120 frames per second and -2,0 Exposure Value Compensation (EV Comp). To have good visualization of the riser base section, a light panel is installed behind the acrylic pipe, shining trough (see setup above ID 3 in Figure 3.1). EV Comp is therefore negative due to the brightness originated from the light panel.

All recordings are stored on a hard drive, which will be delivered in addition to this thesis.

3.3 Experimental procedure

The experimental rig is initially filled with air at atmospheric pressure. The valves in the lab are controlled using the check list for the valves, found in Appx.D. The control valve for the water flowpath is fully opened to 100%. The pump is started and the capacity is slowly adjusted up to 85% to flush out all the air trapped in the system. When the entire system is filled with water and no air, the capacity/frequency is gradually reduced to 78%/38Hz. For centrifugal pump frequency at 38Hz the continuous phase (water) is visually observed to flow at a low rate out of the riser top before air injection is applied. More details on the experimental procedure can be found in Appx.E.

Chapter 4

Experimental results

4.1 Test matrix

Table 4.1: Test matrix

Frequency [Hz]	38	38,5	39	39,5	40
Air $i{\cdot}10^{-3}$ [kg/s]					
Air 1	0	0	0	0	0
Air 2	0,18	0,13	0,11	0,11	0,09
Air 3	0,48	0,42	0,38	0,36	0,35
Air 4	0,81	0,80	0,78	0,77	0,76
Air 5	1,13	1,11	1,10	1,09	1,06
Air 6	1,38	1,35	1,32	1,30	1,29
Air 7	1,79	1,78	1,77	1,76	1,75
Air 8	2,01	2,00	2,00	1,99	1,98
Air 9	2,23	2,23	2,22	2,22	2,21
Air 10	2,58	2,57	2,56	2,57	2,55
Air 11	2,85	2,85	2,85	2,84	2,84
Air 12	4,19	4,19	4,18	4,18	4,19
Air 13	5,50	5,50	5,50	5,49	5,49
Air 14	6,96	6,96	6,96	6,96	6,95

For each frequency, single phase flow of water is logged (see Air 1 in Table 4.1).

The five frequencies follows the same trend for air flow rate for a given Air i, only with some minor discrepancies for the lowest air flow rates. The values for Air 12,13 and 14 have larger increments for air flow rate. These three are included as an insurance for the validation of the experiment. The idea is that the pressure amplitude are supposed to get lower for higher air rate, since more air eventually will change flow regime from slug/churn to annular flow. Amplitude here is defined as peak-to-peak amplitude.

The measured quantities from the experiment are the pressure taken from the riser base (Tag PT 4.13, Table 3.5), the flow rate of air and water (Tag FIT 1.01/FIT 2.02, Table 3.6). For each air flow rate with its respective frequency, the data is logged for approximately 9 minutes.

4.2 Visual observations

When operated in single phase with no air injected, all pump frequencies results in water production (see Appx. Figure A.1, A.20, A.34, A.48 & A.62). This is categorized as a natural flow system, meaning the fluid is able to flow to the surface due to sufficient reservoir pressure.

Oscillating behaviour are defined as a repetitive cyclic pattern for the measured values. The definition for stable behaviour are on the contrary closer to an equilibrium, with no repetitive amplitude of magnitude.

4.2.1 Oscillating

Vertical section

When oscillating behavior is present, the observed flow regime is varying in between single phase water, slug flow and bubbly flow (see Figure 2.7).

Some of the experiments conducted are captured by camera (section 3.2.4 Camera) installed at the riser base. Figure 4.1 shows one oscillating cycle presented by snapshots from the recording. The centrifugal pump frequency is at 38Hz and $\dot{m}_g$=0,81·$10^{-3}kg/s$(U_{sg}=0,24m/s). Snapshot (a) shows single phase water where the liquid column stands still in the riser (see Figure 4.1 *(j)*). The first Taylor bubble (b) enters the riser base, originated from the small u-turn air pocket. The bubbles are growing in length as they continue upwards, due to expansion. The liquid column accelerates and eventually the Taylor bubble from the jumper (c) enters the riser followed by the remaining air (d) flushed out from the jumper. Small slugs (e) continues to enter the riser base due to a constant air injection and high water flow rate. A bubbly flow (f) is present when the water mass flow starts to decelerate. Less air is mixed in the fluid and less bubbles (g & h) enters the riser. Instead of entering the riser, the air is now accumulated once more in the jumper. Eventually the mixture density in the riser column is close to single phase water (i), giving sufficient pressure to stop the liquid production.

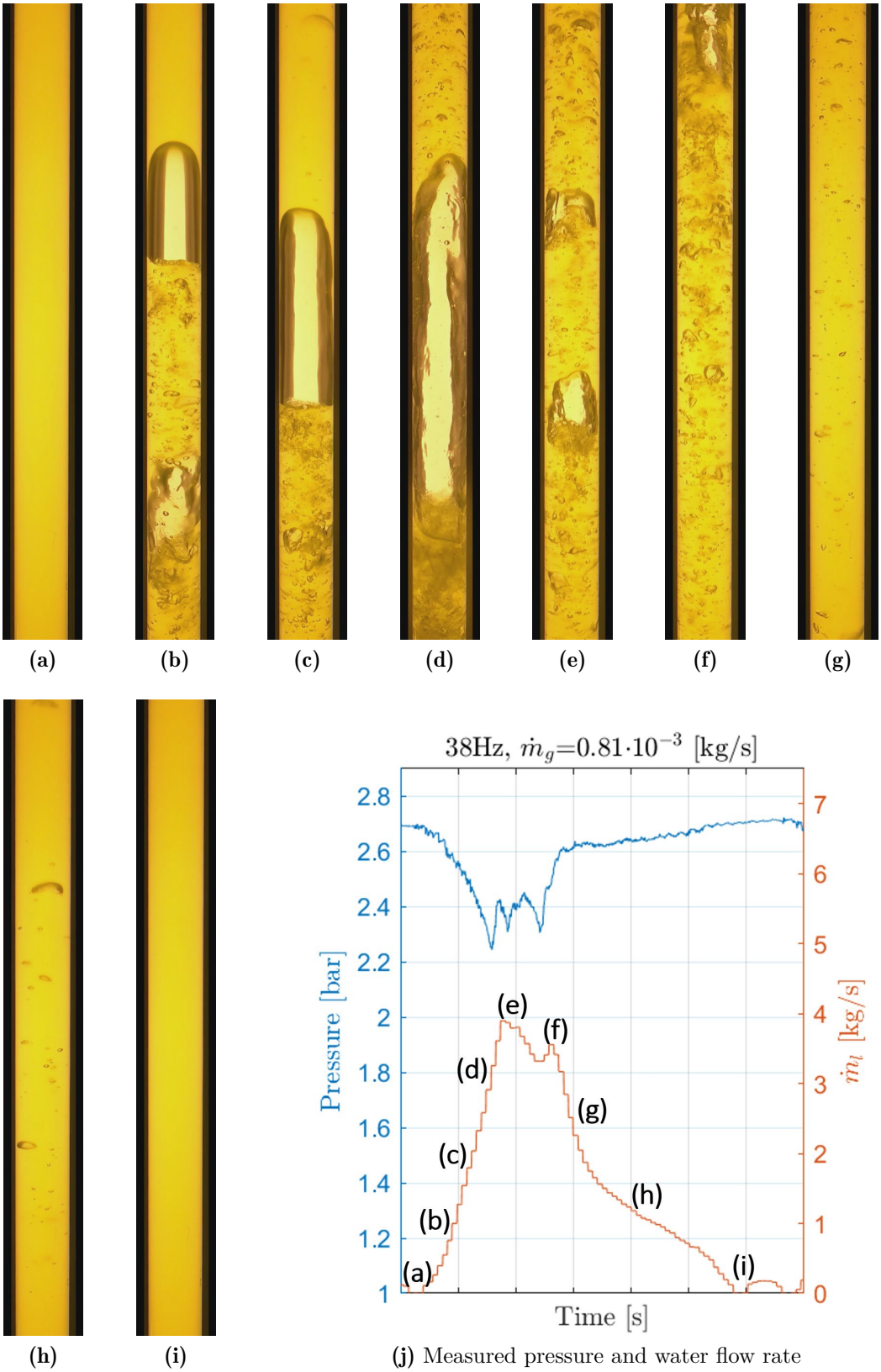

Figure 4.1: Different stages (a-i) at the riser base for one oscillating cycle (j) for pump frequency at 38Hz and injected air flow rate at $\dot{m}_g$=0,81·10$^{-3}kg/s$. Vertical grid lines have 10s increments

Horizontal section

Figure 4.2-4.6 present different stages in the jumper for one oscillating cycle for pump frequency at 38Hz and injected air flow rate at $0{,}81 \cdot 10^{-3} kg/s$. This is exactly the same case as presented in Figure 4.1, where the only change is the relocation of the camera.

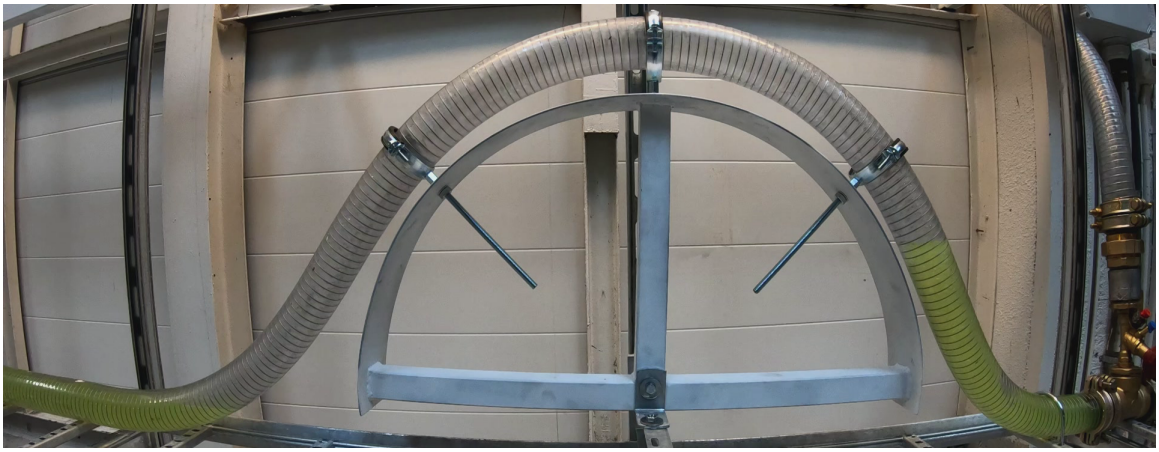

Figure 4.2: Linked to Tag (a) in Figure 4.1

Figure 4.2 shows the jumper where the liquid is flowing from right to left. In this snapshot the liquid stands still. Air is trapped in the jumper geometry, and the liquid is unbalanced, referring to different heights in the liquid columns. The trapped air pushes the liquid upstream.

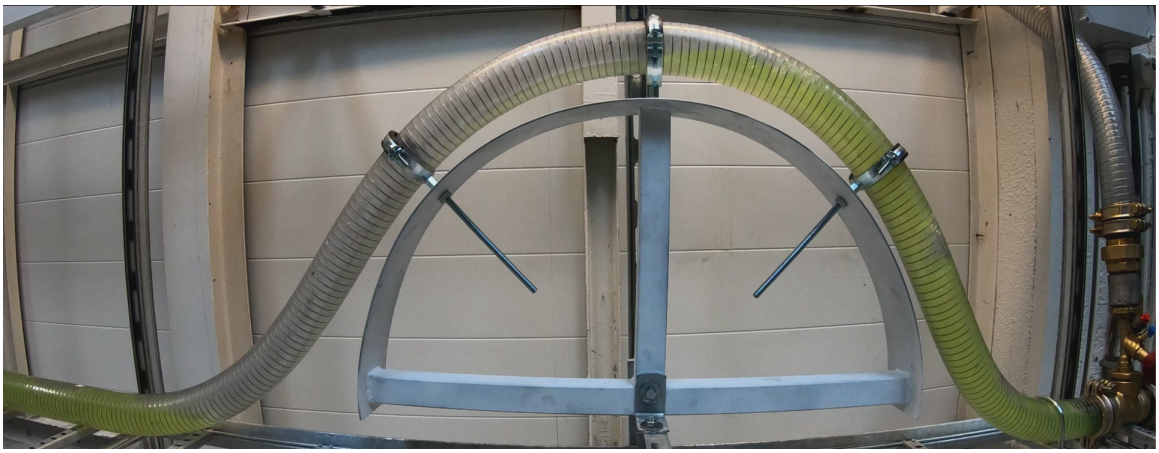

Figure 4.3: Linked to Tag (c) in Figure 4.1

In Figure 4.3 some of the first Taylor bubbles have entered the riser column, decreasing the mixture density, accelerating the liquid inflow. New liquid is now able to flow over the jumper's top, creating a stratified flow in the left section. This flow crashes into the horizontal slug flow, mixing air and water even more due to this impact.

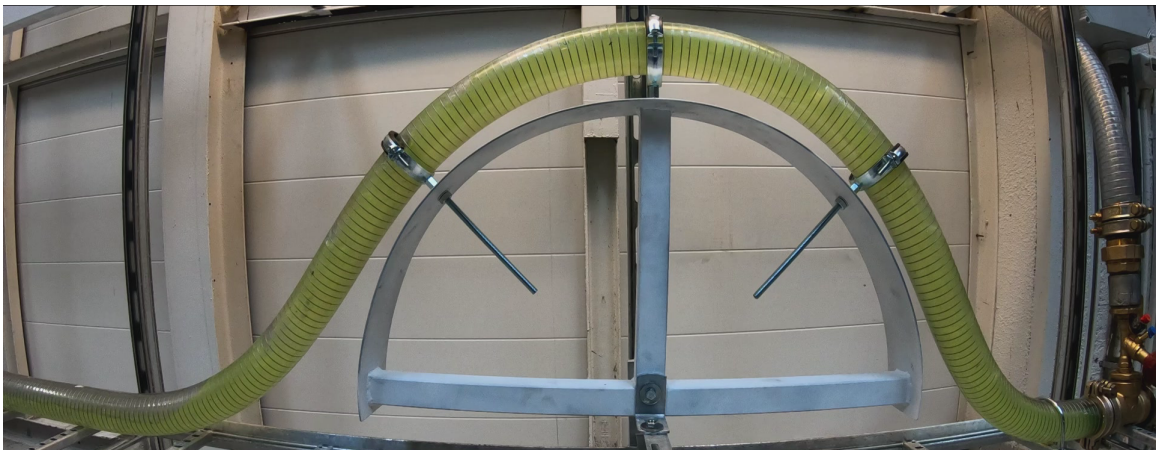

Figure 4.4: Linked to Tag (e) in Figure 4.1

Eventually all of the accumulated air is flushed out from the jumper geometry (Figure 4.4). Air is still injected at a constant rate. Bubbles can now enter the riser base continuously, leading to smaller, but more bubbles. Lower pressure due to aeration of the riser column also increases the liquid inflow to a level which eventually leads to increased mixture density in the riser column.

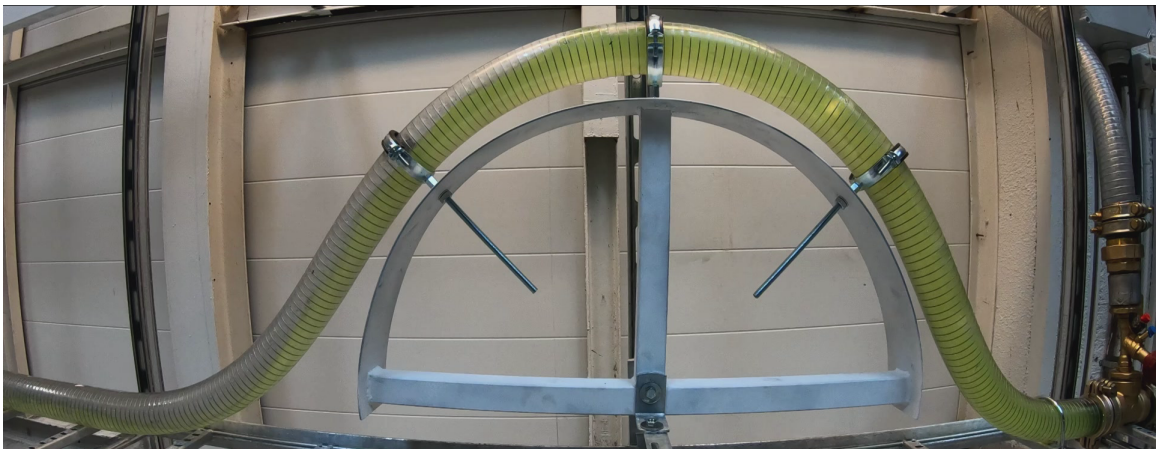

Figure 4.5: Linked to Tag (g) in Figure 4.1

Figure 4.5 shows a developing stratified flow in the left jumper section. Air is now trapped due to liquid blocking, leading to accumulation of trapped air in the jumper. The liquid blocking is pushed further upstream in the horizontal section.

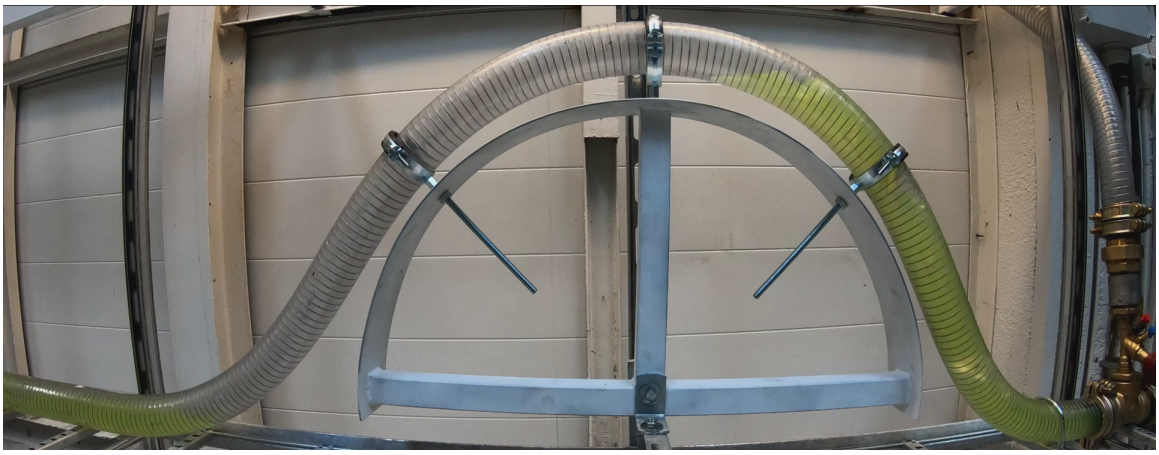

Figure 4.6: Linked to Tag (i) in Figure 4.1

The liquid blocking is now observed in the left bottom corner of Figure 4.6. The trapped air have now accumulated enough to push the liquid further upstream, stopping the inflow of water once more.

4.2.2 Stable

Snapshots from the recording of one single slug bubble passing by the riser base are presented in Figure 4.7. The injected air flow rate is here increased compared to Figure 4.1 and is now at $\dot{m}_g$=2,58·$10^{-3}kg/s$(U_{sg}=0,76m/s). The centrifugal pump frequency is still at 38Hz, but the oscillating behaviour is no longer present in this case. The time needed from snapshot (a)-(i) is under a second. Plot (j) is included to show the trend for the entire video recording. The flow regime trend for the recording is slug flow. Snapshot (a) shows tiny bubbles which are observed in between the slug bubbles. A developing bubble front are presented in (b) and (c). Liquid fallback is observed in the recordings around the bubble. For the snapshots (d)-(i) this phenomena is captured, forming a darker liquid at the tail.

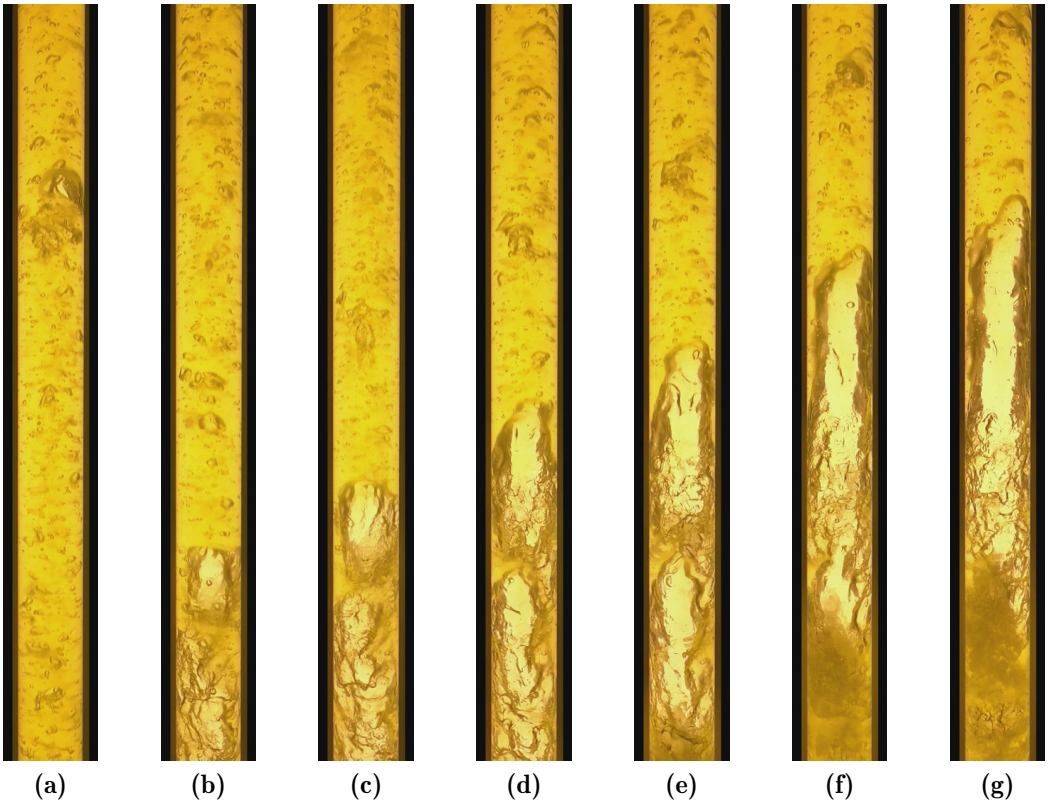

(a) (b) (c) (d) (e) (f) (g)

(h) (i)

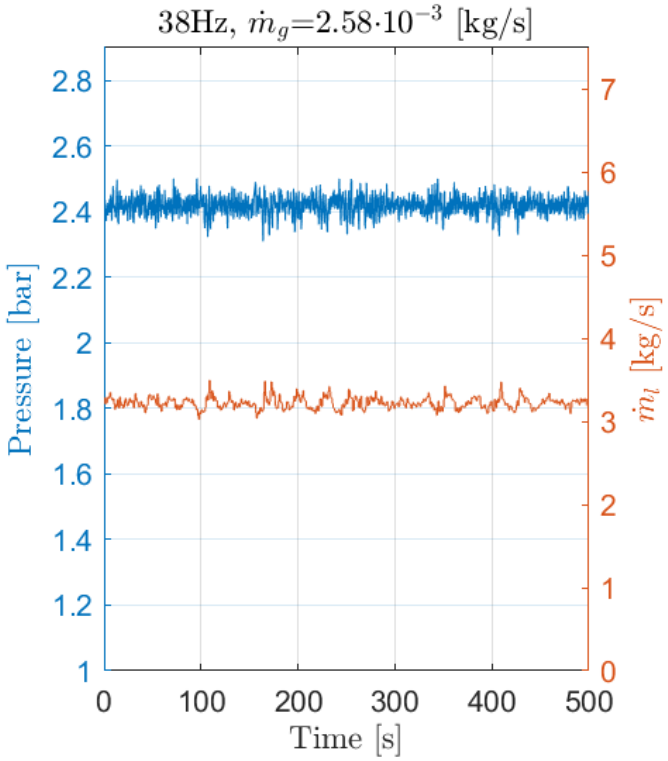

(j) Measured pressure and water flow rate

Figure 4.7: One slug bubble passing by (a-i) for pump frequency at 38Hz and injected air $\dot{m}_g$=2,58·10$^{-3}kg/s$

4.3 Pressure & water flow rate vs time

Some plots for typical behaviour for oscillating and stable flow for frequency at 38Hz are reported in this section. Figure 4.8 shows single phase water logged for $\dot{m}_g$=0kg/s. Stable liquid production (water) is present for the entire logging, but at a very low rate of 0,39kg/s. Measured pressure is also stable at approximately 2,72bar.

Figure 4.9 presents the lowest air injection rate given for this frequency. An oscillating behaviour develops for both the pressure and $\dot{m}_l$. Amplitude for pressure is 0,23bar and has its minimum where the amplitude peaks for $\dot{m}_l$. Measured amplitude for $\dot{m}_l$ is approximately 2,5kg/s. Water production for the system stops between the peaks before it rapidly increases and thereafter rapidly decreases to zero.

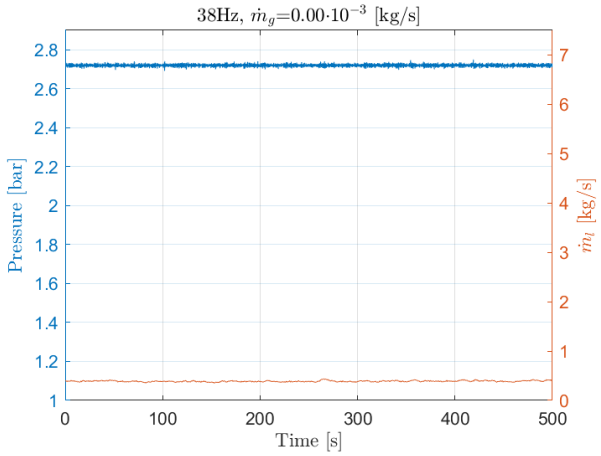

Figure 4.8: Stable flow for Air 1 at 38Hz

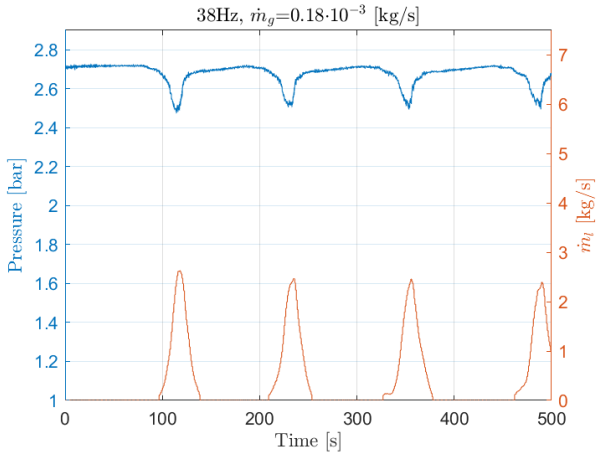

Figure 4.9: Oscillating flow for Air 2 at 38Hz

Figure 4.10 shows a pressure amplitude at approximately 0,52bar. Pressure increases rapidly after reaching the bottom of the curve, and flattens out before another rapidly pressure decrease occurs. The water flow rate have an amplitude of approximately 5kg/s. The peaks for water flow rate matches the negative peaks for the pressure. Water is produced for the entire logging period, but in a oscillating manner.

Figure 4.11 does not present any oscillation of significance for pressure or $\dot{m}_l$. Pressure have its mean value at 2.26bar and $\dot{m}_l$ have a mean value of 3,96kg/s.

Plots for the entire test matrix are reported in Appx.A.1.

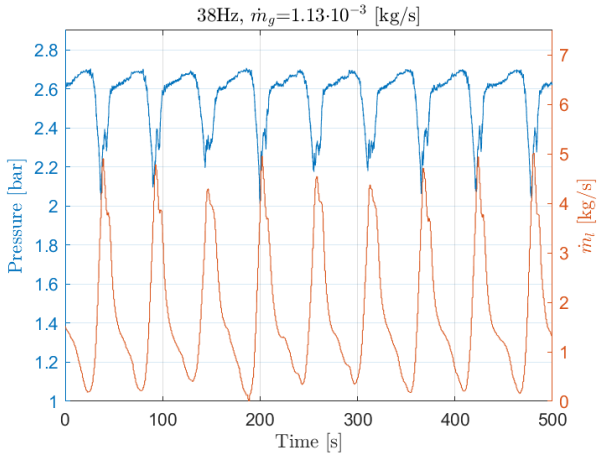

Figure 4.10: Oscillating flow for Air 5 at 38Hz

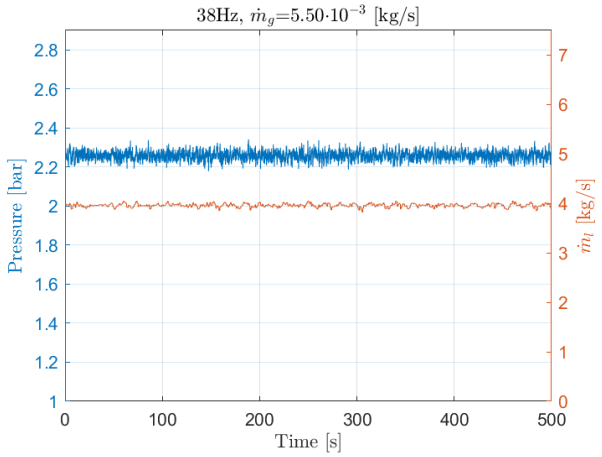

Figure 4.11: Stable flow for Air 13 at 38Hz

4.4 Max/Min values vs superficial gas velocity

Plots for max/min pressure vs U_{sg} are created for each pump frequency included in the test matrix. The same is done for the max/min U_{sl} vs U_{sg}. The max/min values plotted are for a full logging period at 500 seconds. U_{sg} and U_{sl} are calculated from Equation 2.3 and 2.4 respectively. Amplitude is here defined as peak-to-peak amplitude, i.e maximum minus minimum value for a given U_{sg}.

Figure 4.12 show pressure at approximately 2,72bar when U_{sg}=0m/s. Thereafter the amplitude increases until U_{sg}=0,59m/s, where a transition occurs for next increment to U_{sg}=0,66mm/s. The trend for higher U_{sg} values are decreasing amplitude. In Figure 4.13 the U_{sg} values from 0,054-0,33m/s gives no water production when located in the minimum U_{sl} amplitude. The largest amplitude is here when U_{sg}=0,33m/s.

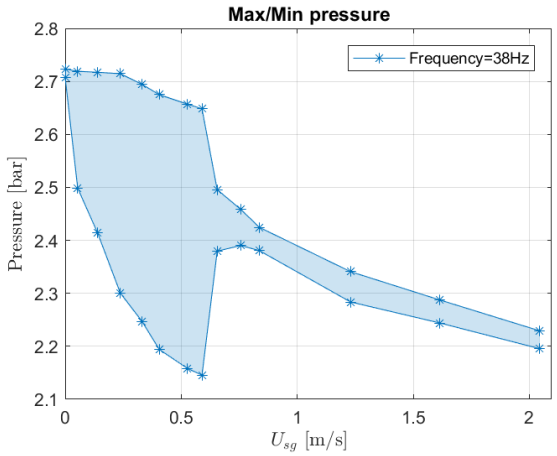

Figure 4.12: Max/Min pressure measured for pump frequency at 38Hz

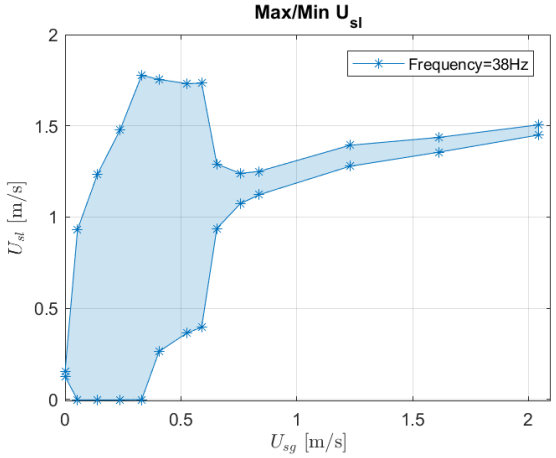

Figure 4.13: Max/Min U_{sl} measured for pump frequency at 38Hz

Figure 4.14 shows slightly higher pressure values (2,73bar) for U_{sg}=0m/s compared with Figure 4.12. Amplitude is increasing in magnitude for higher U_{sg} rates until 0,4m/s. From this value to the next at U_{sg}=0,52m/s the amplitude decreases rapidly. The amplitude decreases further for higher U_{sg} values, except for two points with small deviations for 0,59m/s and 1,23m/s. Figure 4.15 has its transitions point from oscillating to stable when U_{sg}=0,52m/s, which is the same for Figure 4.14. Pump frequency at 38,5Hz gives liquid production for all U_{sg} values, i.e the liquid production does not stop as in Figure 4.13.

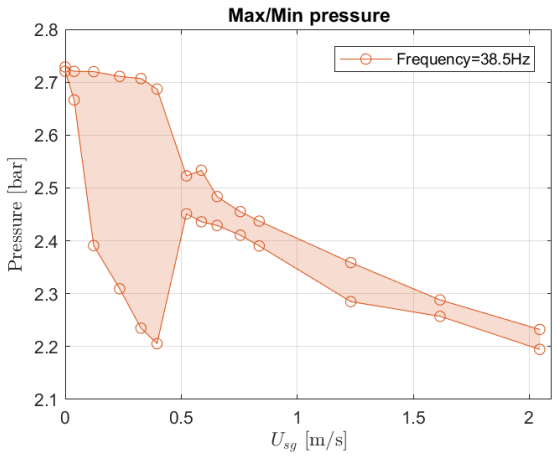

Figure 4.14: Max/Min pressure measured for pump frequency at 38,5Hz

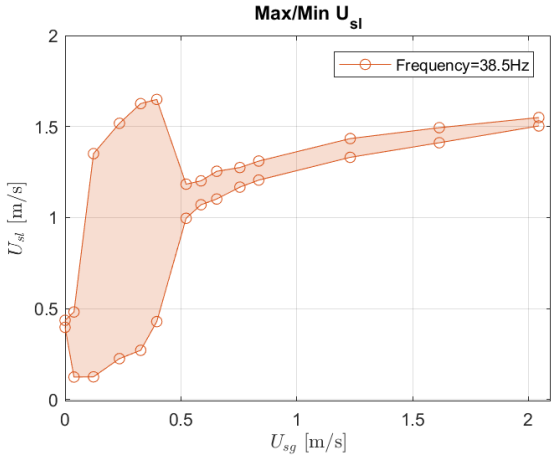

Figure 4.15: Max/Min U_{sl} measured for pump frequency at 38,5Hz

Figure 4.16 rapidly increase in amplitude for U_{sg} values up to 0,32m/s, where a transition to a low amplitude occurs for 0,39m/s. The trend after this value is an amplitude of decreasing magnitude for higher U_{sg} values. Figure 4.17 shows the same transition from oscillating to a more stable regime for the same U_{sg} value.

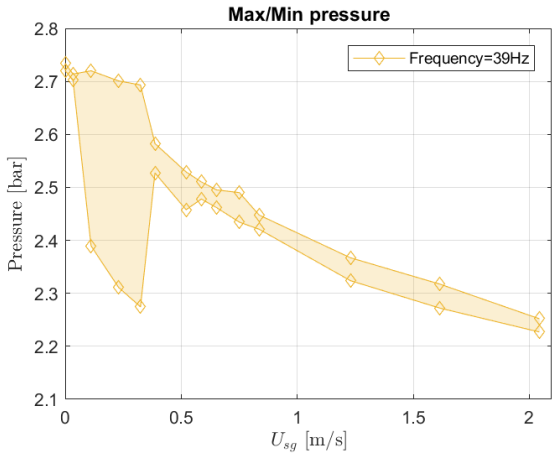

Figure 4.16: Max/Min pressure measured for pump frequency at 39Hz

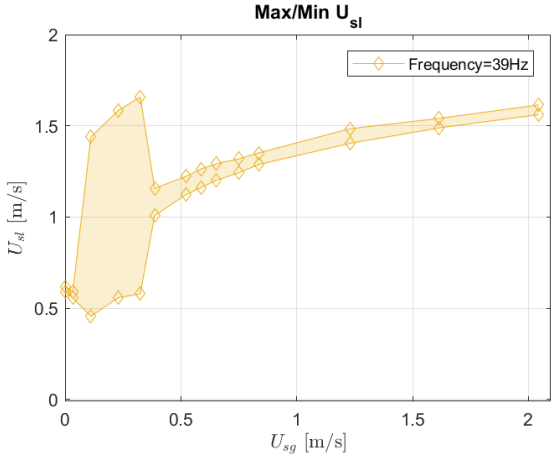

Figure 4.17: Max/Min U_{sl} measured for pump frequency at 39Hz

Figure 4.18 shows the max/min pressure for pump frequency 39,5Hz. No big shifts are observed for the pressure amplitude. The largest amplitude is observed when U_{sg}=0,65m/s. The trend after this value is decreasing amplitude for increased U_{sg}. Figure 4.19 shows stable water production, with reduced slope and increased U_{sl} for higher U_{sg} values.

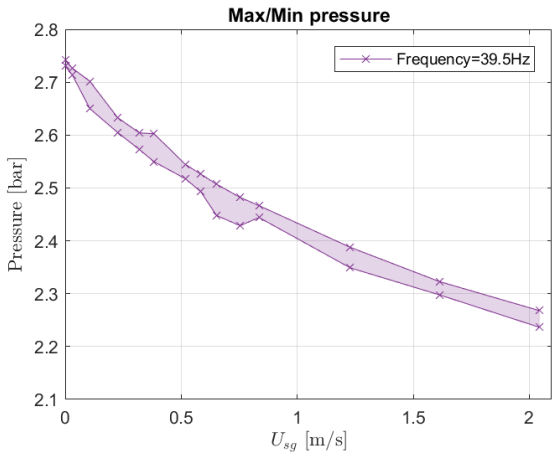

Figure 4.18: Max/Min pressure measured for pump frequency at 39,5Hz

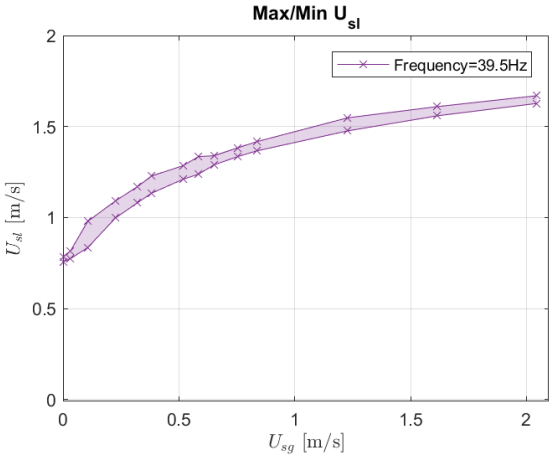

Figure 4.19: Max/Min U_{sl} measured for pump frequency at 39,5Hz

Figure 4.20 presents its greatest amplitude for U_{sg}=1,23m/s. The amplitude does not show any repetitive cyclic pattern of magnitude. Figure 4.21 shows increased U_{sl} for increased U_{sg} values. Stable water production is present for all U_{sg} values tested for this frequency.

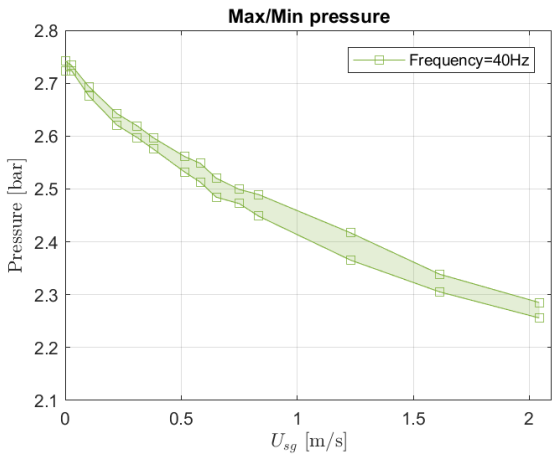

Figure 4.20: Max/Min pressure measured for pump frequency at 40Hz

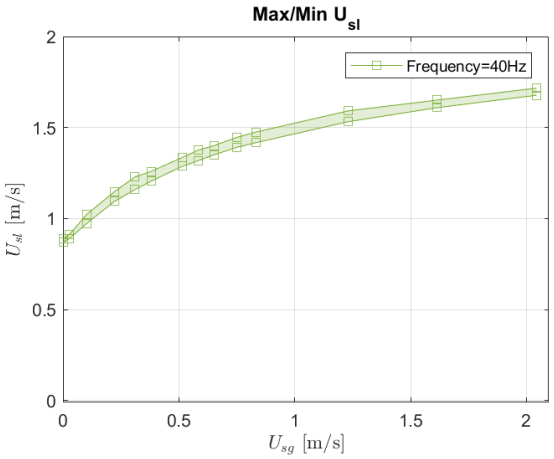

Figure 4.21: Max/Min U_{sl} measured for pump frequency at 40Hz

4.5 Experimental overview plots

Figures 4.12, 4.14, 4.16, 4.18 and 4.20 are combined in one plot (Figure 4.22). The plot shows the difference in amplitude range for the different frequencies with their respective U_{sg} values. Frequencies at 38Hz, 38,5Hz and 39Hz gives oscillating behaviour for the lower U_{sg} region. These three frequencies are close to the same oscillating pattern until a transition occurs to stable flow for a given U_{sg}. Pump frequency at 38Hz gives the largest area for oscillating behaviour. The following frequencies at 38,5Hz and 39Hz presents the second and third largest area for oscillating behaviour, respectively. Frequency values at 39,5Hz and 40Hz does not present the same magnitude in amplitude range, but follows the same pattern for the rest of the frequencies after the transition from oscillating behaviour to stable.

Figures 4.13, 4.15, 4.17, 4.19 and 4.21 are combined into one plot (Figure 4.23). It shows the same trend for oscillating behaviour as Figure 4.22, for the same values for U_{sg}.

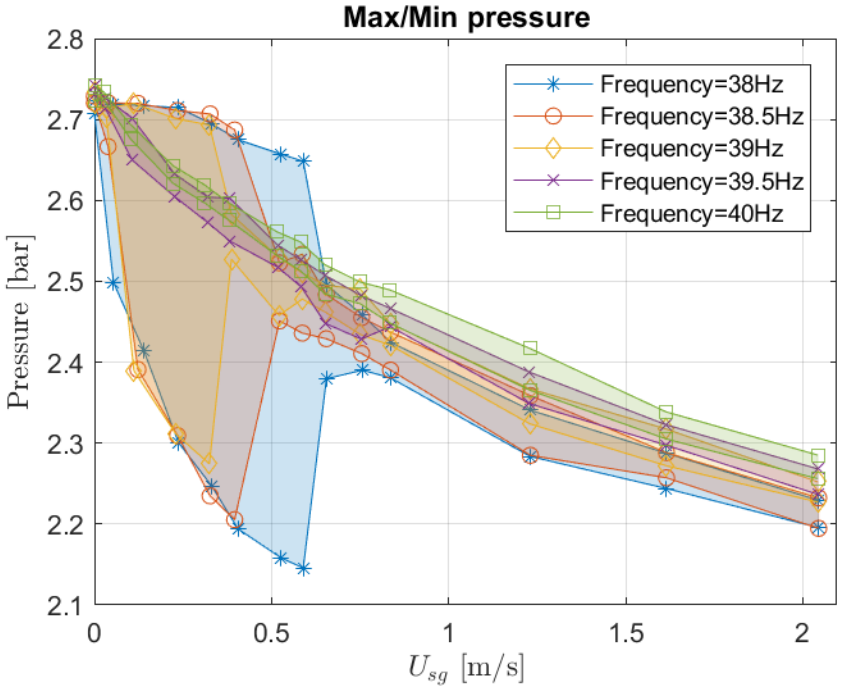

Figure 4.22: Max/Min pressure measured for all pump frequencies

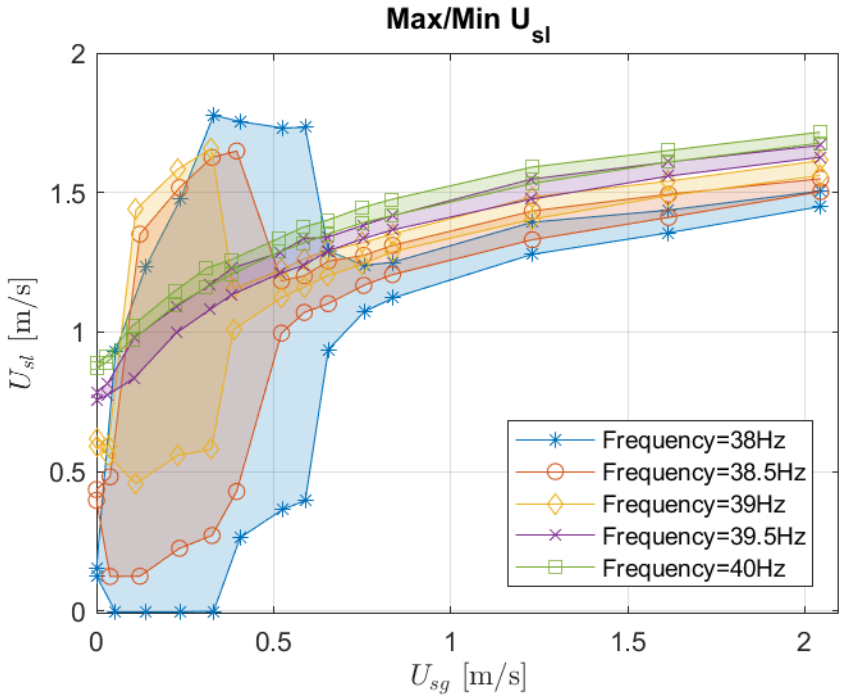

Figure 4.23: Max/Min U_{sl} measured for all pump frequencies

A definition for the transition from oscillating to stable behaviour is defined for Figure 4.24. To be classified as an oscillating behaviour, the values next to a peak in a $\dot{m}_l$ vs time plot needs to drop with a minimum value of $1kg/s$ on either side. This value is $0{,}35m/s$ when calculated to U_{sl} with Equation 2.4. The amplitude is categorized as stable if this criteria is not fulfilled. Figure 4.24 shows a plot for $U_{sl,mean}$ vs U_{sg}, where the above-mentioned definition for oscillating and stable behaviour is applied. The lowest frequency gives the lowest $U_{sl,mean}$ for its respective U_{sg} and highest frequency gives the highest $U_{sl,mean}$ for its respective U_{sg}. The curves follows its respective frequency from high to low in that order.

Frequency at 38Hz gives oscillating behaviour for U_{sg} values between 0,05-0,59m/s, which corresponds to 7 logging sessions. For 38,5Hz, oscillating behaviour are present for U_{sg} values between 0,12-0,40m/s, represented in 4 logging sessions. For this frequency, the $U_{sl,mean}$ decreases when U_{sg} is increased to $0{,}04m/s$. For 39Hz there is 3 oscillating logging sessions presented in this plot. U_{sg} values giving oscillating behaviour are between 0,11-0,32m/s. Also for this frequency, the $U_{sl,mean}$ decreases when U_{sg} is increased from $0m/s$ to $0{,}03m/s$.

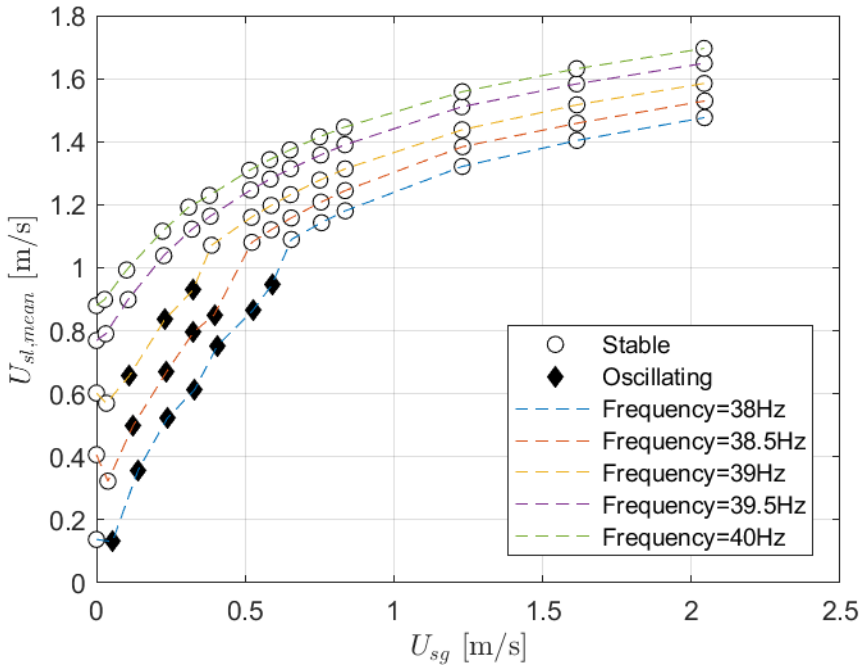

Figure 4.24: Stability map for all frequencies, $U_{sl,mean}$ vs U_{sg}

Figure 4.25 shows the period T vs U_{sg} for the frequencies tested in this case. T is here defined to be the duration in seconds for one oscillating cycle.

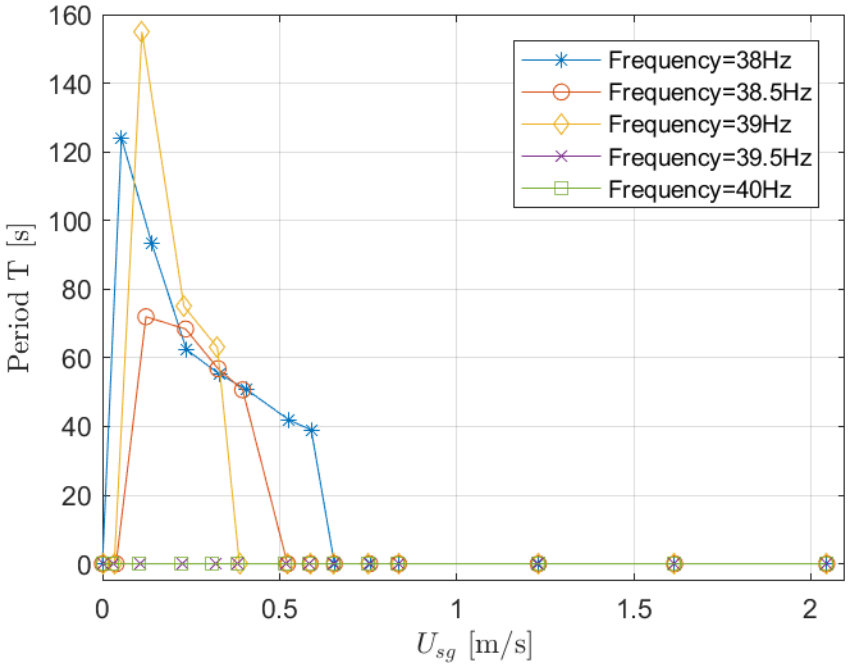

Figure 4.25: Period vs U_{sg} for all frequencies

This plot is calculated with the above-mentioned criteria for the definition for oscillating behaviour. If this criteria is not fulfilled, the period is set to zero in the calculations. This is done to filter out noise and therefore only use well defined peaks in the calculations. For the region where oscillating behaviour is present, frequency at 39Hz gives the largest T=155s, while frequency 38,5Hz gives T=72s for approximately the same U_{sg}=0,12m/s. The lowest period presented in the plot is frequency at 38Hz, with T=39s, when U_{sg}=0,59m/s. When the U_{sg} are equal or above this value, all the other frequencies shows T=0s, which is analog to stable flow behaviour.

4.6 Effect of varying pump frequency

The effect of varying the frequency can be seen in Figure 4.24, where the $U_{sl,mean}$ increases for higher frequency. When the $U_{sl,mean}$ is at a certain value, the oscillating behaviour stops. The effect where the oscillating behaviour are present, are a decreasing range of U_{sg} values, for increased pump frequency. This establishes the fact that the inlet flow pressure is a key value for EDI. In this experiment the inlet flow pressure is directly related to the frequency given by the centrifugal pump, meaning that the frequency itself plays a significant role for the stability in the system.

4.7 Effect of upstream flowline jumper

Figure 4.26 shows the max/min U_{sl} measured from the water flow meter (Table 3.6) without a jumper present, originated from the additional pump-characteristics experiment discussed in section 3.2.1 *Centrifugal pump*. No oscillating behaviour is present for the tested frequencies, in contradiction to Figure 4.23 where oscillating behaviour is present. A jumper plays therefore a significant role, since this geometry allows air to get trapped before it enters the riser base. As seen in Figure 4.26, no oscillating behaviour is present. For this case, the air does not accumulate in the horizontal test-section, but instead enters the riser continuously, giving a stable flow regime.

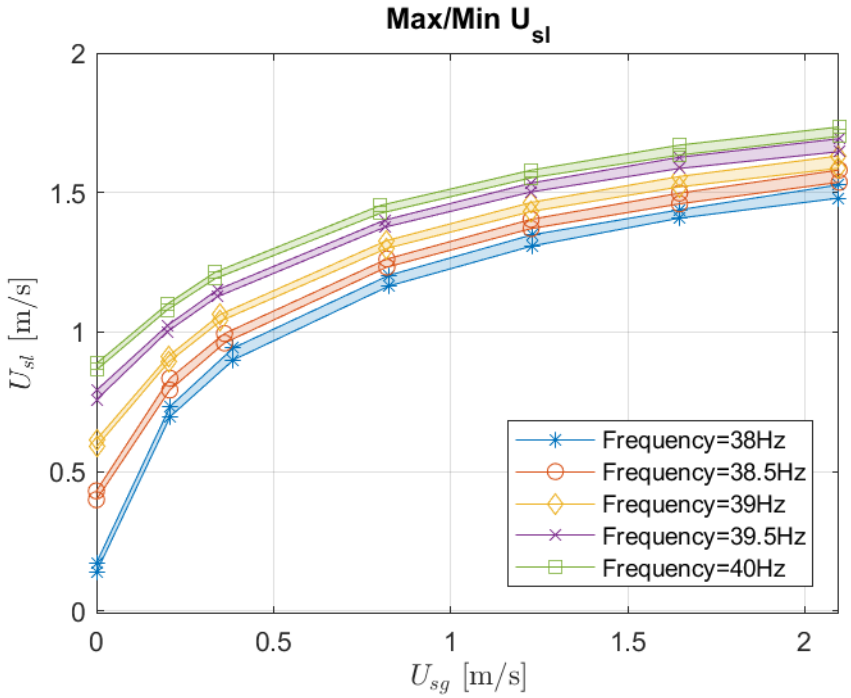

Figure 4.26: Max/Min U_{sl} without jumper

4.8 Air injection

Figure 4.27 shows the air flow rate measured by the Coriolis flow meter for air (Table 3.6). The measured air flow rate is for a case where the pump frequency is at 38Hz. The mean absolute percentage error MAPE is calculated from equation (Tayman and Swanson, 1999)

$$MAPE = \frac{100\%}{n} \sum_{n}^{t=1} \left| \frac{A_t - F_t}{A_t} \right| \tag{4.1}$$

where the A_t represents the average flow rate and F_t the measured flow rate. The MAPE is calculated to 0,72%, which might be attributed to electrical noise or the accuracy to the flow meter. The air flow rate is anyhow ascertained to be constant due to the low error percentage.

For all of the experimental cases the air flow rate is kept constant within each logging session. To avoid variations in the injected air flow rate when the system experiencing oscillating behaviour, the air is kept at 5bar before entering the mixing. This assured a constant and continuously air flow rate at the mixing point.

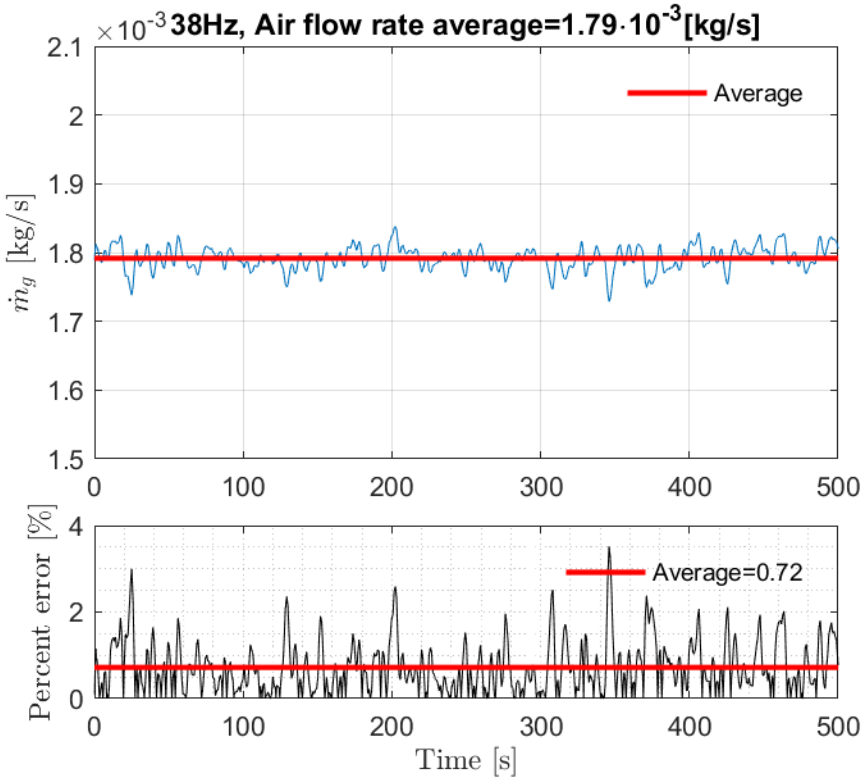

Figure 4.27: Air flow rate vs time with the corresponding percentage error vs time

The air is injected upstream the jumper, and for low air injection rates the air is slowly trapped in the jumper. The air is accumulated at the top, and thereafter filling the downstream part of the jumper. This results in a unevenly distributed liquid column in the jumper, increasing the pressure upstream. The air bubble nose is eventually at the end of the jumper, and thereafter floats all the way to the riser base, and then expands as it continues upwards. As more bubbles enter the riser, this results in a decreased mixture density. Large accumulated air bubbles are now released from the jumper, followed by liquid flushing out the remaining air in the jumper. The water flow rate increases to a certain point before it rapidly decreases/stops. A trend for the period T is decreasing period for the oscillations, for increasing air flow rates injected. Depending on the frequency, higher values for air flow, increases the stability along the U_{sg} axis in Figure 4.25.

4.9 Riser-base pressure

Oscillation in pressure is recorded through a absolute pressure transducer, located at the riser base. The logged pressure can be seen in Appx. Figure A.1-A.80. The pressure gradient is observed to depend largely on the frequency and air injection rate.

When no air is injected, the riser base pressure is close to the hydrostatic pressure (2,70bar) calculated from Equation 2.6. The maximum pressure when air is injected is also close to the hydrostatic pressure when EDI phenomena is present. When the riser base pressure approaches the hydrostatic pressure, liquid is blocking the continuous inflow of air into the riser base. Air is now building up in the jumper, and subsequent penetration of air into the riser base decreases the mixture density. The pressure drops rapidly along with an increased inflow of air. This causes an increased inflow of water, flushing out the remaining air in the jumper, which again restart the oscillating cycle.

4.10 Summary of experimental results

Five different pump frequencies are tested in the new experimental rig, along with a span of injected air flow rates. All of the tested pump frequencies gives a self circulating system. In other words, no injection of artificial air is needed to have liquid production. Figure 4.24 shows that EDI phenomena is present for frequencies at 38/38,5/39Hz. Instability is observed for low air injection rates for the above-mentioned frequencies. The largest area for oscillating behaviour is found at 38Hz, with a decreasing trend for higher frequencies.

Sufficiently high U_{sg} stops the oscillating behaviour. Small bubbles are constantly torn of the air stream, mixing in with the water. The water transports the small bubbles into the riser, keeping the liquid mixture density and hydrostatic pressure lower. This leads to an increased inflow of water and a stable flow in the riser.

Frequencies 39,5-40Hz does not show any oscillating behaviour. The observed phenomena in the jumper is a creation of small bubbles, which continuously enters the riser base. The *escape* of air in the jumper, in form of tiny bubbles, gives insufficient accumulation of air. This results in a continuous inflow of air to the riser base, and therefore a stable flow regime is established.

Chapter 5

Simulation

5.1 OLGA

OLGA is a one-dimension multiphase dynamic flow software. OLGA uses the Eularian formulation to solve two-fluid model on a fixed grid. This program can only handle geometries consisting of straight pipes, therefore some simplifications have been made to the simulation compared to the experimental case. The geometry is already presented in section 3.1.1 *Geometry*. An OLGA input file for a simulation where pump frequency is at 38Hz and injected air mass flow is at $0{,}18{\cdot}10^{-3} kg/s$ is given in Appx.C.

OLGA contains a steady state pre-processor. The routine is to calculate holdup, flow regime, pressure and mass flow along the pipeline. These computed values are stored at the first time step printed to the output file when used as initial conditions for transient simulations (Kjeldby, 2010). Simulation with and without slug tracking have been started using the initial conditions offered from the pre-processor. The pre-processor is used without the energy equation, i.e the simulation is at a constant temperature of 20°C. Results when the slug tracking option in OLGA is enabled is not further processed for all the cases due to inadequate match compared to experimental results. One case is anyhow simulated with slug tracking, for the purpose of the creation of Figure 5.14.

Fluid properties used in the simulation are given in a PVT-table, generated in the software PVTsim. The PVT file is based on pure water representing the liquid phase and air composed of 21% oxygen and 79% nitrogen representing the gas phase.

A centrifugal pump have been added to the simulation. The pump curve from the pump supplier can be seen in Appx.F for model *Perfecta C 100-35*. This curve is implemented in OLGA and tested for a model including the entire facility, where the centrifugal pump is located in the basement. Anyhow, due to poor match to the experimental results, new curves are developed experimentally. New curves have been developed using the absolute pressure transducer located at the inlet of the test-section (ID 7 Table 3.1). The sensor experiences

only single phase water and the centrifugal pump is now implemented at this location (ID F in Figure 5.1) in the simulation. The implemented curves in OLGA can be seen in Figure 3.4.

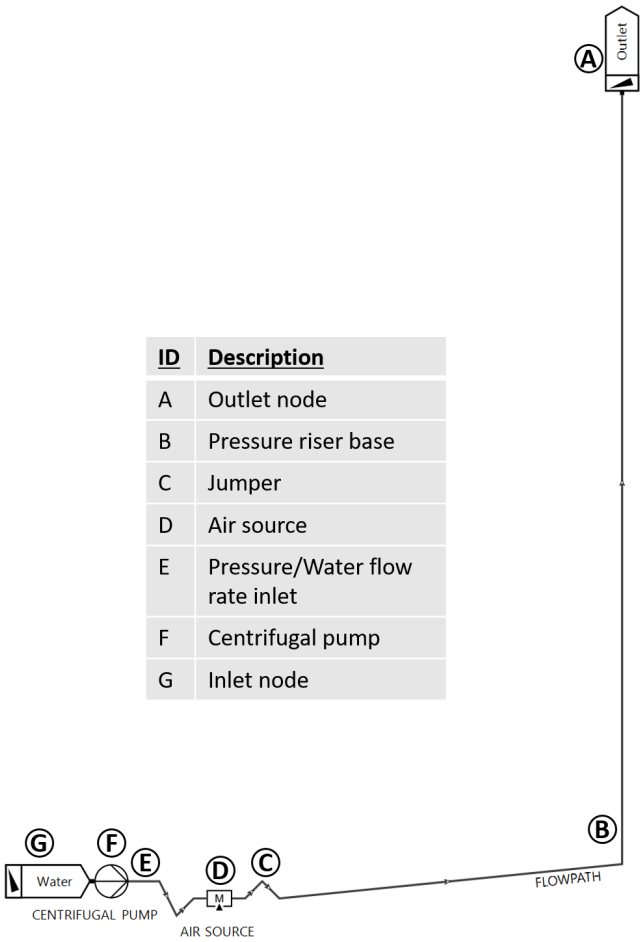

ID	Description
A	Outlet node
B	Pressure riser base
C	Jumper
D	Air source
E	Pressure/Water flow rate inlet
F	Centrifugal pump
G	Inlet node

Figure 5.1: OLGA simulation setup in GUI

Outlet and inlet nodes (ID A & G)have been assigned atmospheric pressure. Lift gas (ID D) is injected at constant flow rate after 200 seconds, giving the centrifugal pump time to stabilize.

The same range of air flow rates in the experiment are tested in the simulations. The simulations are run for 1800 seconds, where only the last 500 seconds are further processed.

5.1.1 Sensitivity

To be able to check the sensitivity for the OLGA model, parametric studies are performed. The different cases are presented in Table 5.1, where MINDT is the smallest time-step allowed in the simulation. Max cell length is the maximum cell length allowed for a pipe length, where increasing this variable gives a coarser grid.

Table 5.1: Sensitivity test for OLGA model

Case	MINDT [s]	Max cell length [m]
1	$1{\cdot}10^{-4}$	0,1
2	$1{\cdot}10^{-4}$	0,4
3	$1{\cdot}10^{-4}$	1
4	$1{\cdot}10^{-6}$	0,4
5	$1{\cdot}10^{-9}$	0,4

Figure 5.2 shows the max/min pressure and Figure 5.3 shows the max/min U_{sl} for the OLGA cases. Pressure is measured at the riser base (ID B) and liquid flow rate at the inlet (ID E). The model have some sensitivity for chosen cell length, referring to case 1-3. Case 3 gives a good match for the minimum pressure in the experiment, but exceeds the maximum U_{sl}. Case 2 and 4-5 shows no significant difference. Lower values than $1{\cdot}10^{-4}$ for MINDT are also tested, but not successfully, due to simulation crash. Case 2 is hence chosen to further processing due to satisfactory results, compared to the tested cases.

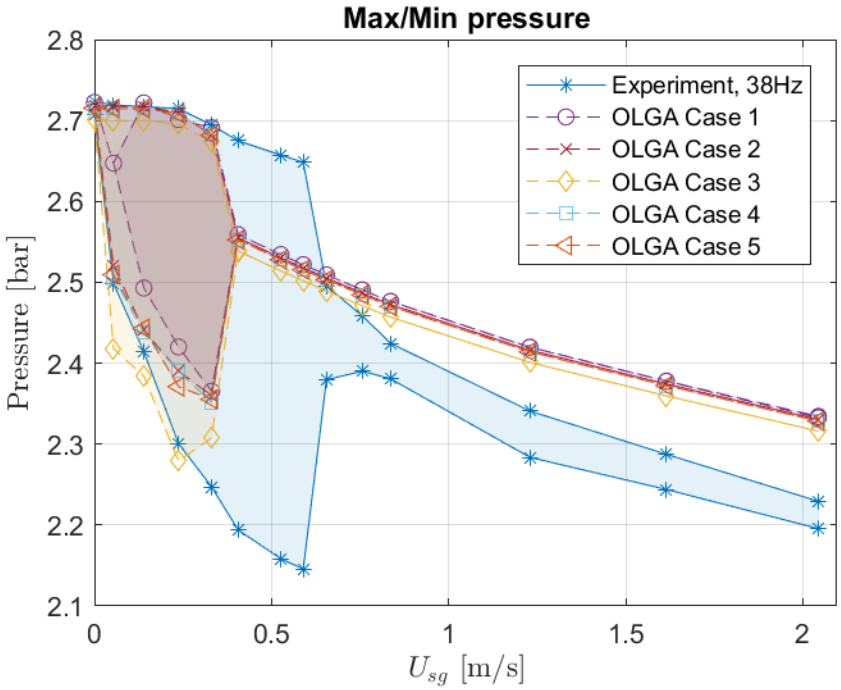

Figure 5.2: Max/Min pressure sensitive test

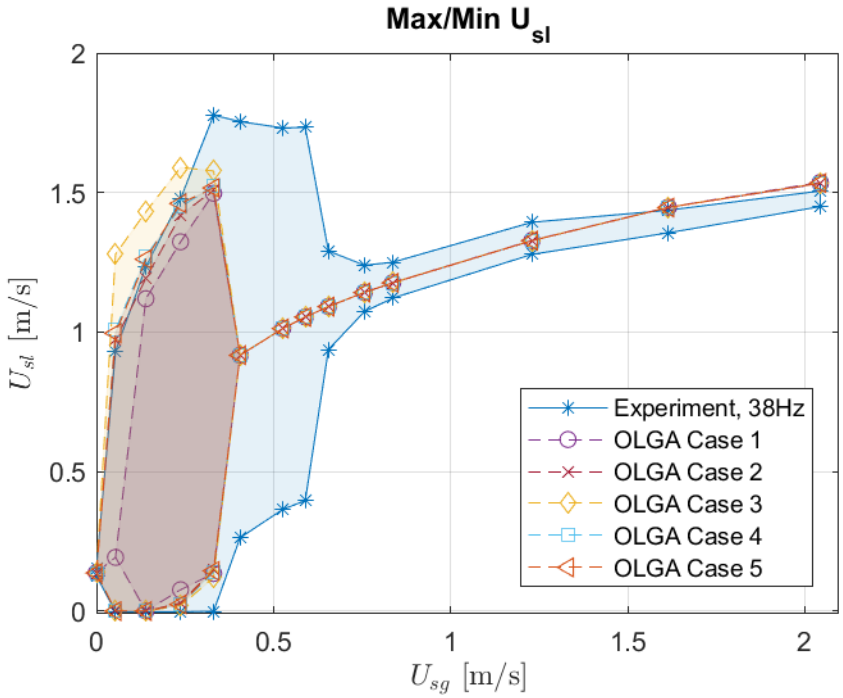

Figure 5.3: Max/Min U_{sl} sensitive test

5.1.2 Simulation result

A comparison for the experimental case vs the OLGA simulated are presented in Figure 5.4-5.13. The corresponding percentage error is calculated and presented under the max/min plots. Equation 4.1 for MAPE is used, where A_t is the average over the experimental max and min values for the respective U_{sg}. F_t is calculated in the same way, representing the simulated values. MAPE is sensitive for small denominators relative to the numerator, and small deviations in error could give unrealistically large changes in absolute percentage error when close to zero. These values are therefore excluded when calculating the absolute percentage error. The reader should also note that the calculated percentage error does not include error the instability area, due to average simplification in the calculation.

Figure 5.4 and 5.5 shows the experimental case with pump frequency at 38Hz. OLGA simulation is displaying oscillating behaviour for low U_{sg}. This behaviour ends at U_{sg}=0,33kg/s and a stable flow regime is present for higher injected air flow rates. The instability area for the simulated case is approximately the half of the experimental case. For the stable flow regime the simulated pressure exceeds the experimental values, but matches the U_{sl} very well with maximum 5% error.

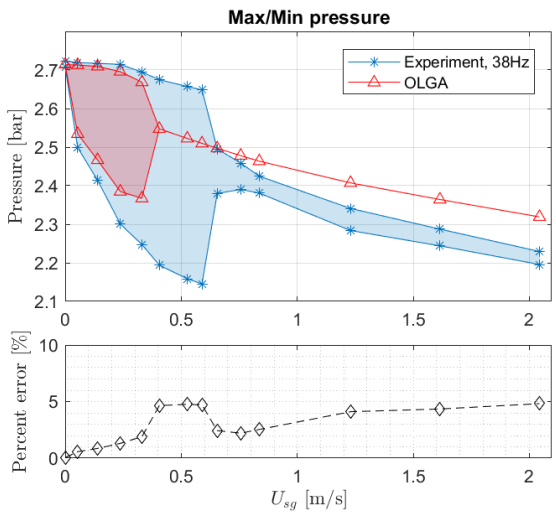

Figure 5.4: Max/Min pressure from experiment at 38Hz vs OLGA

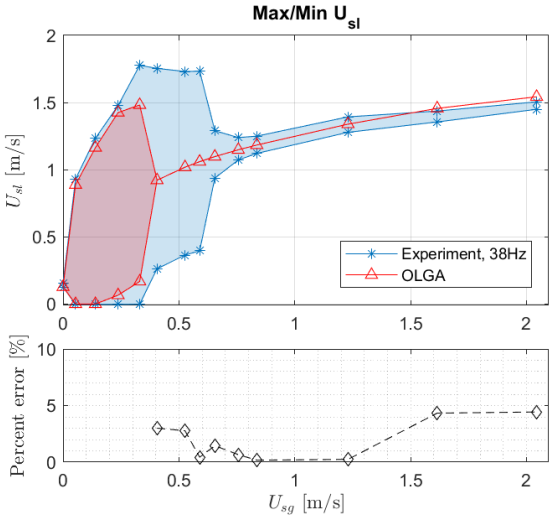

Figure 5.5: Max/Min U_{sl} from experiment at 38Hz vs OLGA

Figure 5.6 and 5.7 gives oscillating behaviour for the lowest air flow rate given to OLGA. The model gives oscillating behaviour for the lowest air rate injected and therefore fails to reproduce the entire instability area, as observed in the experiment. Both pressure and U_{sl} exceeds the experimental values. However, this is a good match with maximum 8% error for pressure and maximum 12% error for U_{sl}.

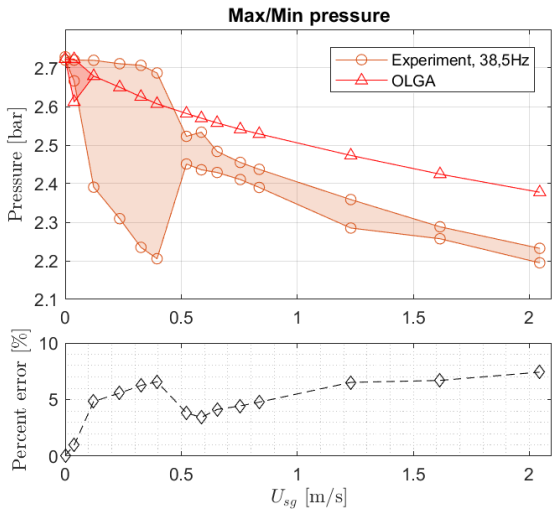

Figure 5.6: Max/Min pressure from experiment at 38,5Hz vs OLGA

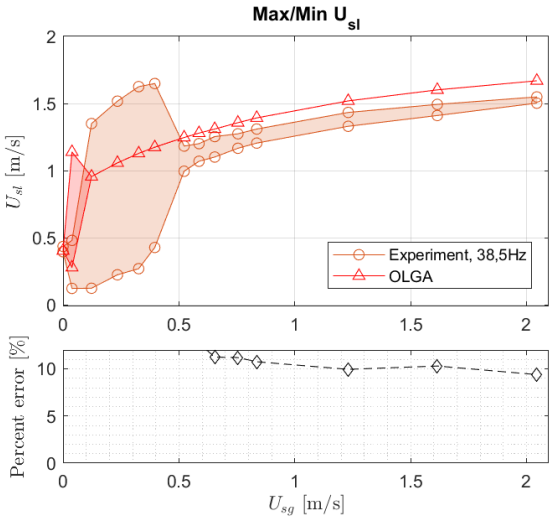

Figure 5.7: Max/Min U_{sl} from experiment at 38,5Hz vs OLGA

In Figure 5.8 and 5.9, no oscillations are observed for the OLGA simulation, in contrast to the experimental case where oscillating behaviour is present for low injected air flow rates. Pressure exceeds the experimental case for higher injected air flow rates, while the U_{sl} matches the experiment for higher air flow rates. Both pressure and U_{sl} have maximum 7% error.

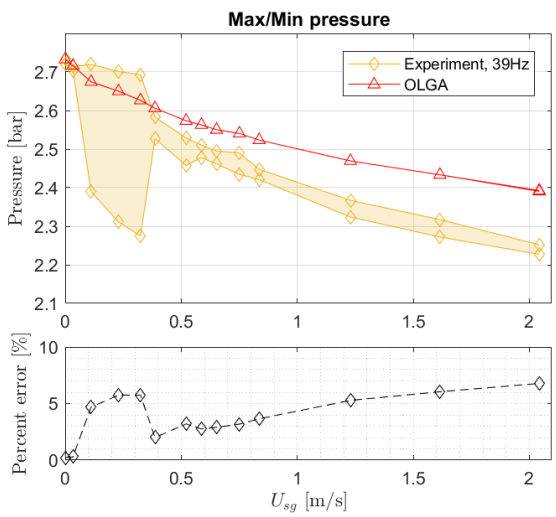

Figure 5.8: Max/Min pressure from experiment at 39Hz vs OLGA

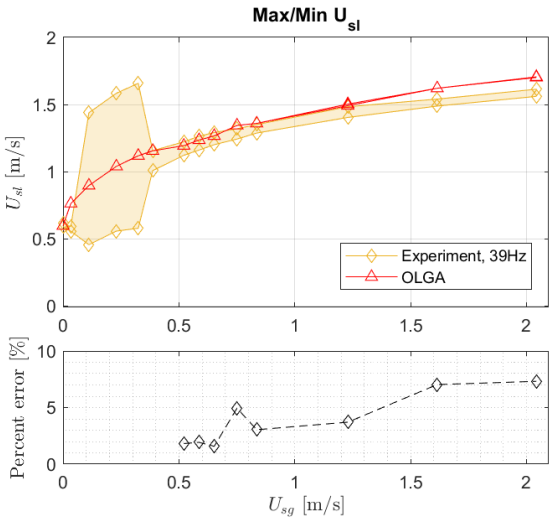

Figure 5.9: Max/Min U_{sl} from experiment at 39Hz vs OLGA

In Figure 5.10-5.13, oscillating behaviour is observed in neither of OLGA model cases, which is the same trend observed in the experiments. The U_{sl} from OLGA matches the experimental case very well with 2% and 1% error for 39,5Hz and 40Hz respectively. The simulated pressure exceeds the measured experimental pressure with maximum 6% error for both 39,5Hz and 40Hz.

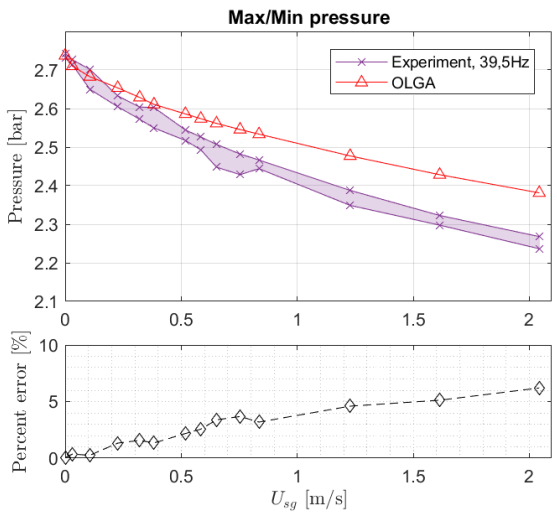

Figure 5.10: Max/Min pressure from experiment at 39,5Hz vs OLGA

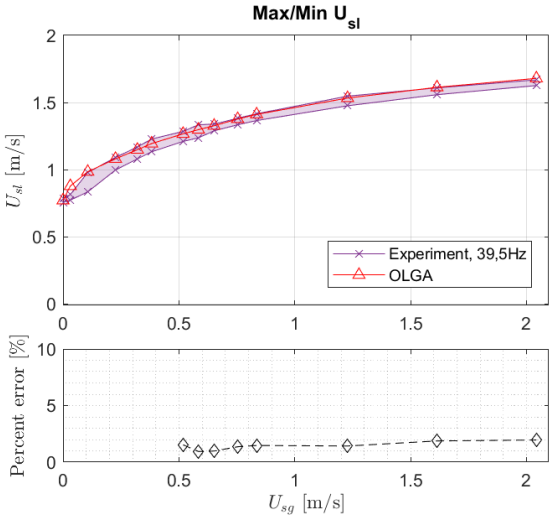

Figure 5.11: Max/Min U_{sl} from experiment at 39,5Hz vs OLGA

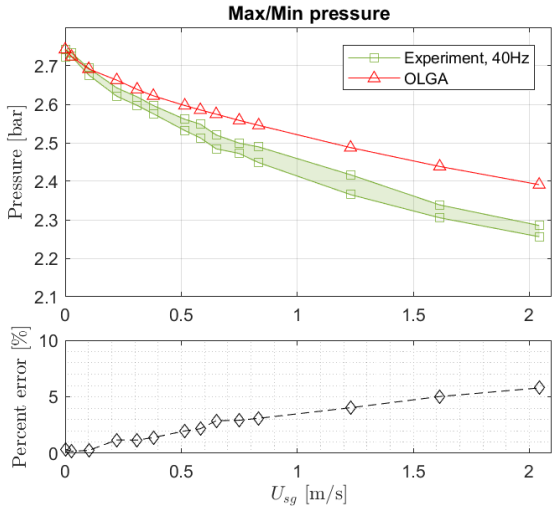

Figure 5.12: Max/Min pressure from experiment at 40Hz vs OLGA

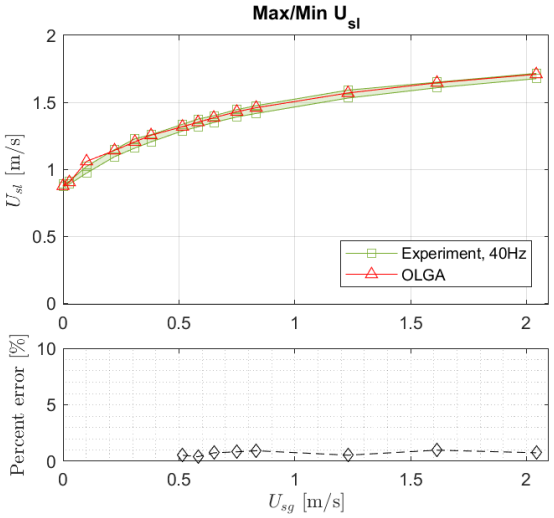

Figure 5.13: Max/Min U_{sl} from experiment at 40Hz vs OLGA

5.1.3 Summary of OLGA results

The numerical simulations in OLGA matches the experimental values very well, if not considering the deviation in stability limits. The maximum percentage error is calculated to 12%, which is quite good.

The oscillating behaviour in the simulated case, either disappears earlier than the experimental, or is not present at all. A reason for this deviation could be the geometrical simplifications in the numerical model. The largest deviation in the geometry is the simplification of the u-turns located at the riser base (Appx.G.3.3). This simplification is necessary since 3-dimensional pipe geometry is not an option in OLGA. Another simplification is the use of straight pipes, when in reality the horizontal section is a flexible hose/pipe, i.e the pipe expands and moves on the cable-ladder. The centrifugal pump used in the experiment is located in the basement (Appx.G.6), while the pump in the simulation is located at the test-section inlet. The change of pump location is due to the location of the pressure sensor (ID 7 Table 3.1) used to plot the new pump-characteristics (Figure 3.4). This fictional change of location could give a discrepancy, due to larger inertia effects present in the experimental setup.

5.2 Instability cycle

Screen-shots from the visualization tool PLOTIT are presented in Figure 5.14. This is OLGA results for the simulated case for 38Hz and air flow rate $0{,}48{\cdot}10^{-3} kg/s$. This case is modelled with slug tracking enabled, with the slug initiation option LEVEL. LEVEL enables initiation of slugs when the change in liquid holdup between two cells are detected. PLOTIT accepts .ppl files from OLGA only if the PROFILEDATA contains the following variables: *Holdup(HOL), Flow-regime(ID), Pipeline diameter(IDIAM),Pressure(PT),* U_g*(UG)* and U_l*(UL)*, in this specific order. The NTNU-inhouse PLOTIT software enables a good visualization of the holdup for the entire test-section, and provide a visual impression of the flow dynamics present for the consecutive time steps.

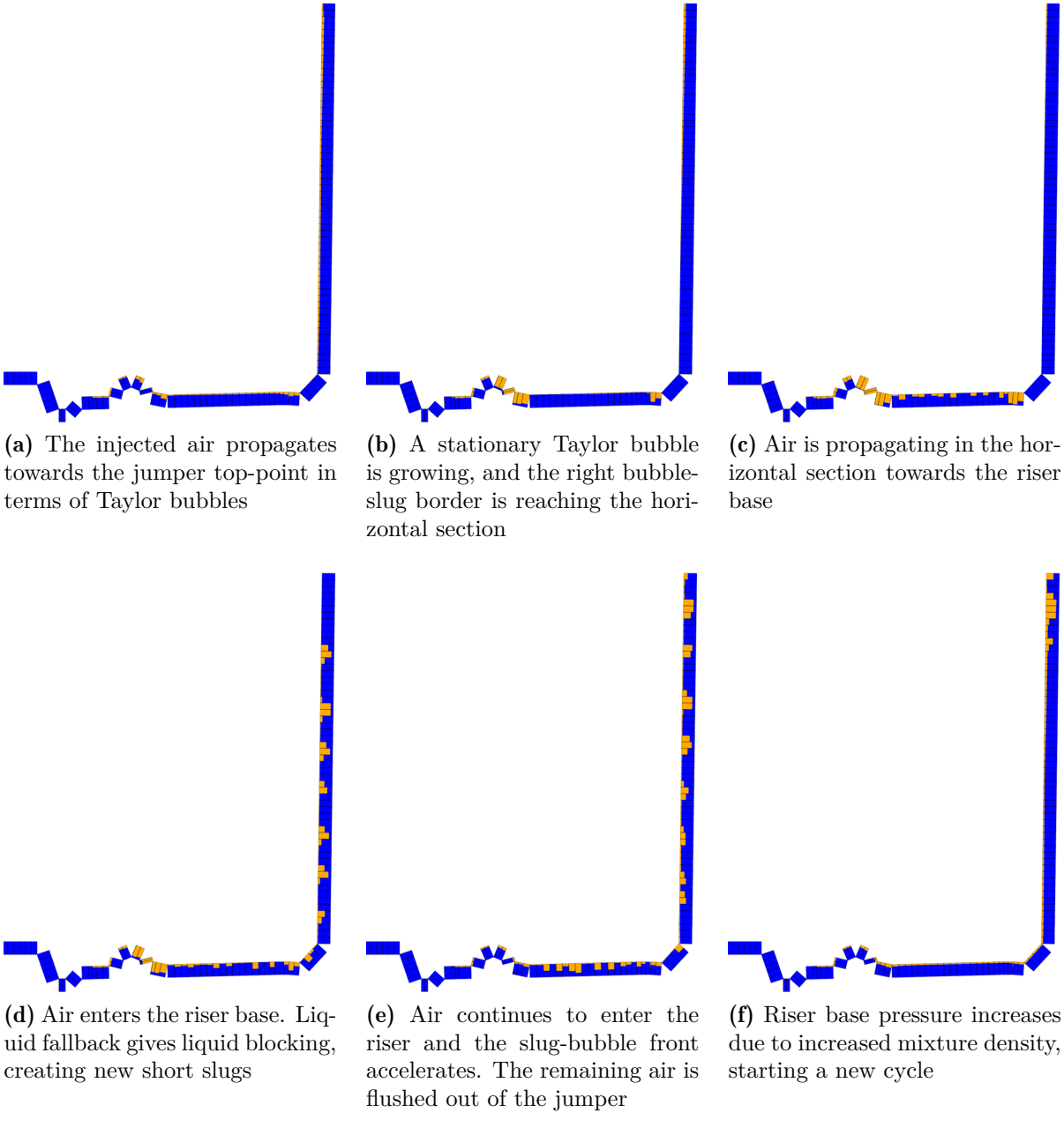

(a) The injected air propagates towards the jumper top-point in terms of Taylor bubbles

(b) A stationary Taylor bubble is growing, and the right bubble-slug border is reaching the horizontal section

(c) Air is propagating in the horizontal section towards the riser base

(d) Air enters the riser base. Liquid fallback gives liquid blocking, creating new short slugs

(e) Air continues to enter the riser and the slug-bubble front accelerates. The remaining air is flushed out of the jumper

(f) Riser base pressure increases due to increased mixture density, starting a new cycle

Figure 5.14: Different stages in one oscillating cycle from PLOTIT, using OLGA results for 38Hz and air flow rate $0{,}48{\cdot}10^{-3} kg/s$. Diameter to length ratio is exaggerated by a factor of 10

5.3 Sluggit

A 1D two-fluid model based on the concept of combined slug tracking and slug-capturing technique is used to simulate two experimental cases (Figure 5.16 & 5.18) reported in Chapter 4 *Experimental Results*. Control volumes are represented by objects bubble and slug sections. Similarly, borders/cell-faces between objects are represented by different types of border objects. Mass, momentum and pressure equations are integrated over the gas and liquid control volumes. The bubble section is converted to a slug section object, when the liquid holdup in a bubble section approaches a user defined limit (= 0.98 in the current study). Similarly, slug to bubble section conversion is applied, when the void fraction in slug reaches a maximum value, or when the slug becomes too short. Complete details of the model can be found in the work by Smith (2017).

The relation between the water mass flow rate and the pressure is obtained from the characteristic pump curves shown in Figure 3.4 for 38Hz frequency, and the equations are shown below,

$$\dot{m}_{pump} = -19,43 \cdot p^2 + 87,1 \cdot p - 92,53 \tag{5.1}$$

$$\dot{m}^{n+1}_{water} = \theta \cdot \dot{m}^{n}_{water} + (1-\theta) \cdot \dot{m}_{pump} \tag{5.2}$$

where θ represents the under relaxation parameter ($0 < \theta < 1$) and p is pressure at inlet section. At each time step, dynamic water mass flow rate was calculated from Equation 5.2 and applied at inlet section.

Simulation results for air mass rate at $1{,}13{\cdot}10^{-3} kg/s$ and $5{,}50{\cdot}10^{-3} kg/s$ for 38Hz pump frequency are presented in Figure 5.15 and 5.17, respectively. A moving average with span 2 seconds is applied on the Sluggit simulation results. In Figure 5.15, strong fluctuations in pressure and water flow rate is observed from simulations, which shows that the simulations failed to capture the periodic oscillations/instabilities observed in experiments as shown in Figure 5.16. The discrepancies in capturing instabilities observed at low flow rates of gas injection can be related to the limitations of the implementation of pump characteristics in the flow model. In the experiment, pump does not respond instantaneously to the change in pressure response and the implementation of pump response time is very critical to predict the instabilities using the flow model. In addition, extrapolation of the pump characteristic curves in range of pressure values, which are outside the limits shown in Figure 3.4, is also another problem for the model. Similar limitations related to geometry as mentioned in section 5.1.3 *Summary of OLGA results*, also need to be accounted in the flow model for improving model predictions.

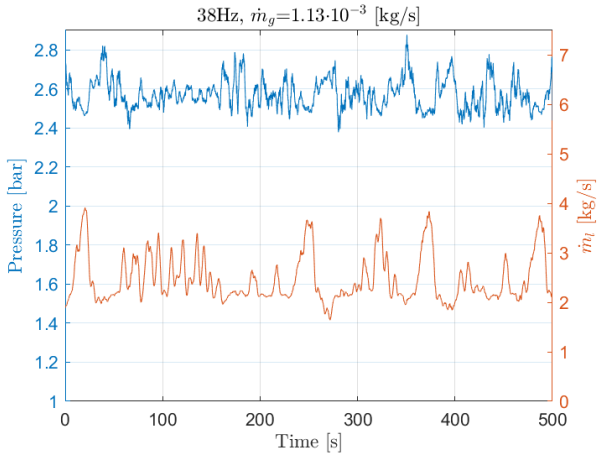

Figure 5.15: Sluggit simulation for 38Hz and air flow rate $1{,}13{\cdot}10^{-3}kg/s$

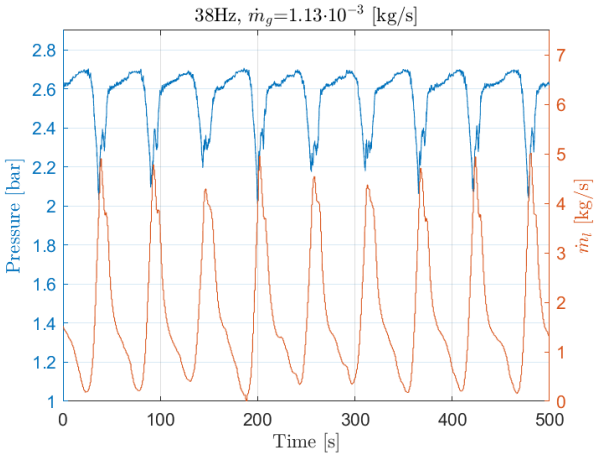

Figure 5.16: Experimental case for 38Hz and air flow rate $1{,}13{\cdot}10^{-3}kg/s$

For the experimental case 38Hz and air flow rate at $5{,}50{\cdot}10^{-3}kg/s$ (Figure 5.18), the pump operates in a stable region and results in almost a constant water mass flow rate and pressure. Simulations are performed with constant water mass flow rate at inlet section instead of using the pump characteristic from Equation 5.2. Figure 5.17 shows the pressure and water flow rate values from the simulation results. Pressure values obtained from simulation are in good agreement with the experiments.

Overall, the internal model failed to predict the instabilities observed at low air flow rate and the model requires improvements for implementation of pump characteristics.

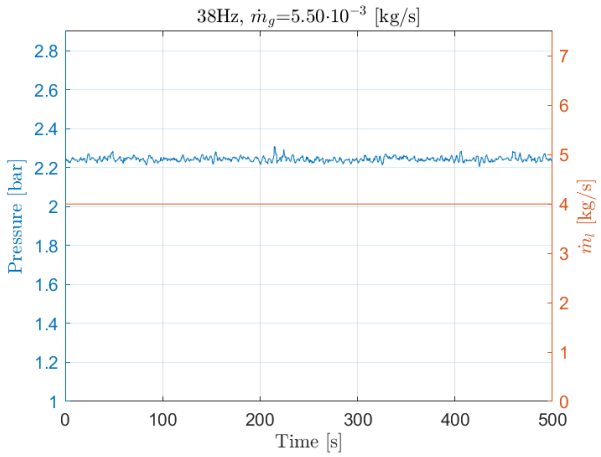

Figure 5.17: Sluggit simulation for 38Hz and air flow rate $5{,}50{\cdot}10^{-3}kg/s$

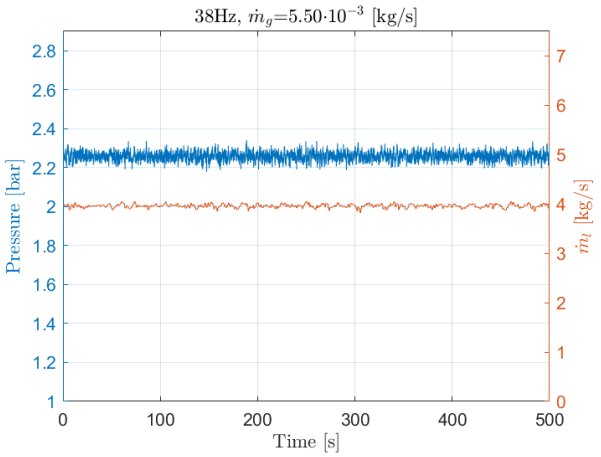

Figure 5.18: Experimental case for 38Hz and air flow rate $5{,}50{\cdot}10^{-3}kg/s$

Chapter 6

Flow regime transition

An extension of the main experiment is conducted for the frequencies 38Hz and 40Hz. The additional air flow rates are presented in Table 6.1. The purpose of this extension are mainly to document the transition from slug flow to annular flow regime. Previous studies (Kassab et al., 2009) have demonstrated experimentally an air-lift pump system and documented its performance, in addition demonstration of the flow regimes, for varying air flow rates. The trend is highest flow rates for water, in the slug-churn flow regime (Figure 6.1).

The referred experimental setup can be comparable to our setup. Instead of using a centrifugal pump, they are using a vertical movable water supply tank, which results in a constant water head. Changing the height also changes the submergence ratio. The submergence ratio is defined as

$$S_r = \frac{H_s}{L} \tag{6.1}$$

where L is the pipe/riser length and H_s is the static depth of water above the riser base.

The air is also injected at the riser base, instead of upstream a jumper geometry, which is done in our case.

Table 6.1: Extended test matrix for pump frequencies 38Hz and 40Hz

Frequency [Hz]	38	40
Air $i{\cdot}10^{-3}$ [kg/s]		
Air 15	11,21	11,41
Air 16	14,10	14,09
Air 17	16,68	16,67
Air 18	19,51	19,49
Air 19	22,48	22,37

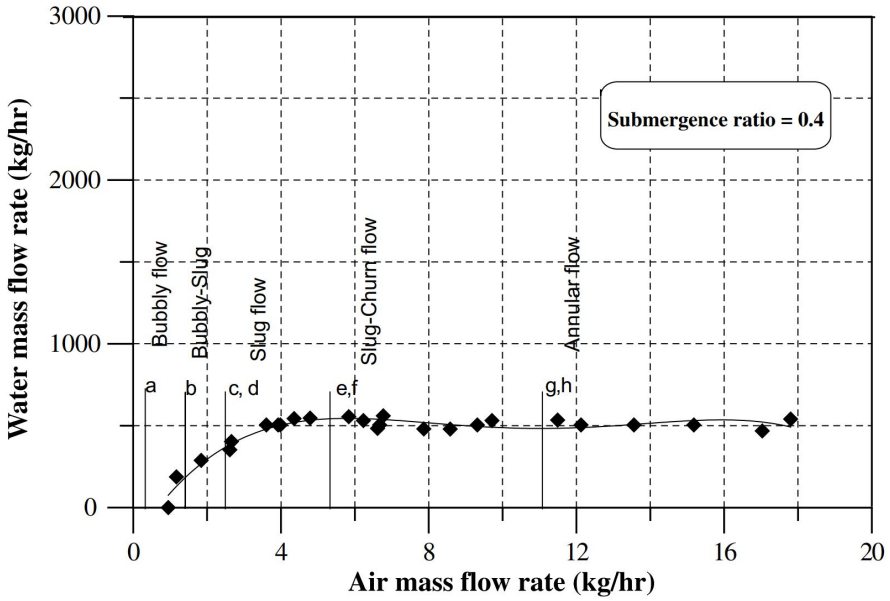

Figure 6.1: Variation of air flow rate with water flow rate at submergence ratio=0.4. Inner diameter is 0,0254m (Kassab et al., 2009)

Figure 6.2 and 6.3 shows the data-sets from the main experiment in addition to five extra air flow rates for both of the extended frequencies.

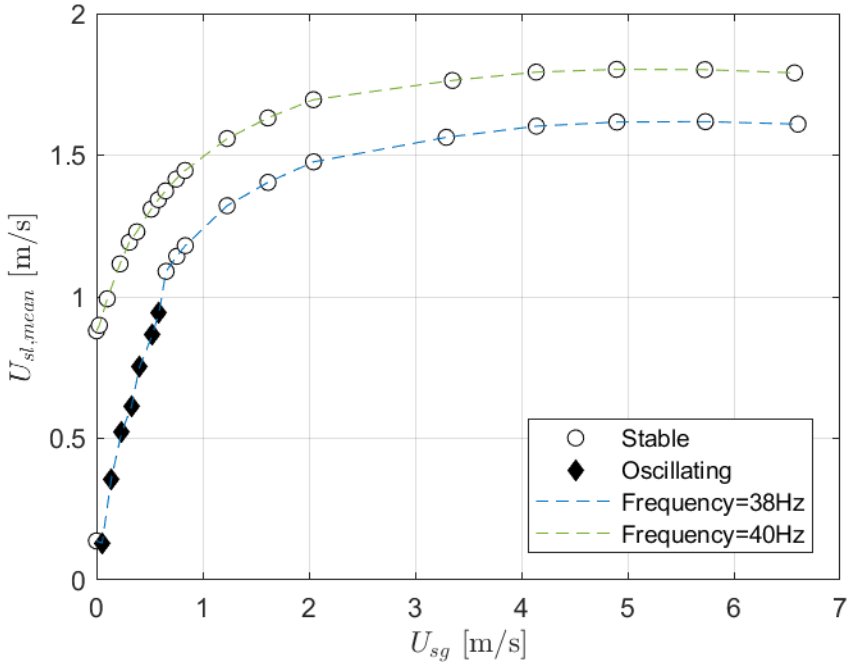

Figure 6.2: Extended stability map for pump frequencies 38Hz and 40Hz, $U_{sl,mean}$ vs U_{sg}

In Figure 6.2 the liquid production peaks when the U_{sg}=5,73m/s for 38Hz and U_{sg}=4,9m/s for 40Hz. The curve trend in Figure 6.2 follows the pattern documented by Kassab et al. (2009) presented in Figure 6.1. The trend in Figure 6.3 are decreasing pressure and slope for higher U_{sg} values for both frequencies.

The flow regimes observed in the main data-set are already discussed in section 4.2 *Visual observation*. In this extension the observed flow regime is slug flow for all of the tested air flow rates for both frequencies. Visual observation of the flow regime are also conducted close to the riser outlet. The slug flow observed here are interpreted to be closer to the slug-annular flow transition compared to the observation at the riser base. According to Equation 2.7, the slug/churn-annular flow transition is calculated to occur when U_{sg}=14,59m/s.

Experiments with higher flow rates could not be conducted due to limitation originated from the air flow meter's maximum flow rate at 0,022kg/s (Table 3.6). Hence the annular flow regime could not be captured.

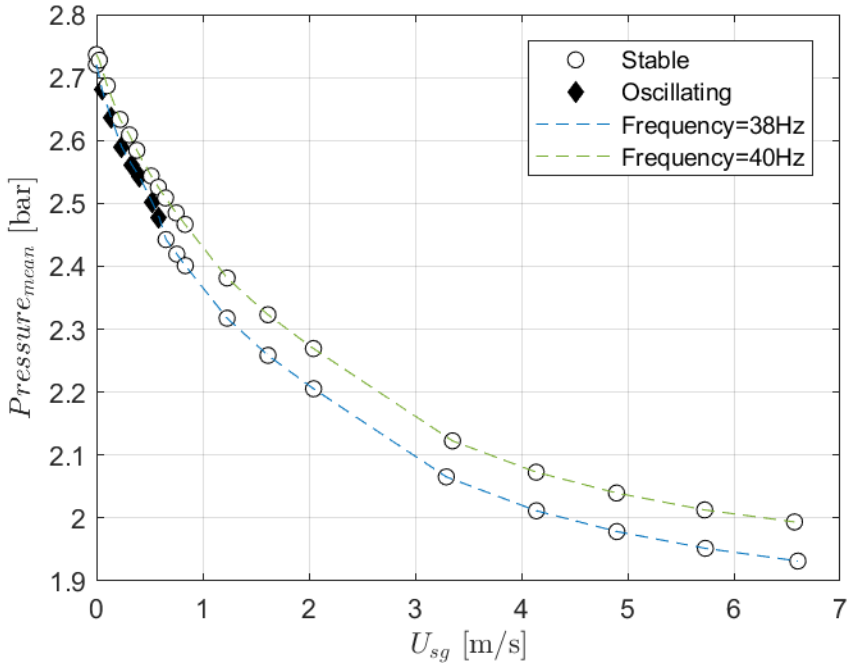

Figure 6.3: Extended stability map for pump frequencies 38Hz and 40Hz, $Pressure_{mean}$ vs U_{sg}

The flow regime present for the highest air flow rate at $22{,}48 \cdot 10^{-3} kg/s$ for 38Hz are captured by the camera installed at the riser base. Snapshots from the camera are presented in Figure 6.4 (a)-(i). Slug flow are present, and a high speed slug bubble is captured passing by. Snapshots with bright sections indicates low holdup, i.e mostly air. The slug bubble passing by is no longer a well defined Taylor bubble due to the high gas velocity. Figure 6.4 (j) shows the trend for pressure and water flow rate for this case. The pressure measured at the riser base is here much more fluctuating. This could be originated from the vibrations in the rig due to the high velocity slugs. Another source could be a decreasing pressure at the high-pressure air side at the mixing point due to high air velocities in the thin supply pipe.

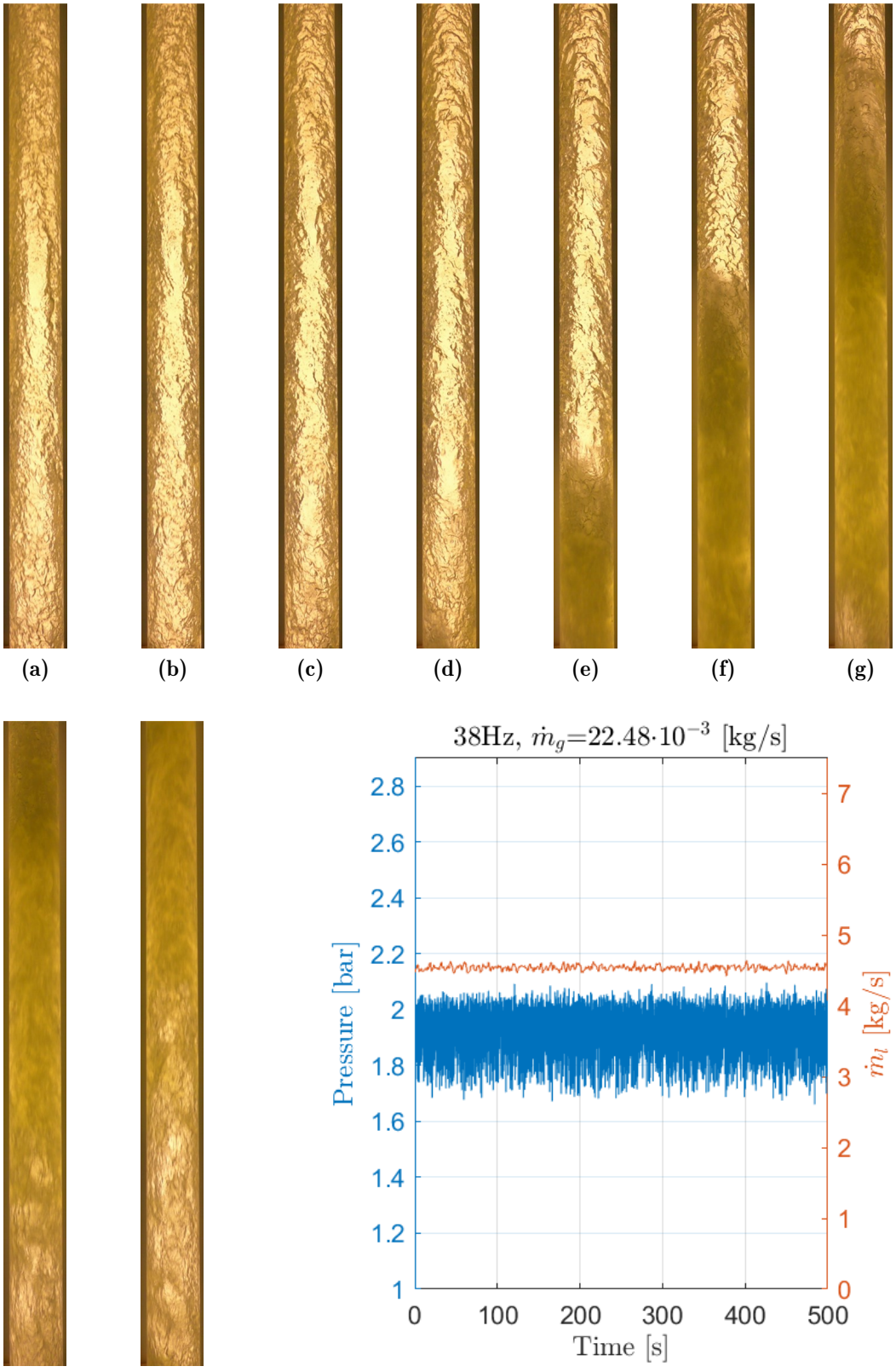

(j) Measured pressure and water flow rate

Figure 6.4: One slug bubble passing by (a-i) for pump frequency at 38Hz and injected air $\dot{m}_g$=22,48·10$^{-3}kg/s(U_{sg}$=6,60$m/s)$. Increments for the snapshots are 1/30 seconds

Chapter 7

Summary and recommendation for further work

A new vertical test-section is installed in the Multiphase Laboratory at NTNU. The purpose for the present study is to demonstrate and document Expansion Driven flow Instability phenomena in long vertical pipes, i.e in long risers or wells. Experiments are conducted for one geometry setup, where the centrifugal pump frequency is varied along with varying the injected air flow rate. EDI is observed for three different pump frequencies and the cyclic behaviour is observed to follow:

1. The injected air propagates towards the jumper top-point in terms of Taylor bubbles, located upstream the riser base
2. A stationary Taylor bubble is growing, and the bubble nose is eventually reaching the horizontal section
3. Air is propagating in the horizontal section towards the riser base
4. Air enters the riser base. Liquid fallback gives liquid blocking, creating new short slugs. Mixture density and hydrostatic head is decreasing along with increasing air volume in the liquid column
5. Air continues to enter the riser and the slug-bubble front accelerates. Air is expanding along the riser. The remaining air is flushed out of the jumper, accelerating the liquid inflow, due to the pressure sensitive pump
6. Riser base pressure increases due to increased mixture density due to high water inflow. The water inflow slows down. Liquid blocking in the horizontal section forces air to accumulate in the jumper, restarting the cycle once more

Five pump frequencies with span 38-40Hz, were studied combined with injected air flow rate with span 0-6,96·$10^{-3}kg/s$. EDI is observed at the three lowest pump frequencies in this study, while the two remaining shows a stable flow regime for all air flow rates. Slug flow regime is observed in the stable regions. For the lowest frequency at 38Hz, the largest span of instabilities are observed. This is the lowest frequency which is able to produce liquid to the surface without injecting artificial air, in this specific test-setup.

In addition to the experiments with a jumper, a stability test is conducted removing the jumper, resulting in no geometry obstacles where air can accumulate. The result is stable flow regime for all of the pump frequencies in combination with injected air flow rates. This result is also used to plot the centrifugal pump curves, later implemented in the multiphase dynamic flow software OLGA and Sluggit.

All of the main experimental cases (Table 4.1) are simulated using OLGA. Results from the simulated cases versus the experimental are compared. EDI is observed in the OLGA simulation, but discrepancies between the two sets of results are substantial regarding the stability limits. The two sets are on the other hand in good agreement if not considering the stability limits with a maximum error of 12%, calculated for the mean values. Sources attributing to discrepancies could be geometrical simplifications and assumptions in the simulated model.

Two cases are simulated using Sluggit. Sluggit fails to reproduce the periodic oscialltions/instabilities observed in the experiment, but is in good agreement with the experimental results when operating in stable conditions.

The extended experiment for higher air flow rates for 38Hz and 40Hz did not successfully demonstrate the transition from slug/churn to annular flow regime, due to limitations in the experimental setup.

The EDI study should be investigated more and recommendation for further work are:

- Effect of friction: Small diameter or more viscous liquid
- Controlled inflow characteristics of both liquid and gas using controlled valve at the inlet
- Systematic investigation of geometry effects
- Investigations into reasons why simulations are more stable than experiments
- Instrumentation installation in the vertical section, i.e ring-probes for holdup and differential pressure transmitters

Bibliography

Adressa. *Her løftes et 20 meter høyt tårn opp på taket på Gløshaugen*. https://goo.gl/images/5k1mVj. Online; accessed 08 December 2017.

Bin, H., Golan, M., et al. (2003). Gas-lift instability resulted production loss and its remedy by feedback control: dynamical simulation results. In *SPE International Improved Oil Recovery Conference in Asia Pacific*. Society of Petroleum Engineers.

Chupin, G. (2003). An experimental investigation of multiphase gas-liquid pipe flow at low liquid loading. *NTNU, Trondheim*.

Cimbala, J. M. and Cengel, Y. A. (2014). Fluid mechanics: fundamentals and applications.

Clegg, J., Bucaram, S., Hein, N., et al. (1993). Recommendations and comparisons for selecting artificial-lift methods (includes associated papers 28645 and 29092). *Journal of Petroleum Technology*, 45(12):1–128.

Guet, S. and Ooms, G. (2006). Fluid mechanical aspects of the gas-lift technique. *Annu. Rev. Fluid Mech.*, 38:225–249.

Hu, B. (2005). Characterization of gas-lift instabilities.

Kanu, E. (2011). Expansion driven unstable two phase flows in long risers and wells. Master's thesis, Institutt for energi-og prosessteknikk.

Kassab, S. Z., Kandil, H. A., Warda, H. A., and Ahmed, W. H. (2009). Air-lift pumps characteristics under two-phase flow conditions. *International Journal of Heat and Fluid Flow*, 30(1):88–98.

Kjeldby, T., Arnult, T., Nydal, O., et al. (2013). Expansion instabilities in long risers: Small scale experiments and simulations. In *16th International Conference on Multiphase Production Technology*. BHR Group.

Kjeldby, T. and Nydal, O. (2012). Modeling of two phase flow expansion instabilities in long risers or wells. *HEFAT 2012*.

Kjeldby, T. B. (2010). Simulation of expansion driven flow instabilities in long risers. Master's thesis, Institutt for energi-og prosessteknikk.

Kjeldby, T. K., Nydal, O. J., et al. (2015). Experiments and simulations of local upstream gas accumulation giving unstable production in a flowline/riser system. *SPE Journal*, 20(03):598–609.

Mayor, T., Pinto, A., and Campos, J. (2008). On the gas expansion and gas hold-up in vertical slugging columns—a simulation study. *Chemical Engineering and Processing: Process Intensification*, 47(5):799–815.

Offshore Energy Today. Technip wins balnaves field subsea installation gig (australia). https://www.offshoreenergytoday.com/technip-wins-balnaves-field-subsea-installation-gig-australia/. Online; accessed 30 January 2018.

Poblano, E., Camacho, R., Fairuzov, Y., et al. (2002). Stability analysis of continuous-flow gas-lift wells. In *SPE Annual Technical Conference and Exhibition*. Society of Petroleum Engineers.

Ravnås, M. (2017). Designing, constructing and testing a vertical multiphase flow rig. *Project work*, pages 1–73.

Shoham, O. (2006). Mechanistic modeling of gas-liquid two-phase flow in pipes.

Smith, I. E. (2017). A 7-field lagrangian slug capturing and slug tracking model with higher order methods.

Taitel, Y., Bornea, D., and Dukler, A. (1980). Modelling flow pattern transitions for steady upward gas-liquid flow in vertical tubes. *AIChE Journal*, 26(3):345–354.

Tayman, J. and Swanson, D. A. (1999). On the validity of mape as a measure of population forecast accuracy. *Population Research and Policy Review*, 18(4):299–322.

Xu, Z., Golan, M., et al. (1989). Criteria for operation stability of gas-lift wells.

Appendix A

Results

A.1 Pressure and water flow rate vs time

A.1.1 Frequency=38Hz

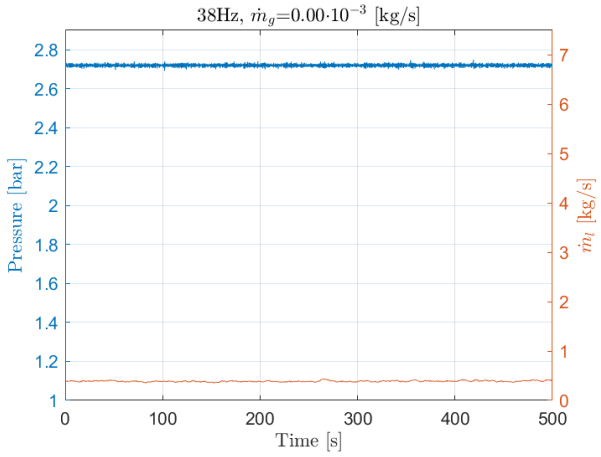

Figure A.1

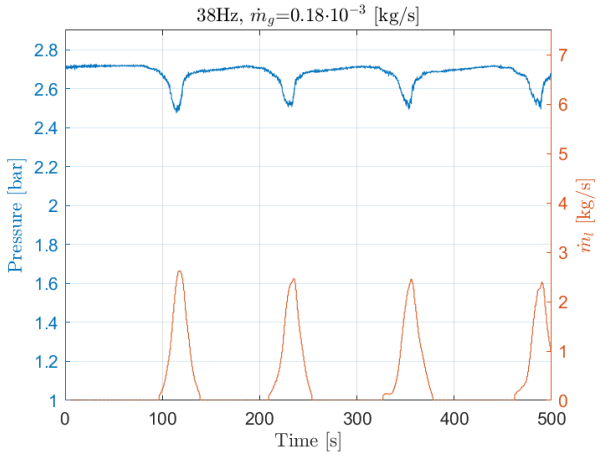

Figure A.2

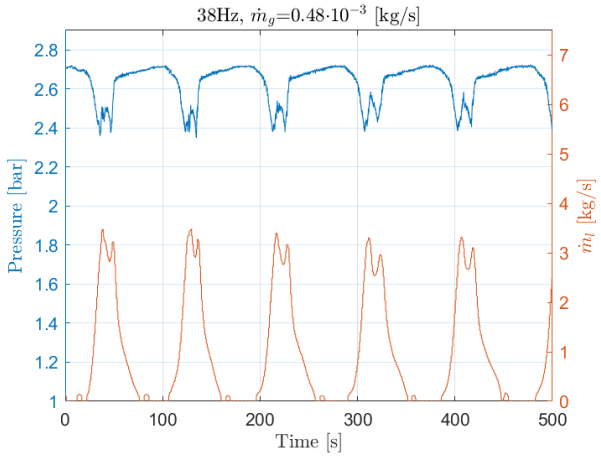

Figure A.3

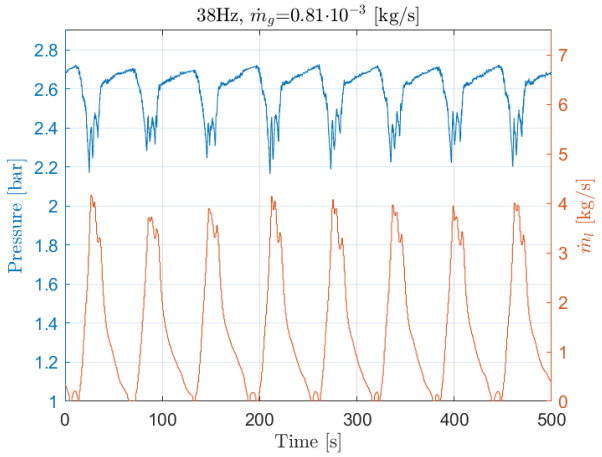

Figure A.4

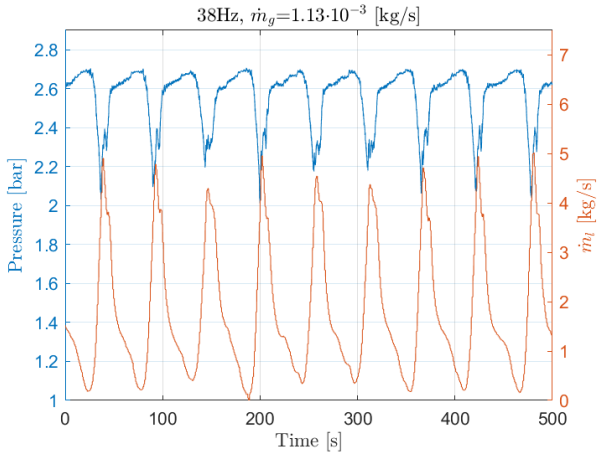

Figure A.5

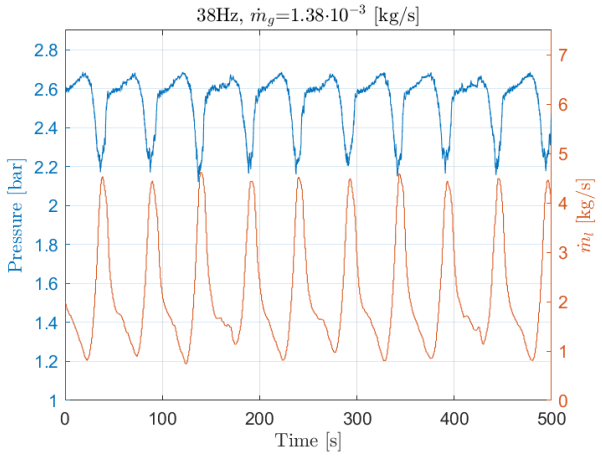

Figure A.6

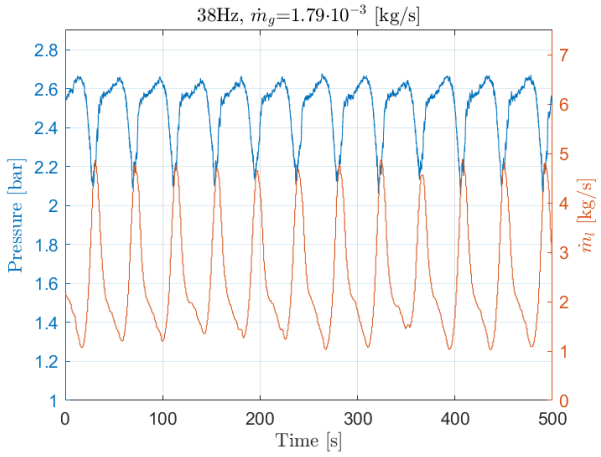

Figure A.7

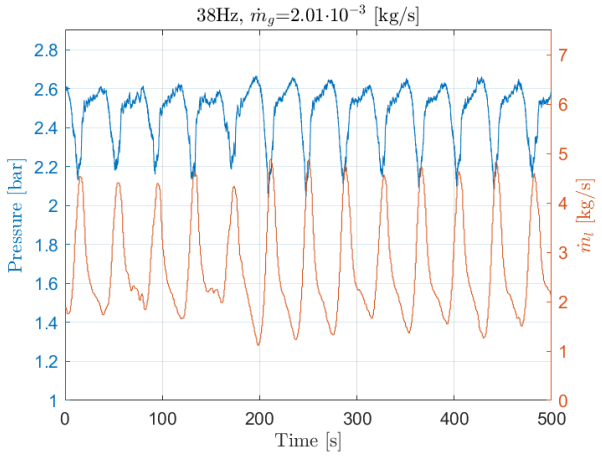

Figure A.8

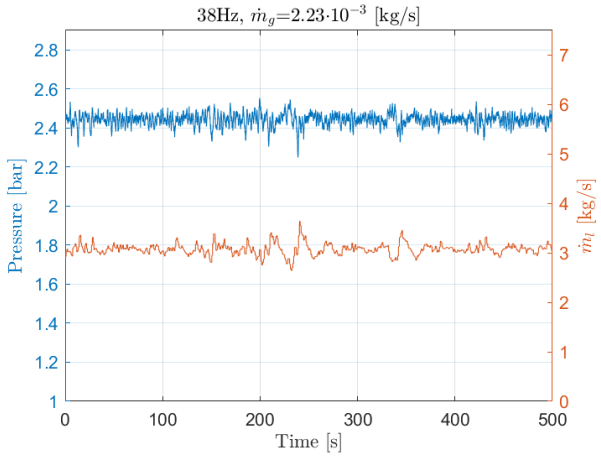

Figure A.9

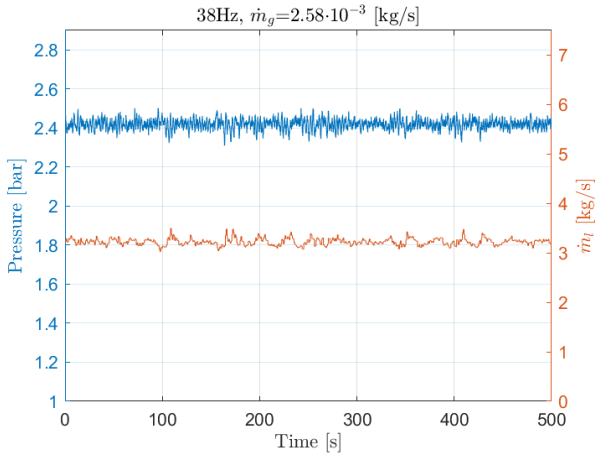

Figure A.10

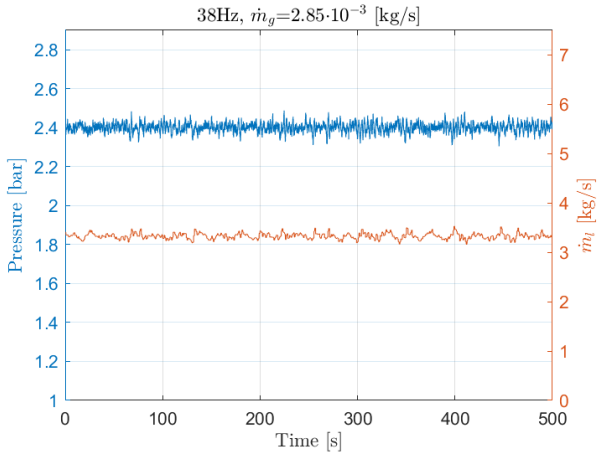

Figure A.11

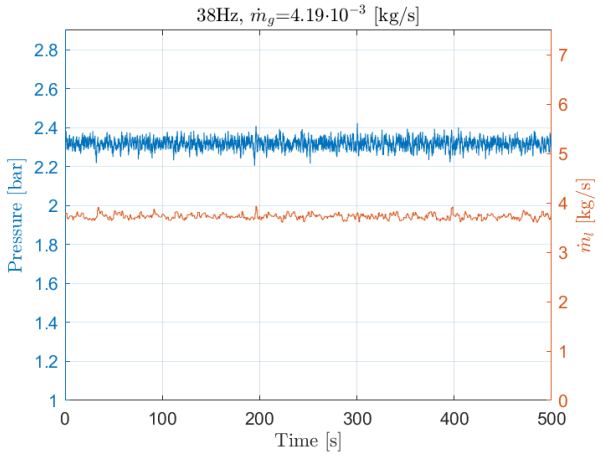

Figure A.12

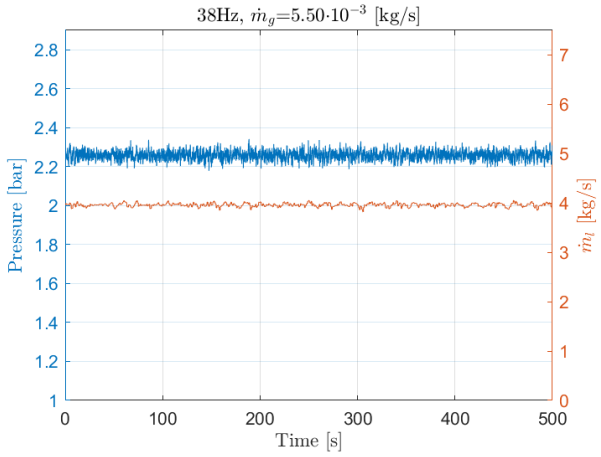

Figure A.13

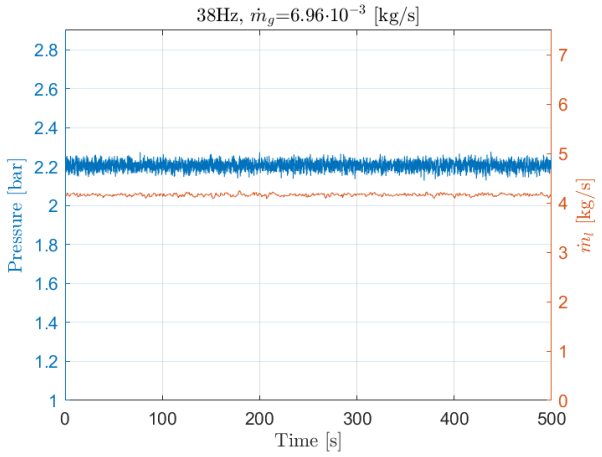

Figure A.14

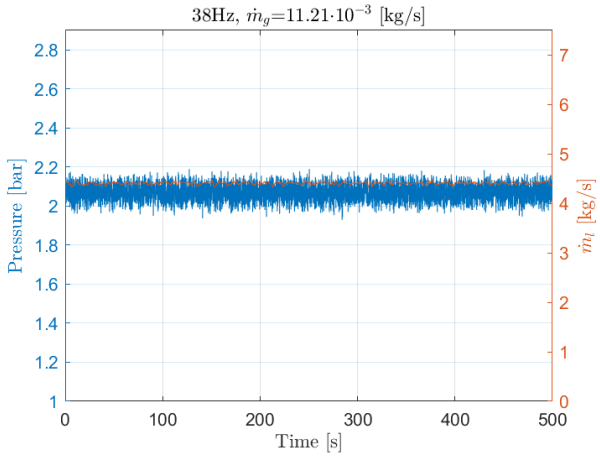

Figure A.15

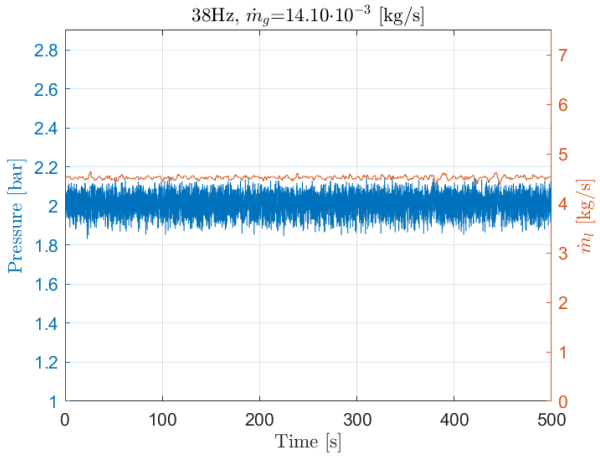

Figure A.16

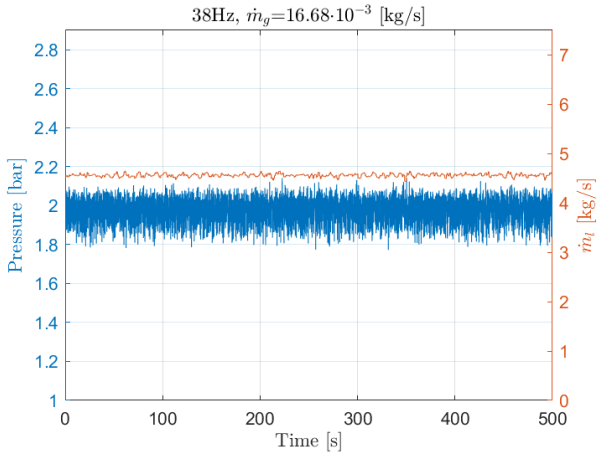

Figure A.17

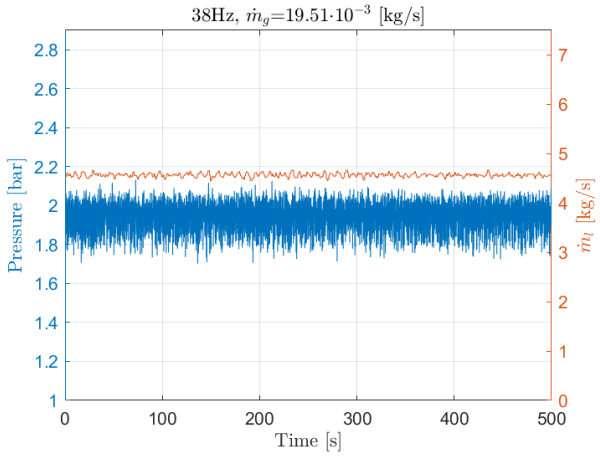

Figure A.18

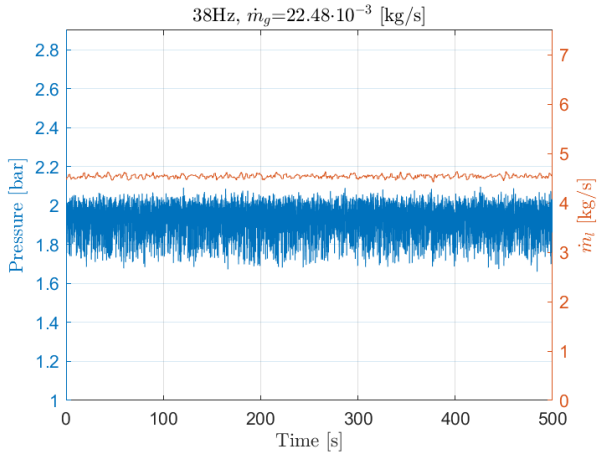

Figure A.19

A.1.2 Frequency=38,5Hz

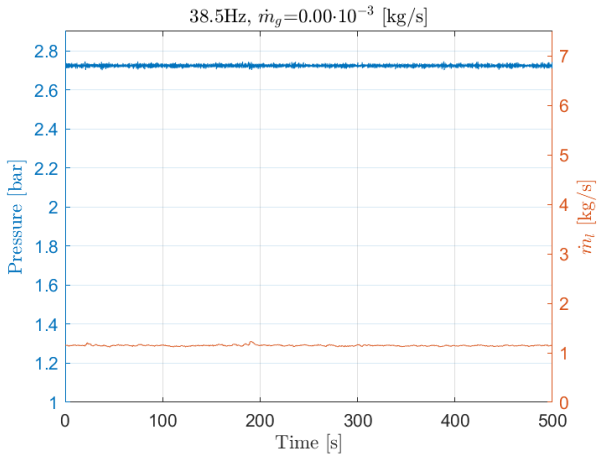

Figure A.20

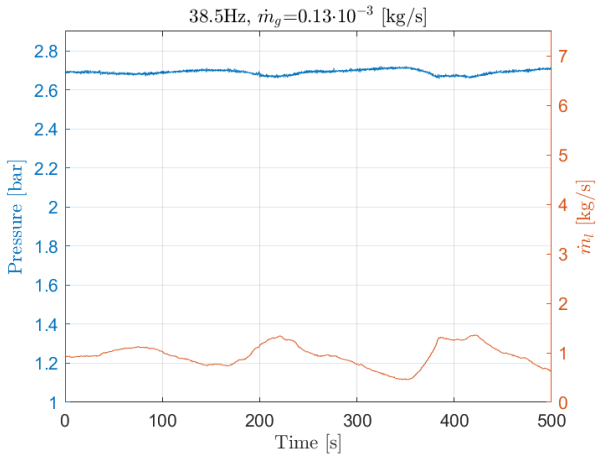

Figure A.21

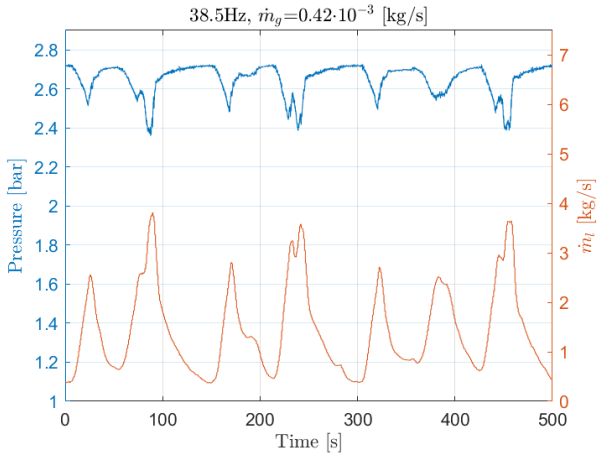

Figure A.22

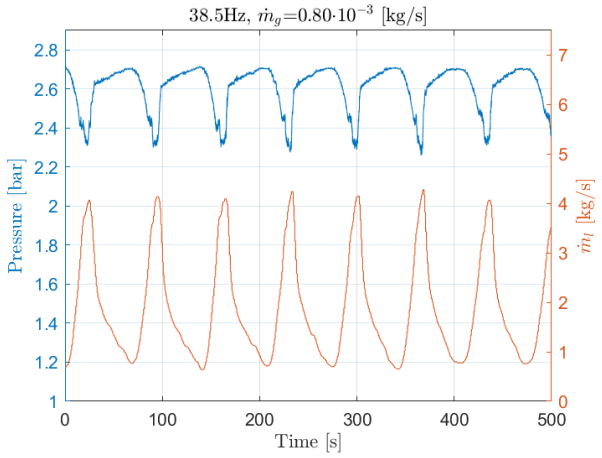

Figure A.23

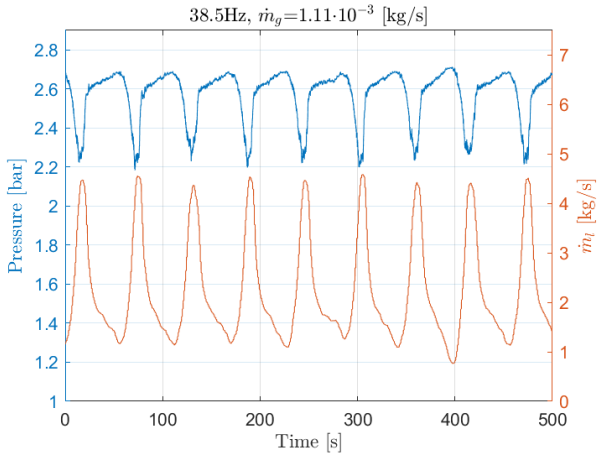

Figure A.24

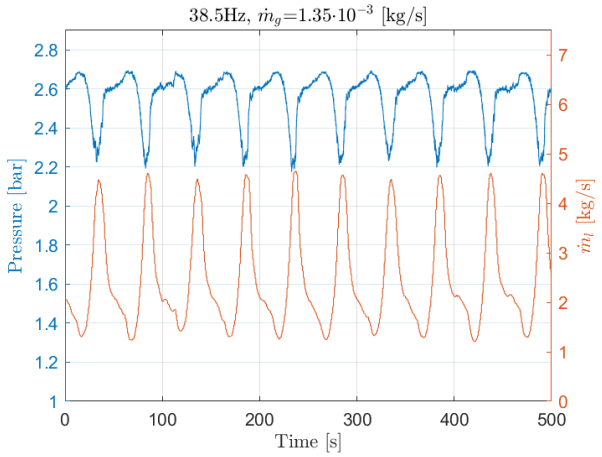

Figure A.25

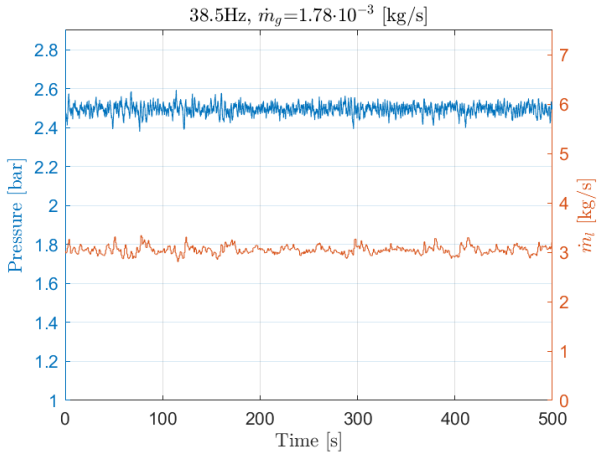

Figure A.26

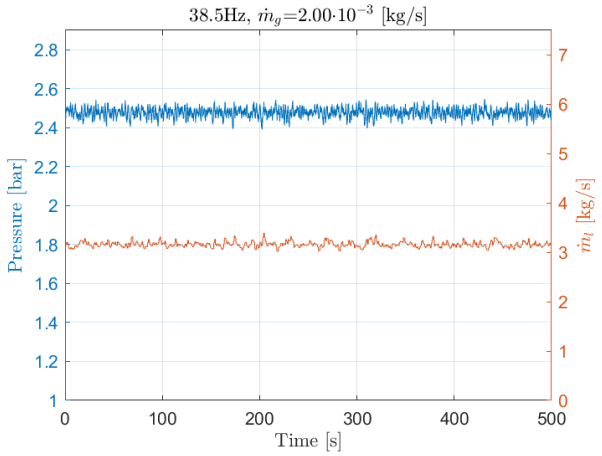

Figure A.27

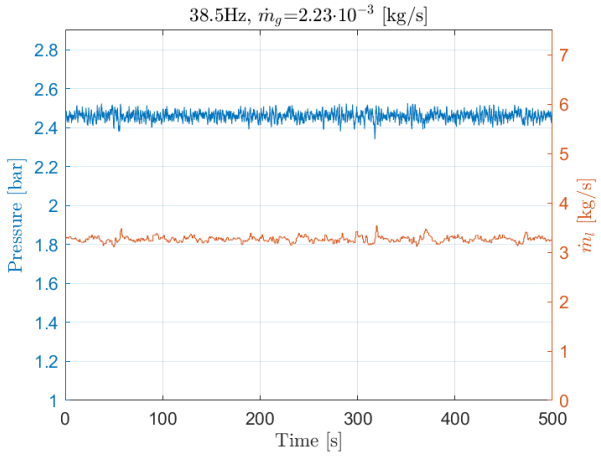

Figure A.28

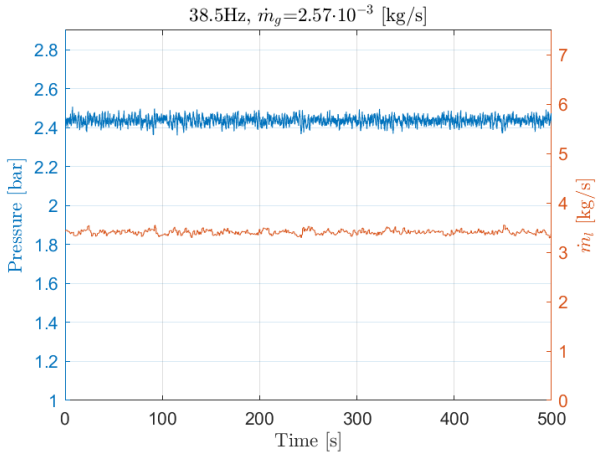

Figure A.29

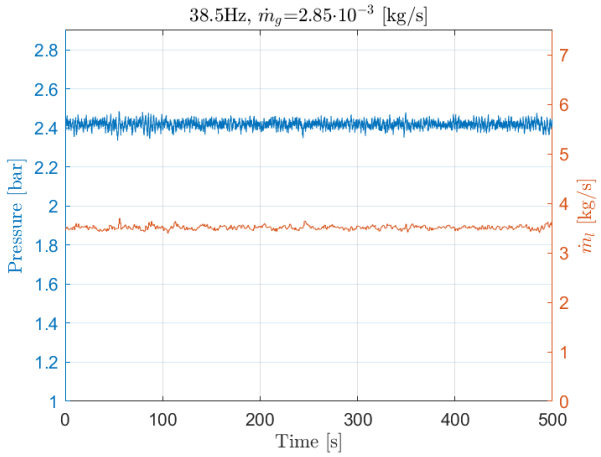

Figure A.30

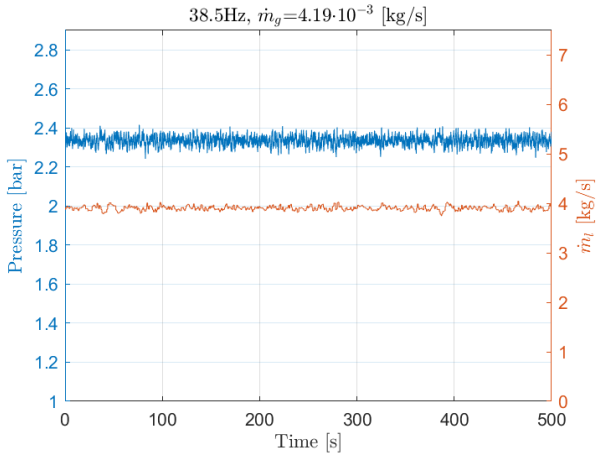

Figure A.31

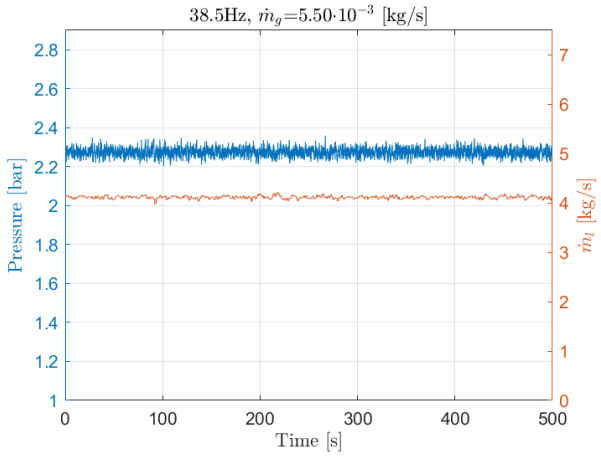

Figure A.32

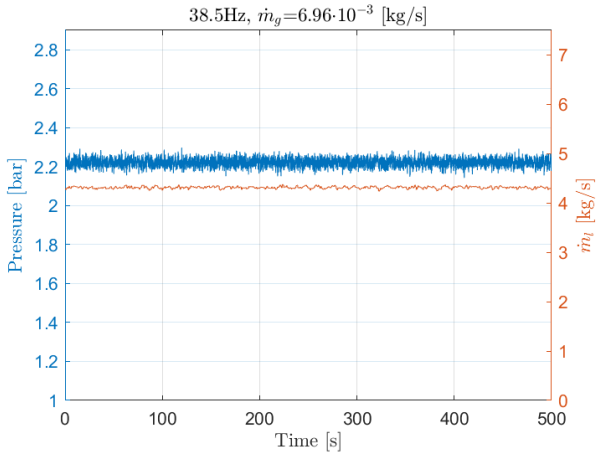

Figure A.33

A.1.3 Frequency=39Hz

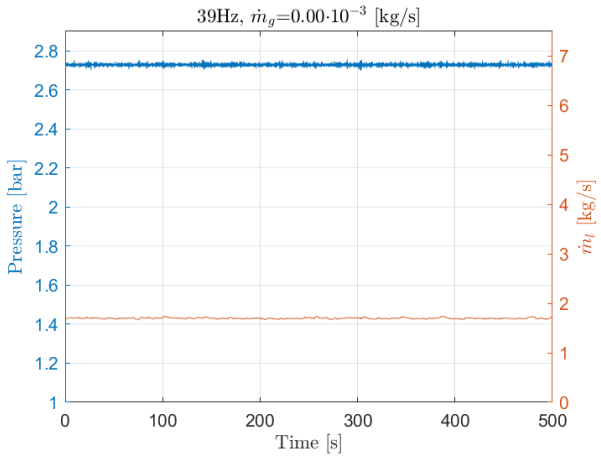

Figure A.34

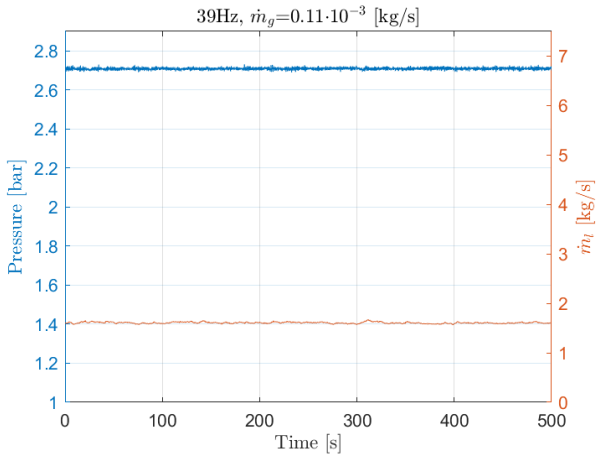

Figure A.35

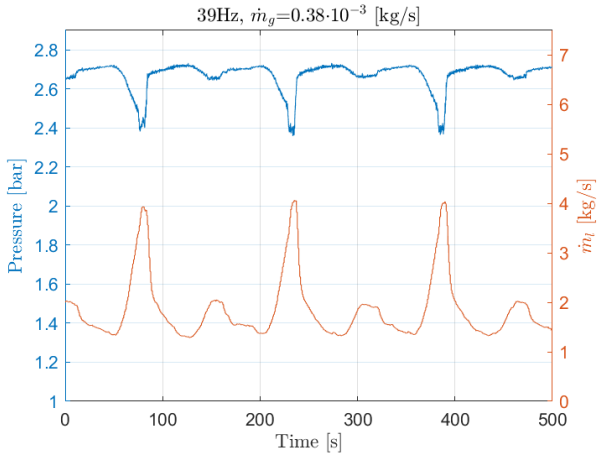

Figure A.36

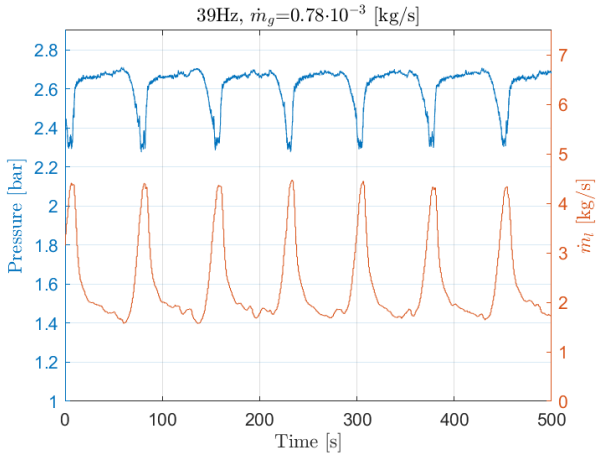

Figure A.37

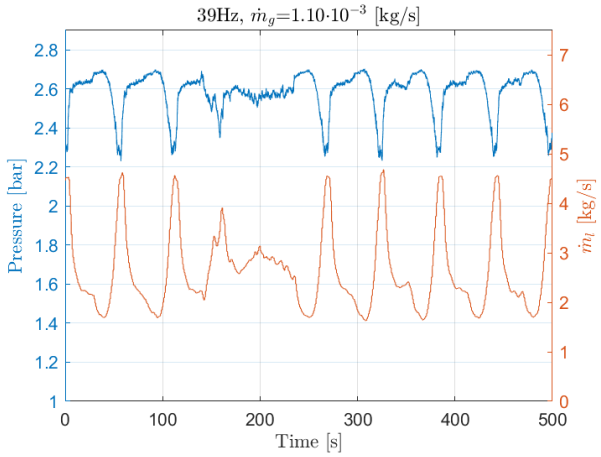

Figure A.38

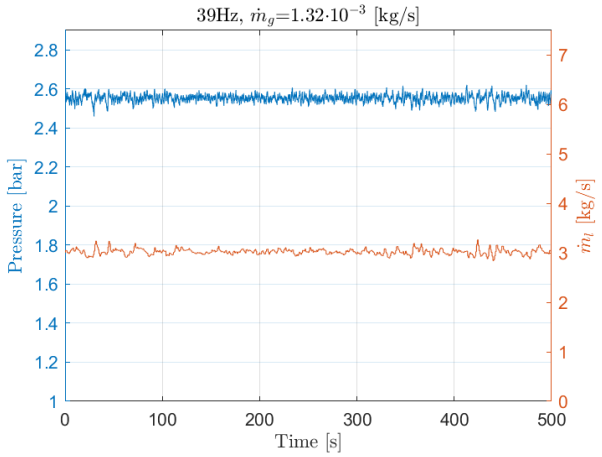

Figure A.39

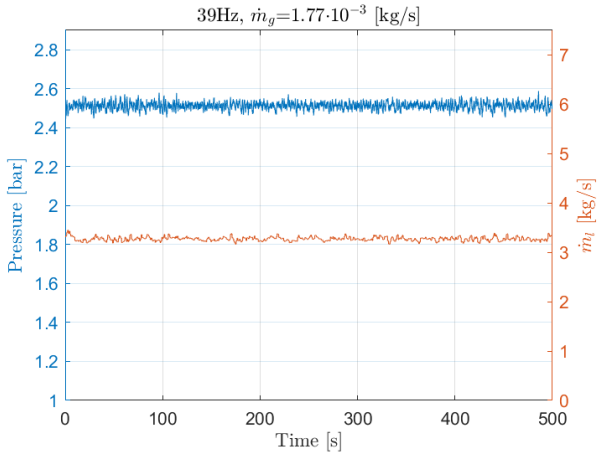

Figure A.40

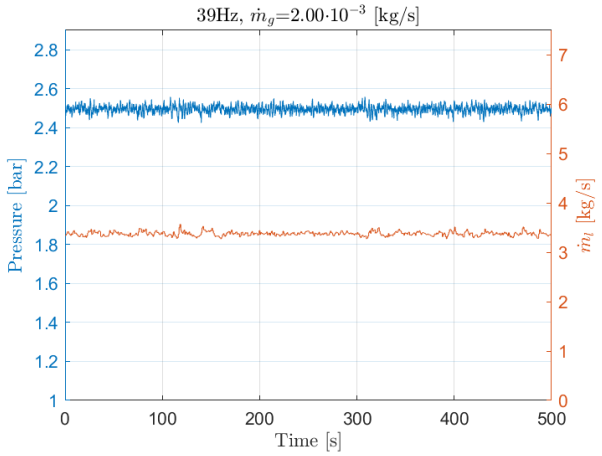

Figure A.41

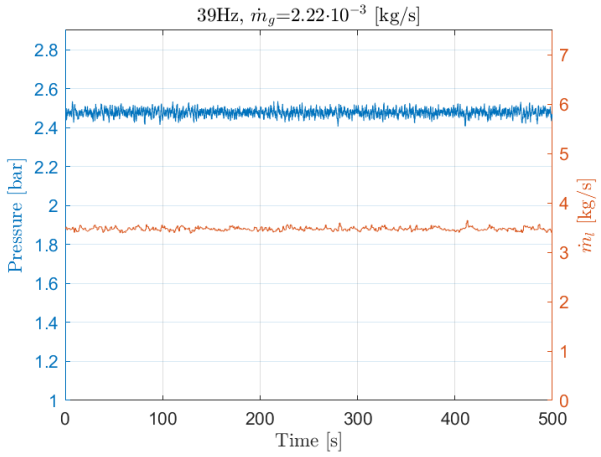

Figure A.42

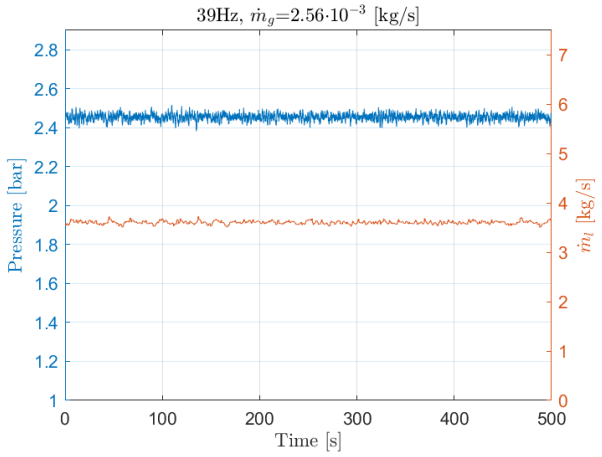

Figure A.43

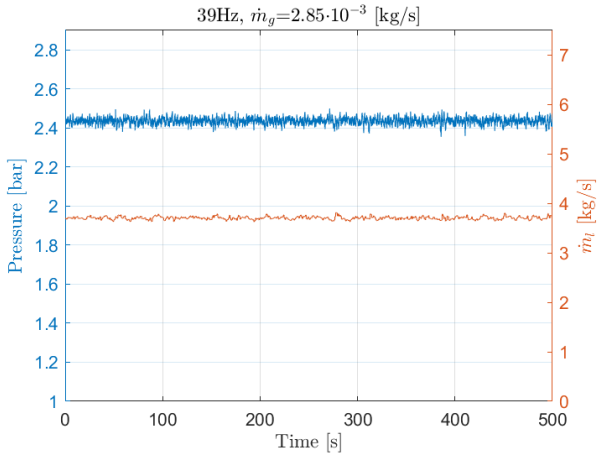

Figure A.44

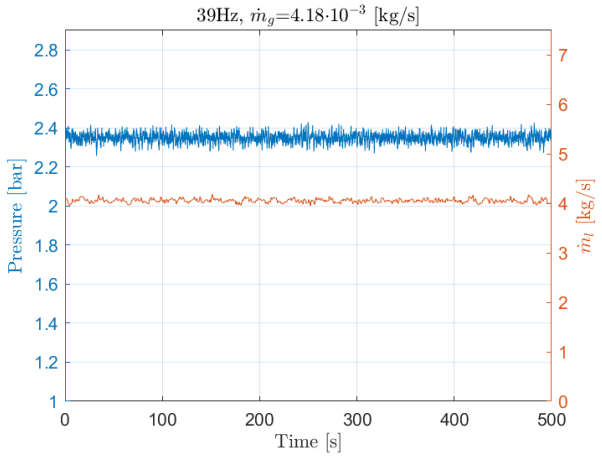

Figure A.45

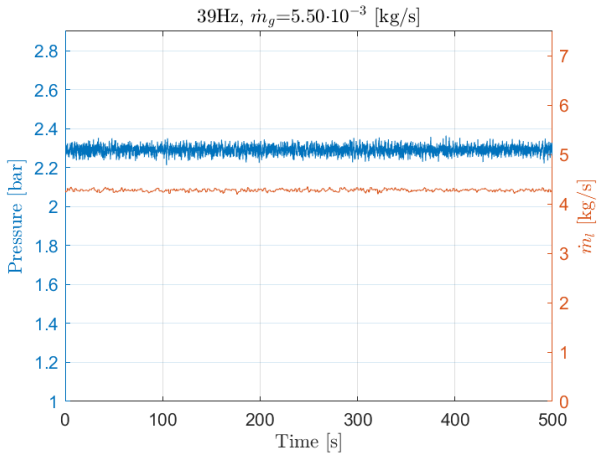

Figure A.46

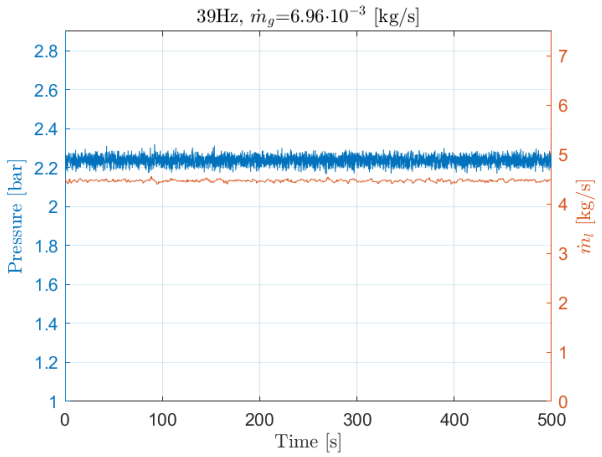

Figure A.47

A.1.4 Frequency=39,5Hz

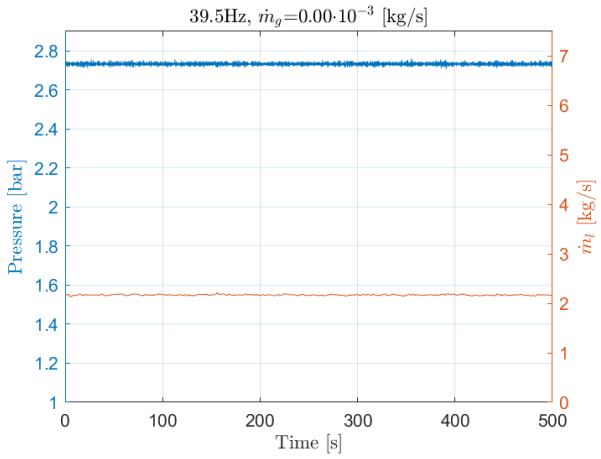

Figure A.48

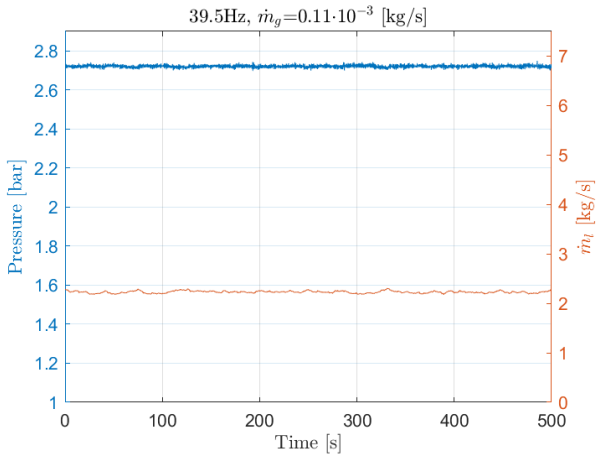

Figure A.49

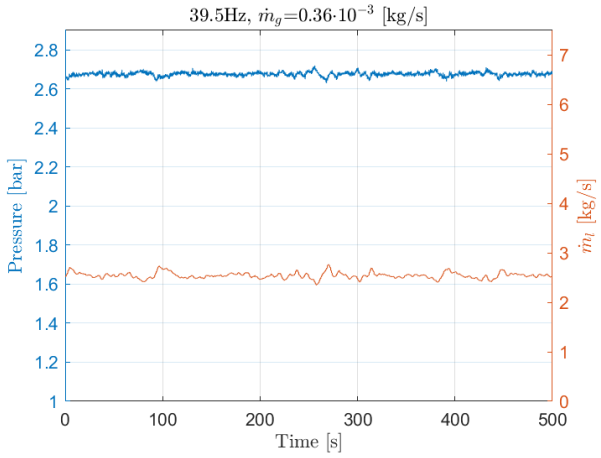

Figure A.50

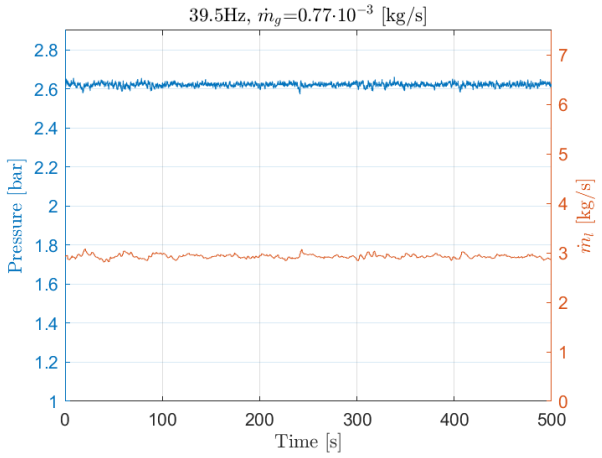

Figure A.51

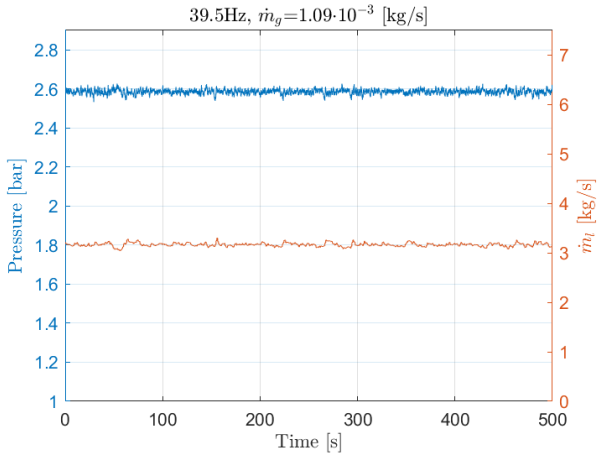

Figure A.52

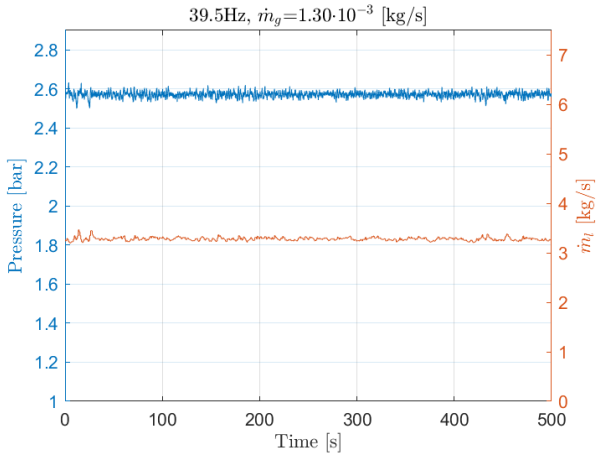

Figure A.53

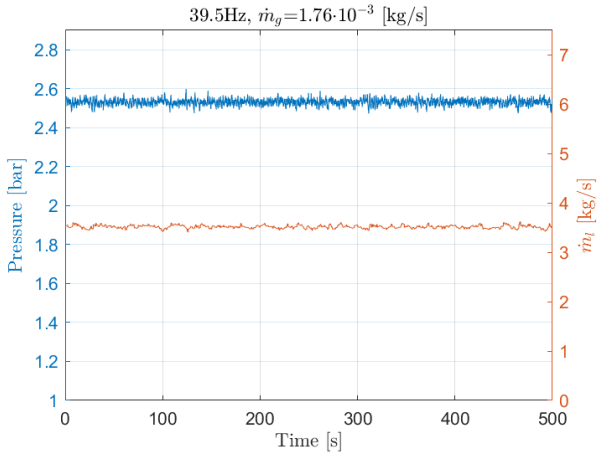

Figure A.54

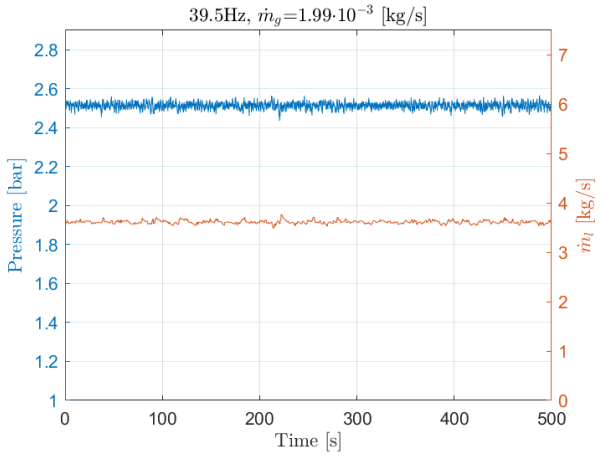

Figure A.55

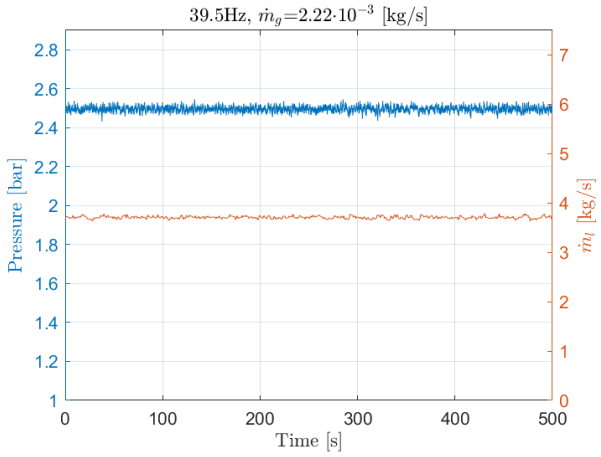

Figure A.56

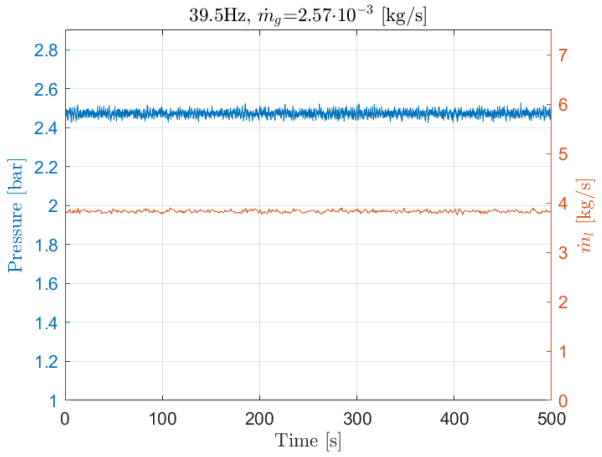

Figure A.57

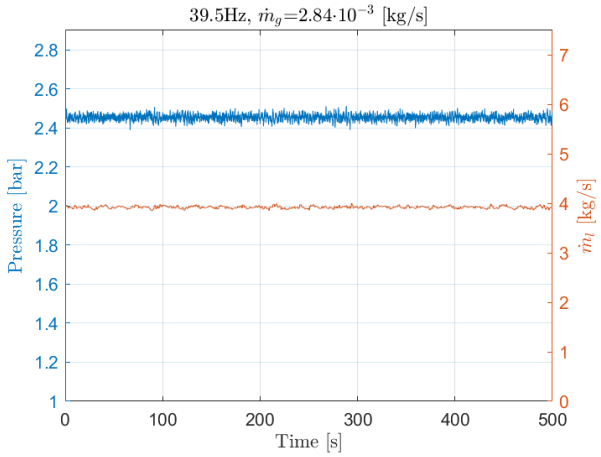

Figure A.58

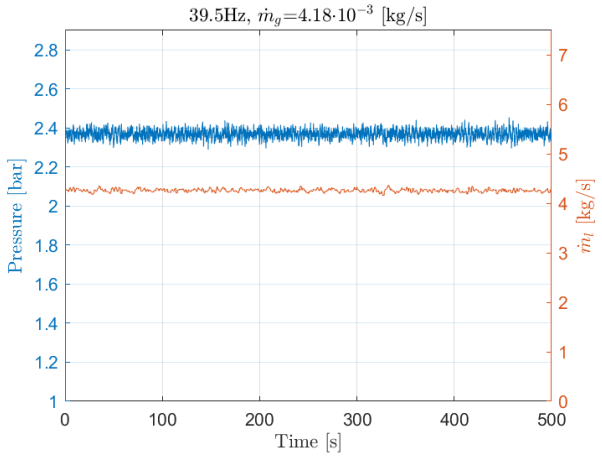

Figure A.59

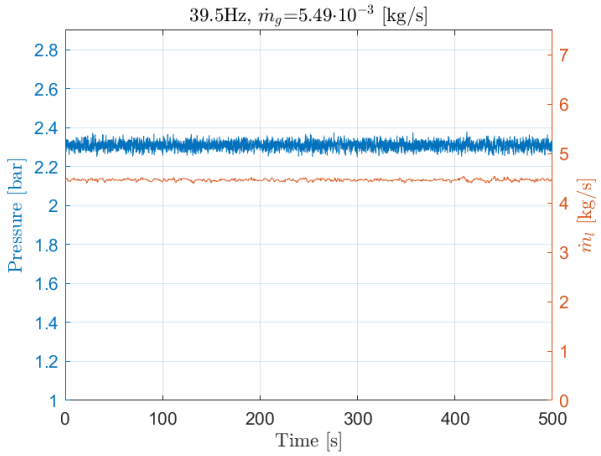

Figure A.60

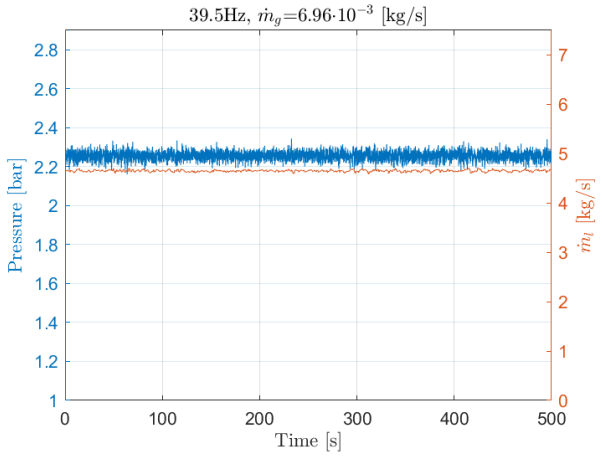

Figure A.61

A.1.5 Frequency=40Hz

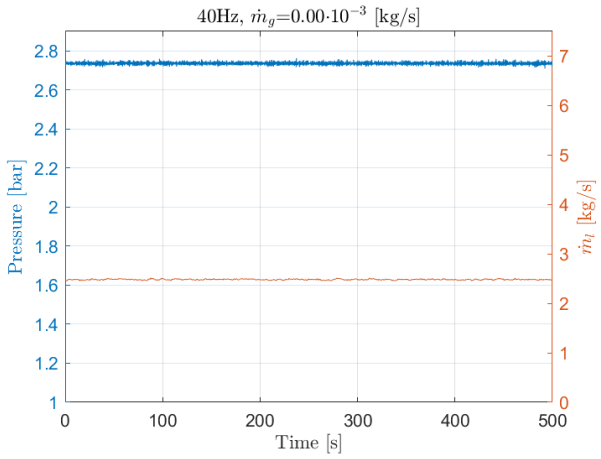

Figure A.62

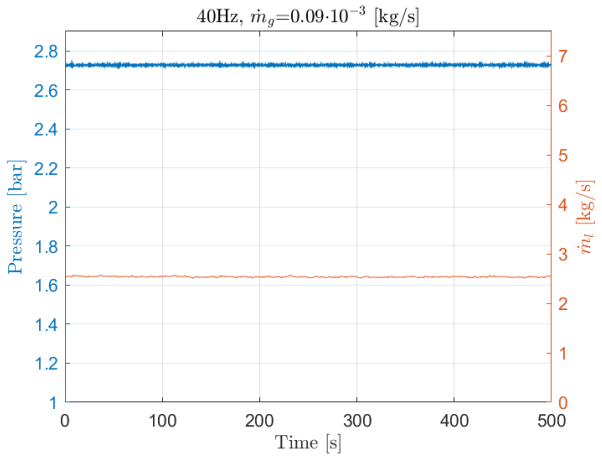

Figure A.63

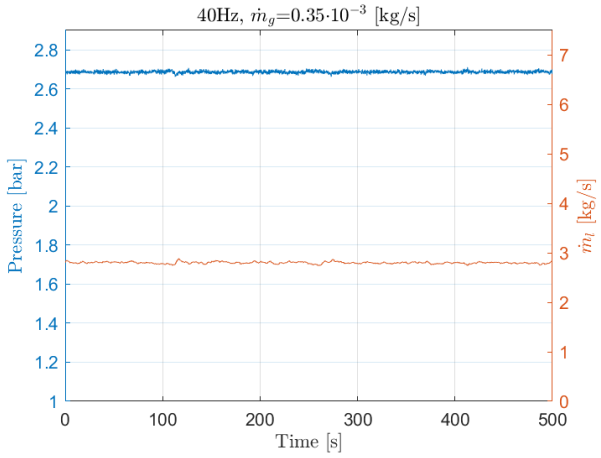

Figure A.64

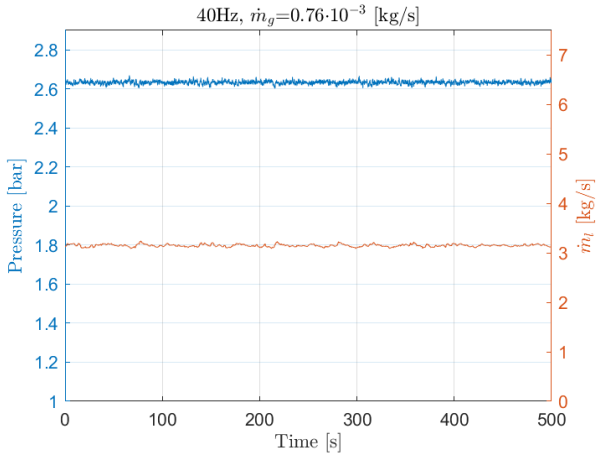

Figure A.65

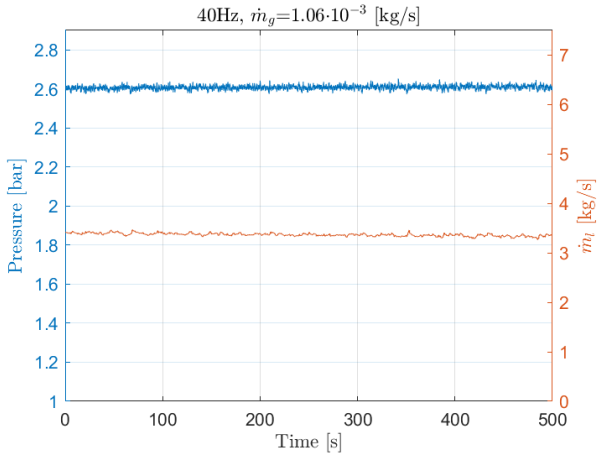

Figure A.66

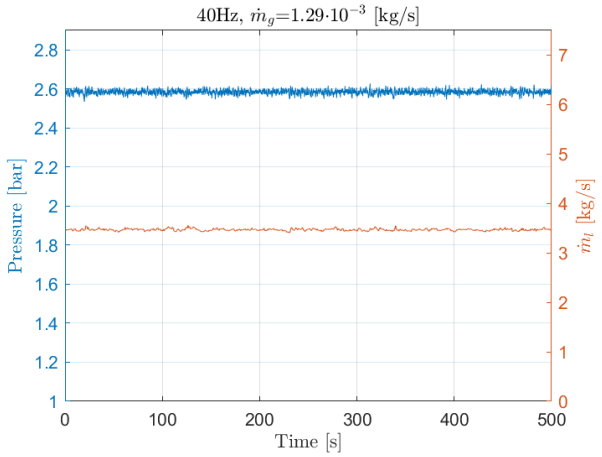

Figure A.67

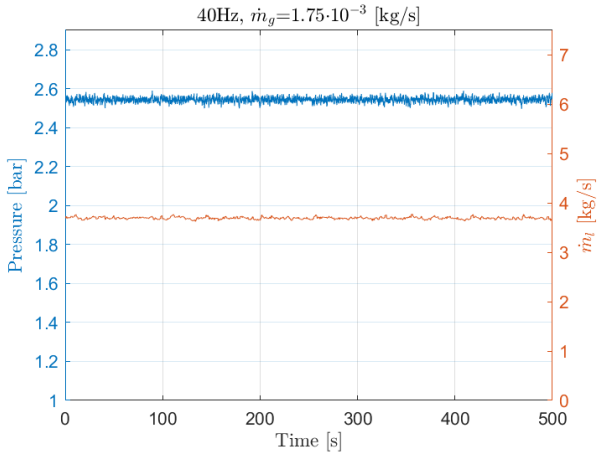

Figure A.68

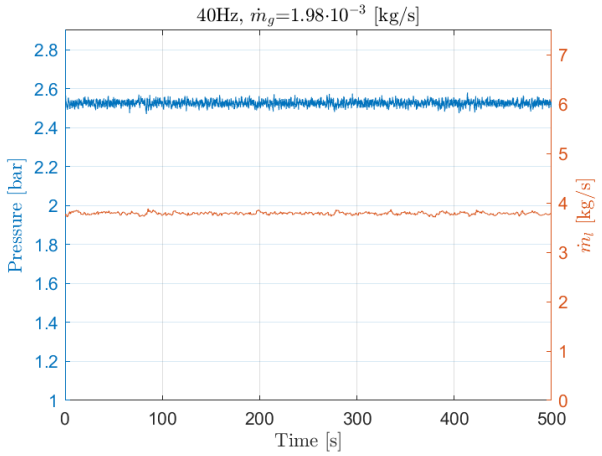

Figure A.69

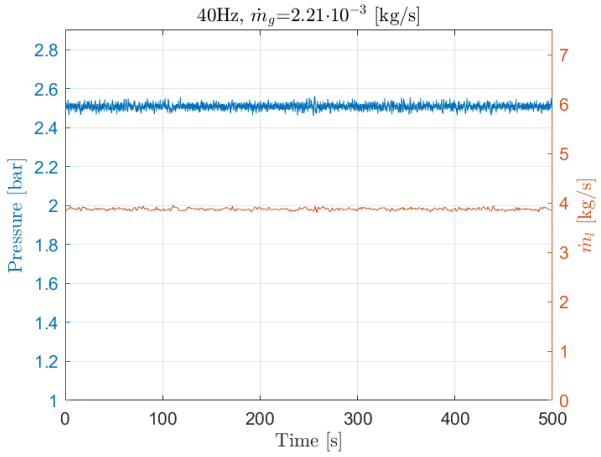

Figure A.70

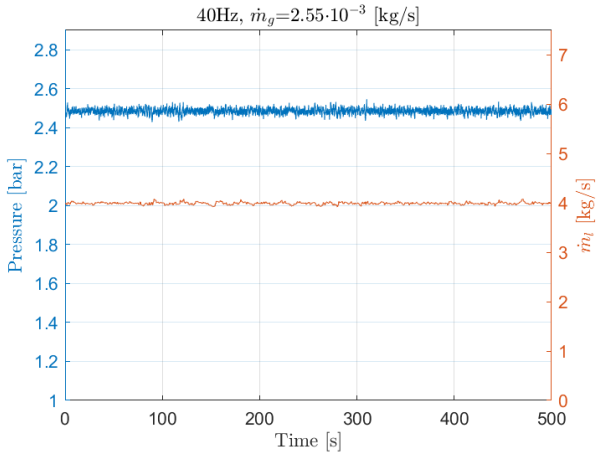

Figure A.71

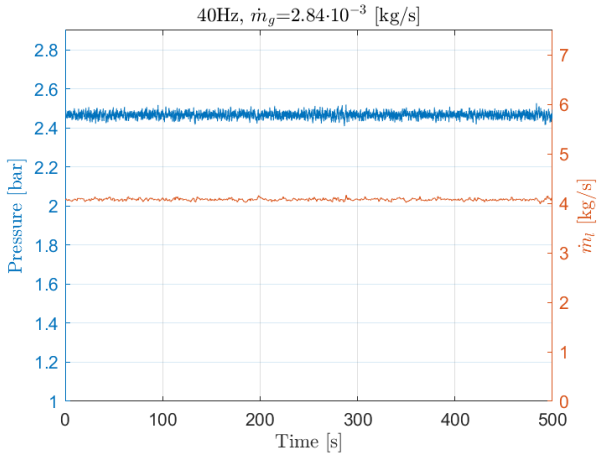

Figure A.72

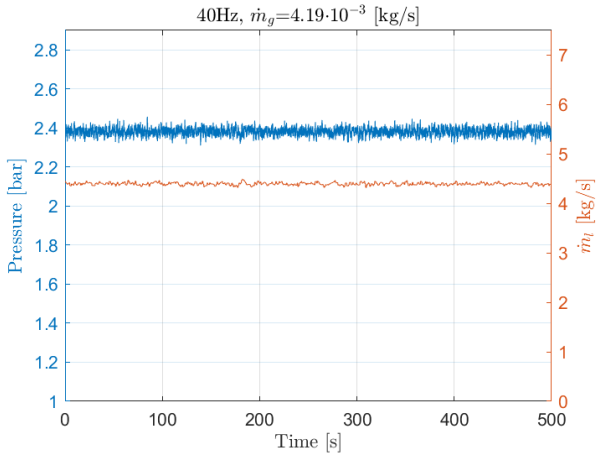

Figure A.73

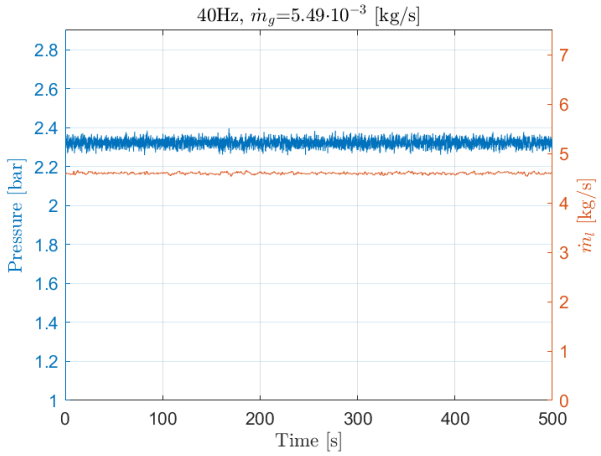

Figure A.74

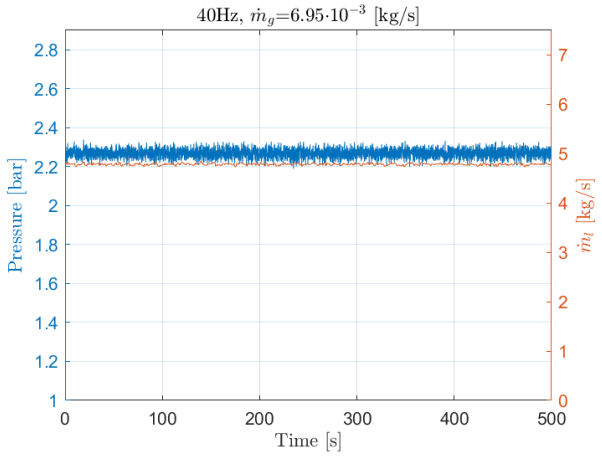

Figure A.75

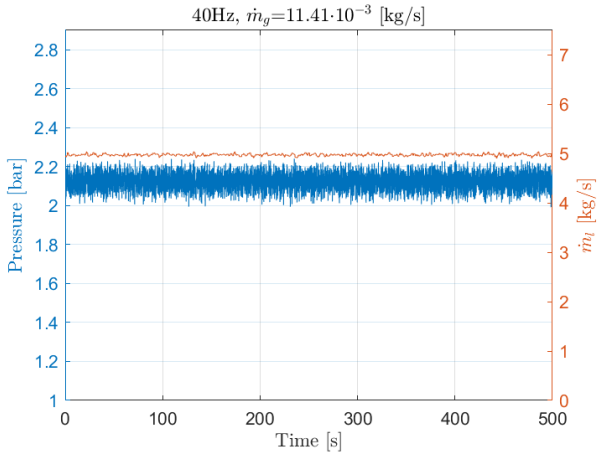

Figure A.76

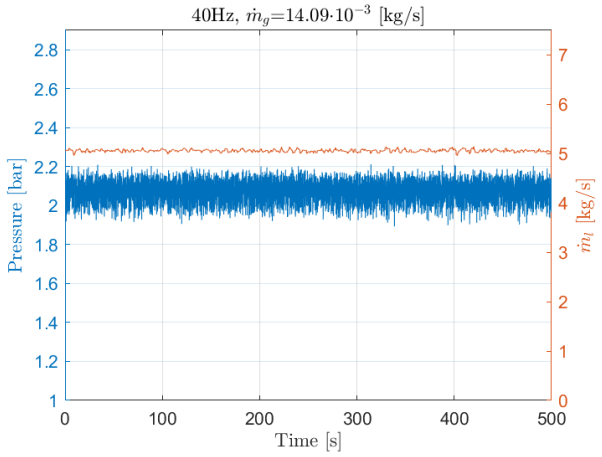

Figure A.77

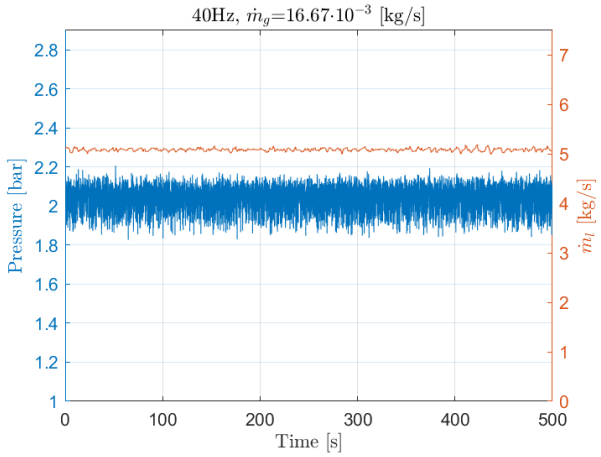

Figure A.78

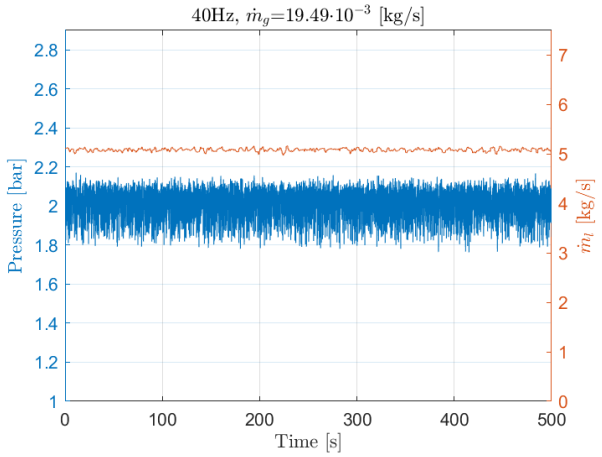

Figure A.79

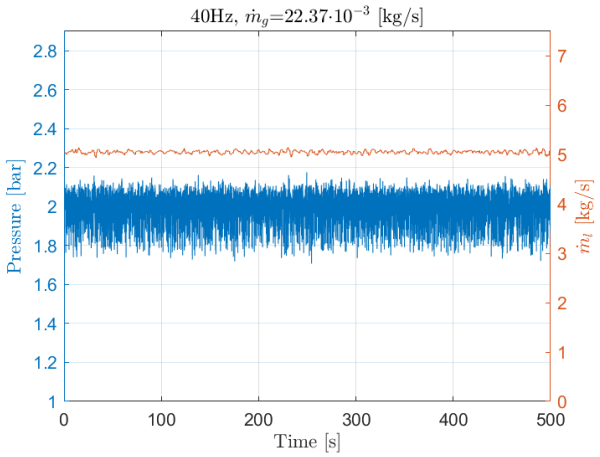

Figure A.80

Appendix B

Risk assessment excerpt

NTNU SINTEF

9 QUANTIFYING OF RISK - RISK MATRIX

The risk matrix will provide visualization and an overview of activity risks so that management and users get the most complete picture of risk factors.

IDnr	Dangerous situation	Probability	Consequences	Combination
1	Oil-water spill: *Slippery floor. Oil/water kept in open containers*	3	B	B3
2	*Eye damage*	2	D	D2
3	*Long way with stair to emergency shut down for air. (Hurry and unsafe way)*	3	C	C3
4	*Loose cables and components around the rig. (Stumbling)*	3	B	B3

Conclusion: The ground around the rig should be dry and clean always.
Routines for removal of oil spillage have to be established.
Air supply shut down valve is preferred connected to the emergency button.

CONSEQUENSES						
	Svært alvorlig	E1	E2	E3	E4	E5
	Alvorlig	D1	D2	D3	D4	D5
	Moderat	C1	C2	C3	C4	C5
	Liten	B1	B2	B3	B4	B5
	Svært liten	A1	A2	A3	A4	A5
		Svært liten	Liten	Middels	Stor	Svært Stor
		PROBABILITY				

The principle of the acceptance criterion. Explanation of the colors used in the matrix

Colour		Description
Red		Unacceptable risk Action has to be taken to reduce risk
Yellow		Assessment area. Actions has to be considered
Green		Acceptable risk. Action can be taken based on other criteria

Appendix C

OLGA input file

```
!****************************************************************************
**************
! Generated with OLGA version 2017.1.0
!****************************************************************************
**************

!****************************************************************************
**************
! Global keywords
!****************************************************************************
**************
OPTIONS TEMPERATURE=OFF, STEADYSTATE=NOTEMP, SLUGVOID=AIR,
CONSOLELOG=OFF, WRITEPVTFILES=YES, \
        MASSEQSCHEME=1STORDER, DEBUG=OFF, TRACERTRACKING=OFF,
TABLETOLERANCE=UNLIMITED, \
        FLOWMODEL=OLGA, SLUGTRACKINGMODEL=OLGA2015
FILES PVTFILE=./gaswatertab.tab
INTEGRATION ENDTIME=30 M, MAXDT=1 s, MAXTIME=30 M, MINDT=1E-04 s,
STARTTIME=0 s, \
        DTSTART=0.0001 s
OUTPUT COLUMNS=6, DTOUT=1000 d
TREND DTPLOT=10 s
PROFILE DTPLOT=1 h
RESTART WRITE=OVERWRITE, READFILE=OFF
ANIMATE DTPLOT=1 s
SLUGTRACKING LEVEL=OFF, HYDRODYNAMIC=OFF, GASENTRAINMENT=VOIDINSLUG

!****************************************************************************
**************
! Library keywords
!****************************************************************************
**************
CENTPUMPCURVE LABEL="PUMPCURVE-38Hz", VOLUMEFLOW=(1.6051, 7.2527, 9.3766,
12.0602, \
        13.5308, 14.594, 15.3059) m3/h, SPEED=(2190, 2190, 2190, 2190,
2190, 2190, \
        2190) rpm, DENSITY=998 kg/m3, EFFICIENCY=(0.78, 0.78, 0.78, 0.78,
0.78, \
        0.78, 0.78) -, HEAD=(17.4769, 16.5642, 16.1568, 15.4874, 15.0812,
14.8322, \
        14.5826) m
CENTPUMPCURVE LABEL="PUMPCURVE-38_5Hz", VOLUMEFLOW=(4.2103, 8.192,
9.9415, 12.6819, 14.1177, \
        15.0923, 15.8455) m3/h, SPEED=(2216, 2216, 2216, 2216, 2216,
2216, 2216) rpm, \
        DENSITY=998 kg/m3, EFFICIENCY=(0.79, 0.79, 0.79, 0.79, 0.79,
0.79, 0.79) -, \
        HEAD=(17.6561, 16.8549, 16.4931, 15.7978, 15.4016, 15.1212,
14.903) m
CENTPUMPCURVE LABEL="PUMPCURVE-39Hz", VOLUMEFLOW=(6.1268, 9.1848, 10.698,
13.3568, \
        14.7308, 15.6654, 16.383) m3/h, SPEED=(2242, 2242, 2242, 2242,
2242, 2242, \
        2242) rpm, DENSITY=998 kg/m3, EFFICIENCY=(0.8, 0.8, 0.8, 0.8,
0.8, 0.8, \
        0.8) -, HEAD=(17.8674, 17.151, 16.8257, 16.1165, 15.7244,
15.4481, 15.2295) m
```

```
CENTPUMPCURVE LABEL="PUMPCURVE-39_5Hz", VOLUMEFLOW=(7.8073, 10.3085,
11.6041, 14.1332, \
        15.4445, 16.3417, 17.0306) m3/h, SPEED=(2269, 2269, 2269, 2269,
2269, \
        2269, 2269) rpm, DENSITY=998 kg/m3, EFFICIENCY=(0.81, 0.81, 0.81,
0.81, \
        0.81, 0.81, 0.81) -, HEAD=(18.1064, 17.4872, 17.1816, 16.4945,
16.1066, \
        15.836, 15.6209) m

CENTPUMPCURVE LABEL="PUMPCURVE-40Hz", VOLUMEFLOW=(8.9131, 11.0935,
12.2482, 14.6479, \
        15.9508, 16.8206, 17.4932) m3/h, SPEED=(2295, 2295, 2295, 2295,
2295, \
        2295, 2295) rpm, DENSITY=998 kg/m3, EFFICIENCY=(0.82, 0.82, 0.82,
0.82, \
        0.82, 0.82, 0.82) -, HEAD=(18.288, 17.7243, 17.4429, 16.7723,
16.3773, \
        16.11, 15.8978) m

!*************************************************************************
**************
! Network Component
!*************************************************************************
**************
NETWORKCOMPONENT TYPE=FLOWPATH, TAG=FLOWPATH_3
 PARAMETERS LABEL=FLOWPATH, LINE=NO, FLUIDTYPE=WATER
 BRANCH FLUID=1
 GEOMETRY LABEL="GEOMETRY-1", YSTART=0 m, ZSTART=0 m
 PROFILEDATA VARIABLE=(HOL, ID, IDIAM, PT, UG, UL)
 INITIALCONDITIONS MASSFLOW=2200 kg/h, INTEMPERATURE=20 C,
OUTTEMPERATURE=20 C, \
        INPRESSURE=1 bara, OUTPRESSURE=1 bara, INVOIDFRACTION=0 -,
OUTVOIDFRACTION=0 -, \
        WATERCUT=1 -
 TRENDDATA ABSPOSITION=14.9696 m, VARIABLE=(GLT, PT)
 SOURCE LABEL="AIR SOURCE", TIME=0 s, SOURCETYPE=MASS, PIPE="Pipe-5",
SECTION=3, \
        GASFRACTION=1 -, TEMPERATURE=20 C,

CENTRIFUGALPUMP LABEL="CENTRIFUGAL PUMP", MAXSPEED=2800 rpm,
CURVEMODE=SINGLEPHASE, \
        EFFIMECH=0.7, VISCMETHOD=OFF, \
        PIPE="PIPE-1", SECTIONBOUNDARY=2, CURVES=("PUMPCURVE-38Hz",
"PUMPCURVE-38_5Hz", \
        "PUMPCURVE-39Hz", "PUMPCURVE-39_5Hz", "PUMPCURVE-40Hz"),
TWOPHASEOPTION=CALCMULTIPLIERS, \
        ONECURVEPERSPEED=YES, USEPHASEMULT=NO
 PIPE ROUGHNESS=1.5E-05 m, LABEL="Pipe-1", NSEGMENT=6,
LSEGMENT=(0.346123, 0.357706, \
        0.38247, 0.424095, 0.244803, 0.244803) m, LENGTH=2 m, ELEVATION=0
m, DIAMETER=0.06 m
 PIPE ROUGHNESS=5E-05 m, LABEL="Pipe-2", NSEGMENT=4, LSEGMENT=(0.363578,
0.363578, \
        0.363578, 0.309267) m, LENGTH=1.4 m, ELEVATION=-1.25 m,
DIAMETER=0.06 m
 PIPE ROUGHNESS=5E-05 m, LABEL="Pipe-3", NSEGMENT=2, LSEGMENT=(0.158877,
0.141123) m, \
```

```
        LENGTH=0.3 m, ELEVATION=0 m, DIAMETER=0.06 m
 PIPE ROUGHNESS=5E-05 m, LABEL="Pipe-4", NSEGMENT=2, LSEGMENT=(0.204403,
0.295597) m, \
        LENGTH=0.5 m, ELEVATION=0.35 m, DIAMETER=0.06 m
 PIPE ROUGHNESS=5E-05 m, LABEL="Pipe-5", NSEGMENT=4, LSEGMENT=(0.427372,
0.230326, \
        0.230326, 0.361975) m, LENGTH=1.25 m, ELEVATION=0.03185 m,
DIAMETER=0.06 m
 PIPE ROUGHNESS=5E-05 m, LABEL="Pipe-6", NSEGMENT=2, LSEGMENT=(0.221852,
0.183748) m, \
        LENGTH=0.4056 m, ELEVATION=0.375 m, DIAMETER=0.06 m
 PIPE ROUGHNESS=5E-05 m, LABEL="Pipe-7", NSEGMENT=2, LSEGMENT=(0.195314,
0.210286) m, \
        LENGTH=0.4056 m, ELEVATION=0.155 m, DIAMETER=0.06 m
 PIPE ROUGHNESS=5E-05 m, LABEL="Pipe-8", NSEGMENT=2, LSEGMENT=(0.229576,
0.176024) m, \
        LENGTH=0.4056 m, ELEVATION=-0.155 m, DIAMETER=0.06 m
 PIPE ROUGHNESS=5E-05 m, LABEL="Pipe-9", NSEGMENT=2, LSEGMENT=(0.102943,
0.0998568) m, \
        LENGTH=0.2028 m, ELEVATION=-0.1875 m, DIAMETER=0.06 m
 PIPE ROUGHNESS=5E-05 m, LABEL="Pipe-10", NSEGMENT=3, LSEGMENT=(0.158281,
0.233195, \
        0.308524) m, LENGTH=0.7 m, ELEVATION=-0.1426 m, DIAMETER=0.06 m
 PIPE ROUGHNESS=5E-05 m, LABEL="Pipe-11", NSEGMENT=14,
LSEGMENT=(0.354019, 0.397549, \
        0.435748, 0.393508, 0.393508, 0.393508, 0.393508, 0.393508,
0.393508, \
        0.417407, 0.375974, 0.330928, 0.285424, 0.2419) m,
LENGTH=5.2 m, \
        ELEVATION=0.1325 m, DIAMETER=0.06 m
 PIPE ROUGHNESS=5E-05 m, LABEL="Pipe-12", NSEGMENT=2, LSEGMENT=(0.201998,
0.198002) m, \
        LENGTH=0.4 m, ELEVATION=0 m, DIAMETER=0.06 m
 PIPE ROUGHNESS=5E-05 m, LABEL="Pipe-13", NSEGMENT=2, LSEGMENT=(0.227117,
0.272883) m, \
        LENGTH=0.5 m, ELEVATION=-0.033 m, DIAMETER=0.06 m
 PIPE ROUGHNESS=5E-05 m, LABEL="Pipe-14", NSEGMENT=4, LSEGMENT=(0.346671,
0.409486, \
        0.221921, 0.221921) m, LENGTH=1.2 m, ELEVATION=0.8275 m, \
        DIAMETER=0.06 m
 PIPE ROUGHNESS=5E-05 m, LABEL="Pipe-15", NSEGMENT=43,
LSEGMENT=(0.438316, 0.433082, \
        0.428181, 0.423647, 0.419504, 0.415764, 0.41243, 0.409496,
0.406948, 0.404763, \
        0.402916, 0.401374, 0.400106, 0.399078, 0.398255, 0.397606,
0.397103, \
        0.396718, 0.396427, 0.396212, 0.396055, 0.395942, 0.395862,
0.395806, \
        0.395768, 0.395742, 0.395725, 0.395714, 0.395707, 0.395702,
0.3957, 0.395698, \
        0.395698, 0.395696, 0.395696, 0.395696, 0.395696, 0.395696,
0.395696, \
        0.395696, 0.395696, 0.395696, 0.395696) m, LENGTH=17.28 m,
ELEVATION=17.28 m, \
        DIAMETER=0.06 m
 TRENDDATA CENTRIFUGALPUMP="CENTRIFUGAL PUMP", VARIABLE=PUMPGL
 TRENDDATA SOURCE="AIR SOURCE", VARIABLE=(GGSOUR, GTSOUR)
 TRENDDATA PIPE="Pipe-2", SECTION=1, VARIABLE=(GLT, PT)
```

```
ENDNETWORKCOMPONENT

!************************************************************************
**************
! Network Component
!************************************************************************
**************
NETWORKCOMPONENT TYPE=MANUALCONTROLLER, TAG=MANUALCONTROLLER_1
 PARAMETERS LABEL="PUMP CONTROLLER", RANGECHECK=OFF, TIME=0 s,
SETPOINT=0.78, STROKETIME=10 s
 TRENDDATA VARIABLE=CONTR
ENDNETWORKCOMPONENT

!************************************************************************
**************
! Network Component
!************************************************************************
**************
NETWORKCOMPONENT TYPE=MANUALCONTROLLER, TAG=MANUALCONTROLLER_2
 PARAMETERS LABEL="AIR CONTROLLER", TIME=(0, 200) s, SETPOINT=(0,
0.000183), MODE=AUTOMATIC, \
        STROKETIME=10 s
 TRENDDATA VARIABLE=CONTR
ENDNETWORKCOMPONENT

!************************************************************************
**************
! Network Component
!************************************************************************
**************
NETWORKCOMPONENT TYPE=NODE, TAG=NODE_1
 PARAMETERS LABEL=Inlet, TYPE=PRESSURE, LINE=NO, TOTALWATERFRACTION=1 -,
GASFRACTION=0 -, \
        TEMPERATURE=20 C, PRESSURE=1 atm, FLUID=1, FLUIDTYPE=WATER
ENDNETWORKCOMPONENT

!************************************************************************
**************
! Network Component
!************************************************************************
**************
NETWORKCOMPONENT TYPE=NODE, TAG=NODE_2
 PARAMETERS LABEL=OUTLET, TYPE=PRESSURE, LINE=NO, TOTALWATERFRACTION=-1 -
, GASFRACTION=1 -, \
        TEMPERATURE=20 C, PRESSURE=1 atm, FLUID=1, FLUIDTYPE=GAS
ENDNETWORKCOMPONENT

!************************************************************************
**************

ENDCASE
```

Appendix D

Check list valves

Up Stairs

Water

Centrifugal Pumps	**FIT 2.0.1**	*Small water c.v*	HV11003 Close	HV11002 Open	HV11004 Open	HV11005 Close	HV11007 Close	HV11008 Close	HV11010 Open			
	FIT 2.0.2	*Large water c.v.*	HV11003 Close	HV11002 Open	HV11004 Close	HV11005 Open	HV11006 Open	HV11007 Close	HV3014 Close	HV11009 Close		
		Small water c.v.	HV11003 Close	HV11002 Open	HV11004 Close	HV11005 Open	HV11006 Open	HV11007 Open	HV11008 Close	HV3014 Close	HV11009 Close	HV11010 Open
	FIT 2.0.3	*Large water c.v.*	HV11003 Close	HV11002 Open	HV11005 Close	HV11004 Open	HV11008 Close	HV11007 Open	HV11006 Close	HV3014 Close	HV11009 Close	
		Small water c.v.	HV11003 Close	HV11002 Open	HV11004 Open	HV11005 Close	HV11007 Close	HV11008 Close	HV11010 Open			

Screw Pumps	**FIT 2.0.2**	HV11003 Close	HV11002 Open	HV11004 Close	HV11005 Open	HV11006 Open	HV11007 Close	HV3014 Close	HV11009 Open
	FIT 2.0.3	HV11003 Close	HV11002 Open	HV11004 Open	HV11005 Close	HV11006 Close	HV11007 Open	HV11008 Close	HV3014 Close	HV11009 Open

S-riser	HV11011 Close	HV11012 Open	HV2017 Open
Horizontal line	HV11011 Open	HV11012 Close	HV4001 Open

Long Horizontal line	HV11011 Close	HV11012 Open	HV2013 Open

OIL

Centrifugal Pumps	**FIT3.02**	*Large Oil c.v .*	HV3029 Close	HV3011 Close	HV3012 Open	HV3013 Close	HV3014 Close	HV3015 Close	HV3016 Open	HV3018 Open	HV3017 Close	HV3020 Close
	FIT3.01	*Small Oil c.v*	HV3029 Close	HV3011 Close	HV3012 Open	HV3013 Close	HV3014 Close	HV3015 Open	HV3016 Close	HV3017 Close		

Screw Pumps	**FIT3.02**		HV3011 Open	HV3012 Close	HV3013 Close	HV3014 Close	HV3015 Close	HV3016 Open	HV3018 Open	HV3017 Close	HV3020 open

S-riser	HV3021 Open	HV3022 Close	
Horizontal line	HV3021 Close	HV3022 Open	HV4002 Open

Long Horizontal line	HV3021 Open	HV3022 Close	HV3023 Open

AIR

FIT 1.01	HV10010 Open	HV10009 Close	HV10008 Close	HV10006 Open	HV10007 Close	HV10004 Close	HV10003 Close
FIT 1.02	HV10010 Close	HV10009 Open	HV10008 Close	HV10007 Open	HV10006 Close	HV10004 Close	HV10003 Close

S-riser	HV10011 Open	HV10012 Close	HV10002 Open	HV10001 Open
Horizontal line	HV10011 Close	HV10012 Open	HV4003 Open	

Long Horizontal line	HV10011 Open	HV10012 Close	HV10013 Open

Air for control Valves	HV1003 Open

Full Name:	**Date:**

Down Stairs

Water

Large Screw Pump	HV2008 □Open	HV2002 □Close	HV2001 □Close	HV3004 □Open	HV3003 □Open
	HV3005 □Close	HV3009 □Open	HV3010 □Open	HV3008 □Close	HV2009 □Close
	HV2010 □Open	HV2011□Open	HV2006 □Close	HV2007 □Close	
Small Screw Pump	HV2008 □Open	HV2002 □Close	HV2001 □Close	HV3004 □Open	HV3003 □Close
	HV3005 □Open	HV3006 □Open	HV3008 □Open	HV3010 □Close	HV2009 □Close
	HV2010 □Open	HV2011 □Open	HV2006 □Close	HV2007 □Close	HV3007 □Close
Large Centrifugal Water Pump	HV2002 □Close	HV2008 □Close	HV2001 □Close	HV2003 □Open	HV2004 □Open
	HV2006 □Open	HV2007□Close	HV2011 □Open	HV2010 □Close	
Small Centrifugal Water Pump	HV2002 □Close	HV2008 □Close	HV2001 □Close	HV2003 □Open	HV2005 □Open
	HV2007 □Open	HV2006 □Close	HV2011 □Open	HV2010 □Close	

OIL

Large Centrifugal Oil Pump	HV3023 □Open	HV2001 □Close	HV2002 □Close	HV3027 □ Open	HV3026 □ Close	HV3028 □ Open
Small Centrifugal Oil Pump	HV3023 □Open	HV2001 □ Close	HV2002 □Close	HV3024 □Open	HV3025 □Open	HV3026 □Open
	HV3028 □Close					
Large Screw Pump used with small tank	HV3001 □Open	HV3002 □ Close	HV3003 □ Close	HV3004 □ Close	HV3009 □Open	HV3010 □ Open
	HV2009 □ Open	HV2010 □ Close	HV3008 □Close			
Small Screw Pump used with small tank	HV3001 □Open	HV3002 □ Close	HV3003 □Open	HV3005 □Open	HV3004 □ Close	HV3006 □Open
	HV3007 □ Close	HV3008 □Open	HV3010 □ Close	HV2009 □ Open	HV2010 □ Close	

AIR

Main Air supply valve HV1001 □Open

open on~10 degree and wait until pressure stabilizes, then open fully

Appendix E

Experimental procedure

Before staring pumps etc. the check list for the valves (Appx.D) must be controlled. Flowlines used in this experiment are higlighted in Figure 3.3. Check also that the air-tank Tag A-002 is at 5bar, if not, adjust the choke-valve next to the tank.

Start-up

1. Visually inspect the test-section and open the water flowline valves.
2. Check the air-bypass valves (see Tag HA-192 Figure 3.3) and close if open. Open valve Tag HA-195. Check the manual air control valve at the mixing, this should be closed.
3. Check that the valves are closed at the inlet for the other test facilities.
4. Open control valve for water (V 2.02) to 100% in LabVIEW.
5. The large centrifugal pump can now be started. Capacity is slowly increased to 85%. Water is now supposed to flow up in the riser. If not, stop pump and check valves.
6. If the water is circulating in the system, continue by opening the control valve for air (V 1.02) slowly. Pay attention to the flow rate for air in LabVIEW. When not increasing, open the valve with 1% more. Stop at 95% capacity.
7. Reduce pump capacity to 78%/38Hz.
8. Air can now be injected to a desired mass flow rate by opening the manual control valve at the mixing.

Stop

1. Stop water flow by slowly reduce the pump capacity until the pump is of.
2. Close control valve for water (V 2.02)

3. Close the manual air control valve at the mixing.
4. Close the air control valve (V 1.02)
5. Switch air flowline over to large flow meter.
6. Open air bypass valve (Tag HA-192 Figure 3.3) slowly. Open the air control valve (V 1.02) in LabVIEW once again slowly up to 30%. Water is now flushed out of the riser. Let air clean the pipe for 10 minutes.
7. Close the main air valve (HV-1001) in basement and air supply for control valves (HV-1003)

Appendix F

Centrifugal pump

Perfecta C 100-14, C 100-19, C 100-24, C 100-29, C 100-35

Cirkulationspump för värme och kyla

Teknisk information

Pumphus	Gjutjärn, SS0120
Pumphjul	Gjutjärn, SS0120
Packningar	Teadit el. likv
Mek axeltätning	Kol/kisel/ Viton/EPDM
Anslutningar:	Fläns DN100 PN16
Arbetstryck:	Max 10 bar
	Min 0,05 bar vid 50 °C
	Min 0,8 bar vid 80 °C
	Min 1,4 bar vid 110 °C
Vätsketemp:	Max 120 °C
	Min -20 °C
Omgivningstemp:	Max 40 °C

Montering

Pumpar med en vikt över 20 kg bör monteras på pelare.
Pumpen kan monteras med horisontell eller vertikal motoraxe beroende på om pelarealternativet valts.

Motordata

Motorn är en fläktkyld, kullagrad motor med förlängd axel av rostfritt stål. Motorskydd skall användas.

Spänning/Frekvens:	(-14,-19,-24) 3x230/400 V /50 Hz
	(-29,-35) 3x400/690 V /50 Hz
Skyddsform:	IP54

Beteckning	Art Nr	Motor Effekt (kW)	Märkström (A)	Varvtal (rpm)	H (mm)	Vikt (kg)
C 100-14	6231960	2,2	6,75/11,7	2800	415	55
C 100-19	6197170	3	10,5/6,7	2800	418	61
C 100-24	6197140	4	15/8,7	2800	435	65
C 100-29	6197130	5,5	10,7/6,2	2800	435	83
C 100-35	6197110	7,5	14,7/8,5	2800	455	86

Märkströmsuppgifter är nominella. Alternativa spänningar offereras.

Tvillingpumpar

Pumpen finns även i tvillingutförande. Bygglängd 500mm.

Tillbehör	**Art nr**	**Höjd**
Fotplatta C	6293890	125 mm till rörcentrum
Pelare A	6293900	435-755 mm
Vibrationsdämpare	6293910	8 mm
Motfänsar, svets 2-pack	6220450	
Frekvensomformare	6298040	(2,2-4kW)
Frekvensomformare	6298050	(4-7,5kW)
Differenstryckvakt	6298060	(1-16mvp)
Differenstryckvakt	6298070	(1-25mvp)
Rostskyddsbehandling	6298480	

Reservdelar	**Art nr**
Drivsida C 100-14 3x230/400V	6234030
Drivsida C 100-19 3x230/400V	6198940
Drivsida C 100-24 3x230/400V	6198930
Drivsida C 100-29 3x400/690V	6198920
Drivsida C 100-35 3x400/690V	6198910

Kapacitetsdiagram

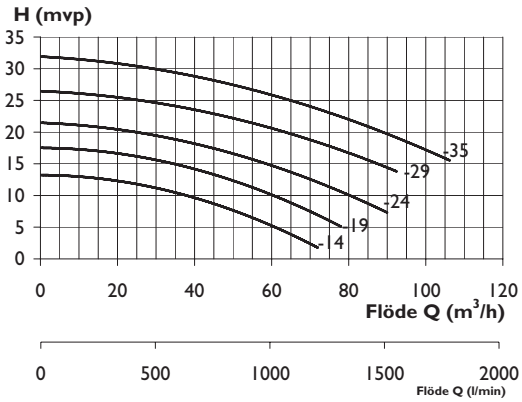

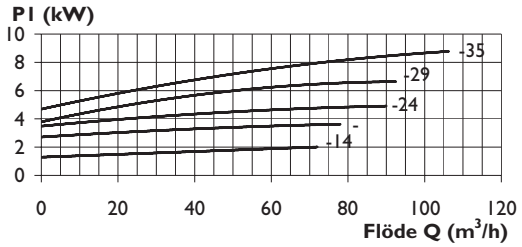

Måttskiss

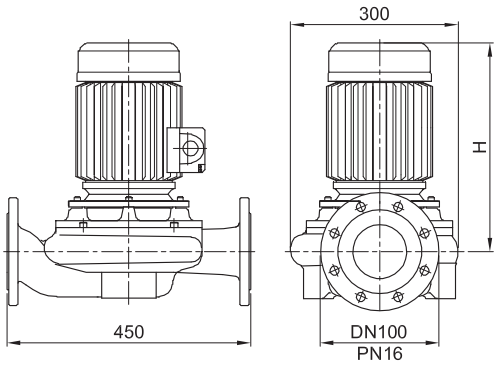

Med reservation för tekniska ändringar

Appendix G

Experimental facilities

G.1 Riser

Figure G.1 displays the top of the riser where the riser and drainage is connected to the separator tank. The separator riser inlet is aligned over the riser and connected with a pipe coupling. This is used between every pipe length in the riser. The acrylic pipe is 60mm inner diameter.

Figure G.1: Riser

The acrylic clamps are used to attach the acrylic pipe to the rail. The space between the clamps are set to 1m, which is quite close due to possible shaking and shocks originated from slugs.

G.2 Separator

The air-liquid separator (Figure G.2a) is installed at the top of the riser to separate air out of the system before the fluid continues in the flexible drainage pipe. The separator is built of rolled plates and thereafter welded together. Attachment brackets are welded on-sight to ensure correct position over the vertical riser pipe.

The separator lid (Figure G.2b) have deflection plates welded on the inside of the lid to ensure separation of gas and liquid. Deflection plates are attached to the lid to have a clear view down in the tank and riser pipe, if an inspection is performed.

The separator tank is designed (Figure G.3a & G.3b) and built at the multiphase laboratories.

(a) **(b)**

Figure G.2: (a) Separator tank, (b) Separator lid

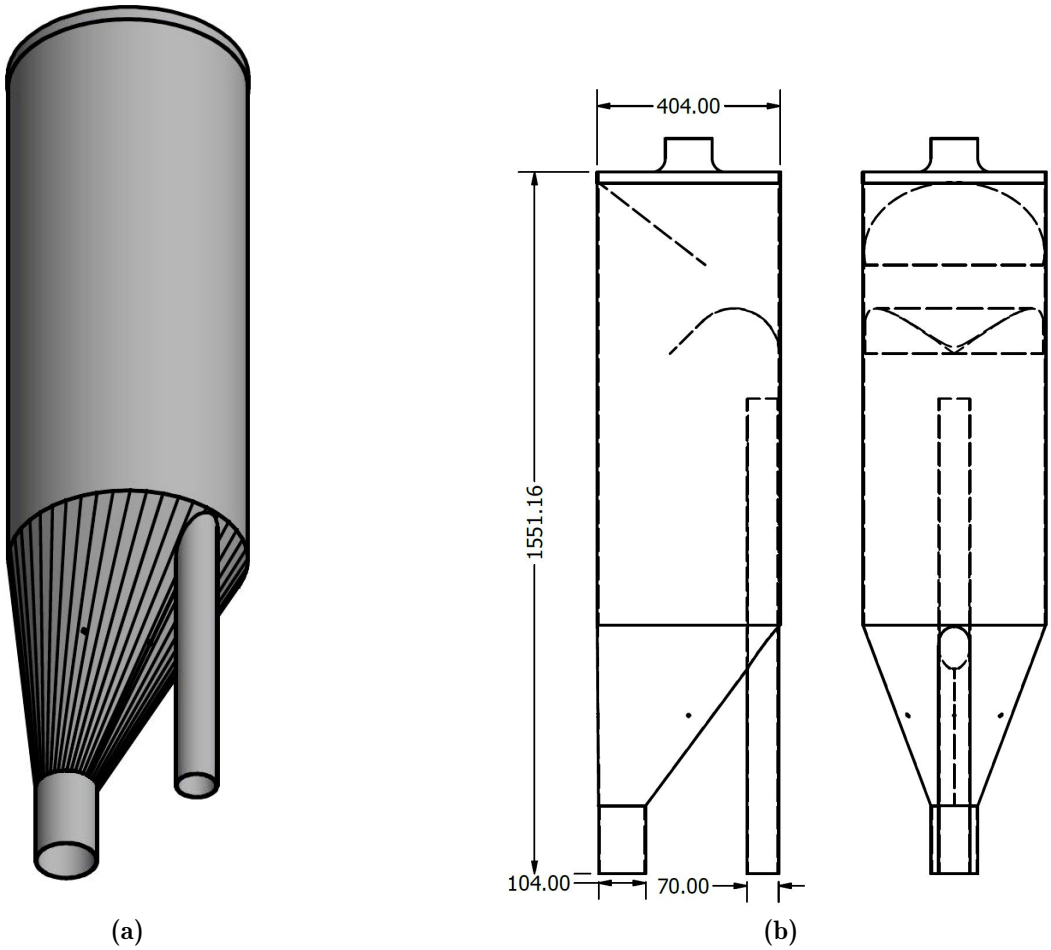

Figure G.3: (a) Separation tank (Figure G.2a) , (b) Separation tank with internals

G.3 Horizontal test-section

Figure G.4 displays the horizontal section for this experiment. A grid have been installed on the wall to have the flexibility to adjust the cable ladder to various geometry settings. The grid is built of several vertical rails, with the cable ladder supporters standing normal at the rails. The support can easily be adjusted within the rail to a desired level.

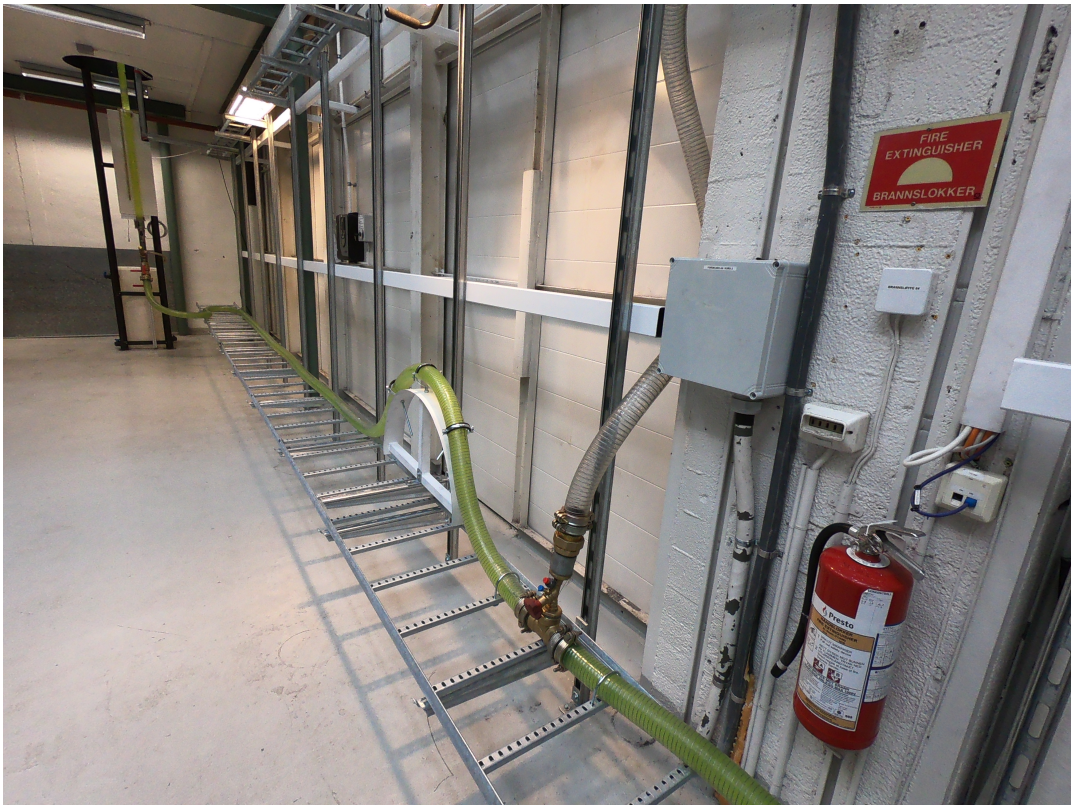

Figure G.4: Horizontal test-section

G.3.1 Air injection

Air is injected from the vertical hose into the water (Figure G.5). The air have a pressure of approximately 5bar, and the control valve for air further upstream is fully opened. The flow rate of air is controlled by the manual balancing valve, displayed in the figure. The valve is adjusted manually until the desired flow rate is read from the flow meter FIT 1.01 (Table 3.6). The location of the balancing valve is at the mixing point to ensure high pressure air at this location, avoiding instability problems due to compressibility.

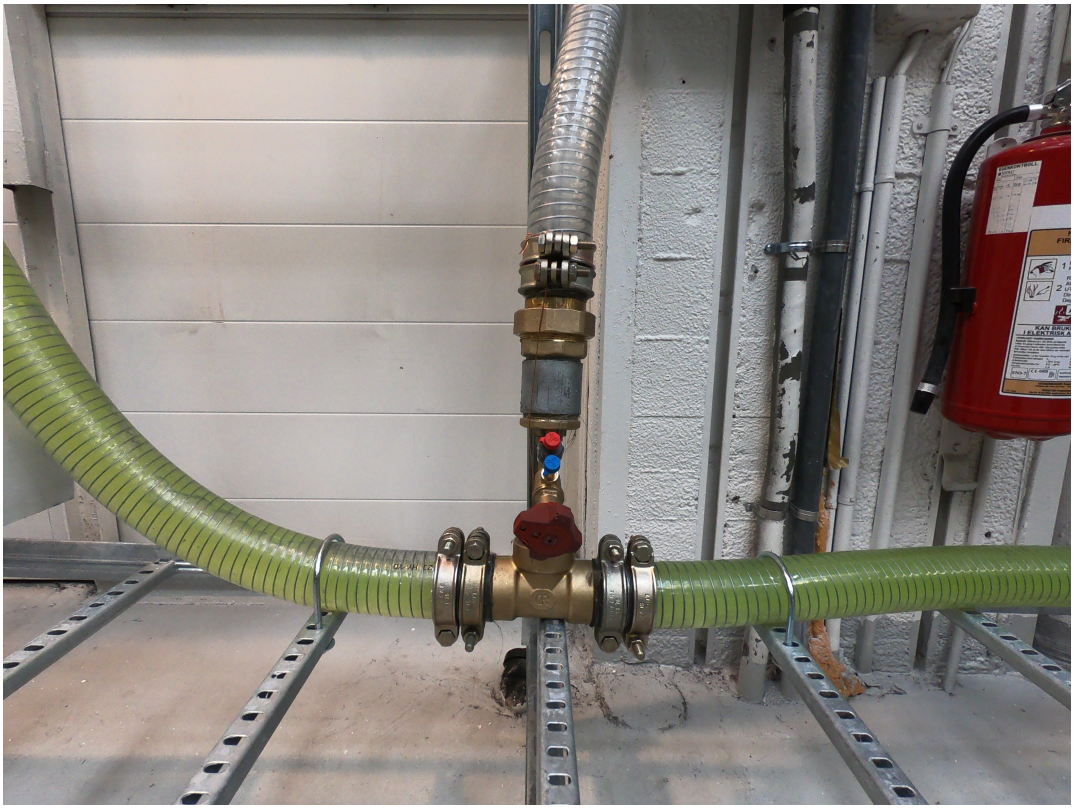

Figure G.5: Air injection

G.3.2 Jumper

This handmade *jumper* (Figure 2.1) in Figure G.6 have the purpose of allowing entrapment of air before the riser inlet. Its mounted on a support which is attached to the rail-grid. The pipe-clamps can be adjusted to increase the radius for this geometry.

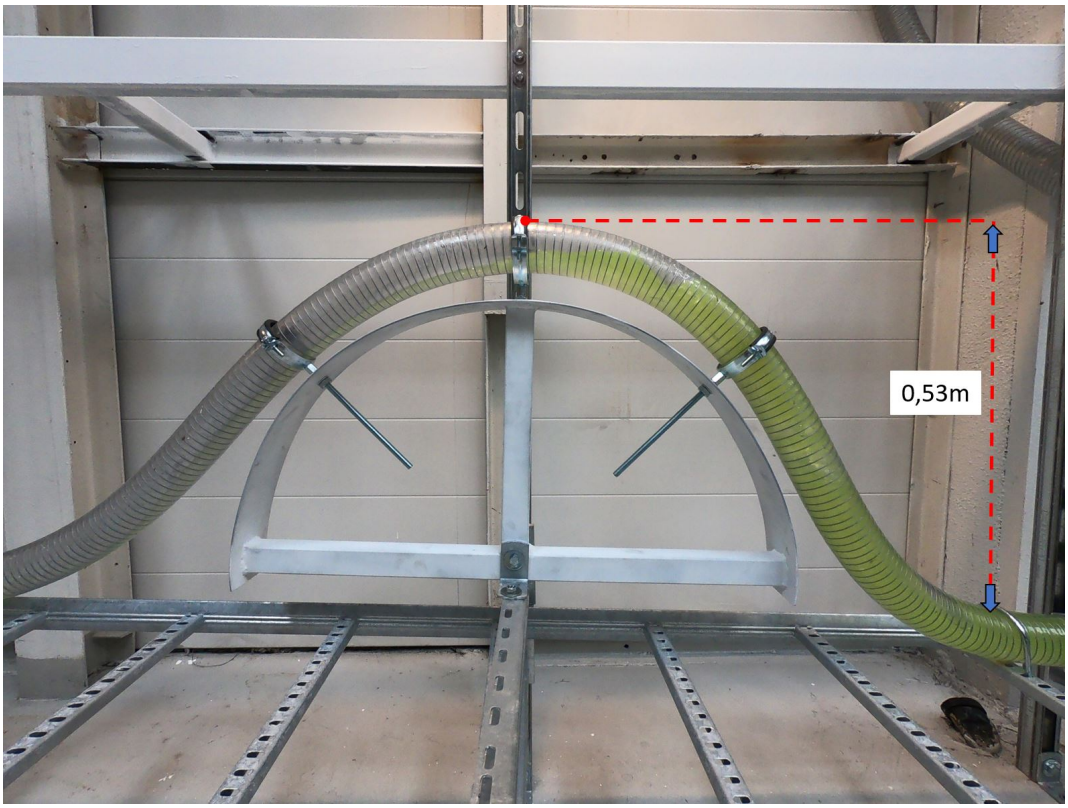

Figure G.6: Jumper

G.3.3 Turns

Before the riser inlet there are some sharp turns (Figure G.7). The u-turn laying on the cable ladder allows a small entrapment of air since the cable ladder is slightly inclined. In the geometry described in Chapter 3, these turns are unfolded, and represented only by length and elevation.

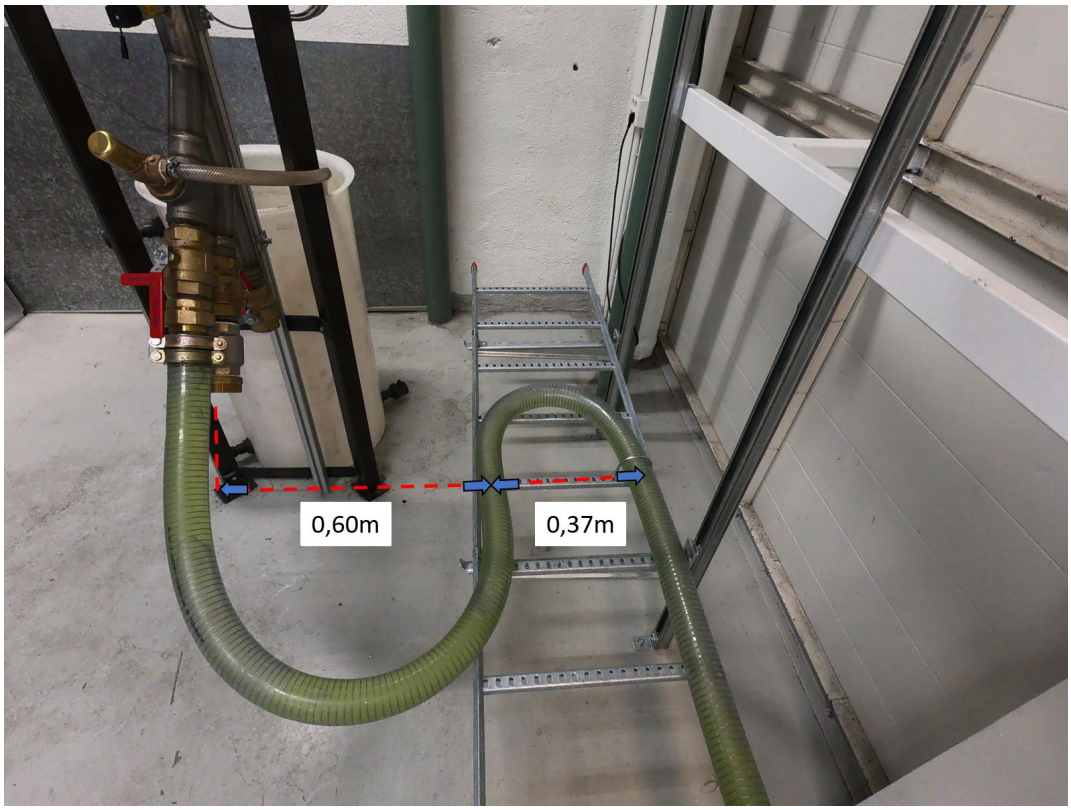

Figure G.7: Turns

G.4 Connection to existing

Air and water flows are taken from the existing facility. Branches are installed for both of them and required valves are installed to be able to switch easily between the different experiments conducted in the lab.

Figure G.8 displays the connection area and the letter tags are described in the figure text. This figure also displays the bypass from the air to water and the function is to blow out the remaining water when cleaning the rig after an experiment.

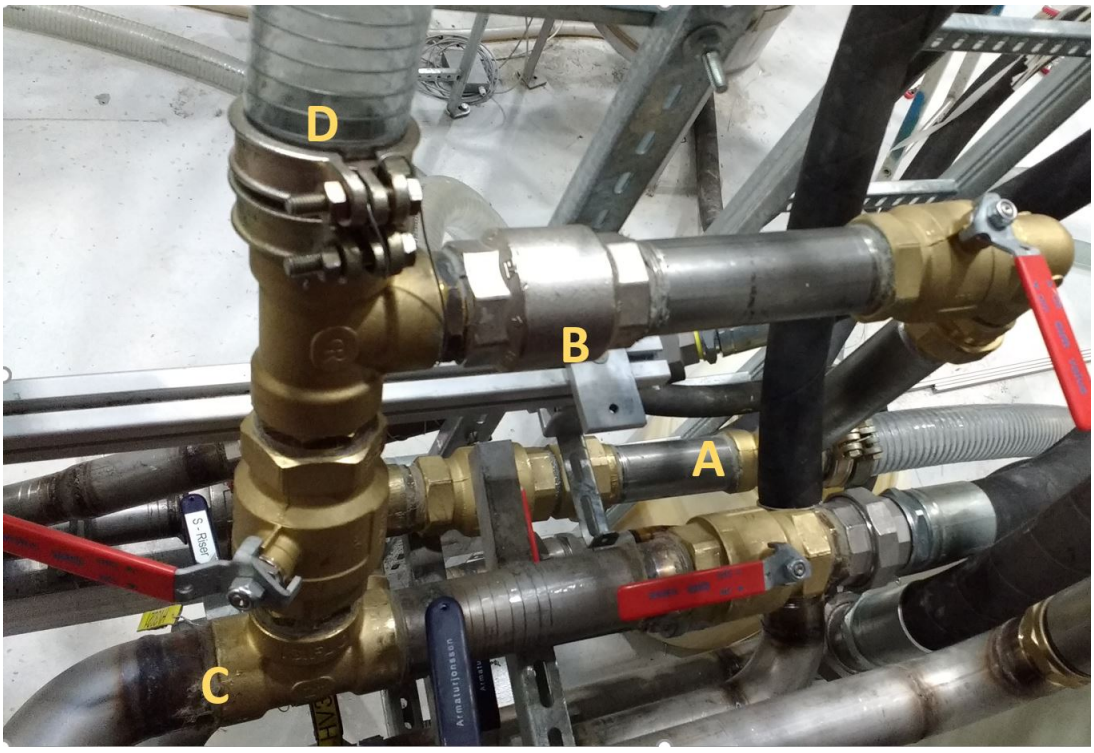

Figure G.8: Connection to existing, A=Water supply, B=Check-valve, C=Air supply, D=Air supply to mixing

G.5 Drainage

G.5.1 Horizontal drainage

This section of the drainage (Figure G.9a) consist of rigid 3m lengths of black *PP*-pipes. 30 meters pipe is needed to connect the flexible riser drainage and the oil-water separator (see Figure 3.3 Tag F-002)

For the horizontal pipe sections, the fall is set to 1:105, which is standard for drainage pipe for water. Clamps are installed with 1,10m space, which is standard for horizontal 110mm plastic pipes.

(a) **(b)**

Figure G.9: (a) Rigid drainage pipe , (b) Flexible drainage

G.5.2 Vertical drainage

This section consists of approximately 40m flexible drainage pipe with i.d 100mm. The pipe is mounted underneath the staircase outer edge (Figure G.9b). For attachment, WG-band is used since this is available in the lab. The spiral staircase is also one of the many fire escape routes in the lab. Therefore, in addition to mentioned straps, steel wire is also installed due to higher fire resistance, to keep the staircase free from obstacles, in the event of a fire.

G.6 Technical-room

The technical-room have several pumps available, but for this experiment the large centrifugal pump is used marked with E in Figure G.10. Letter G represents the air tank at 5 bar supplying the air further downstream. Upstream this tank there is an even bigger air tank at 7bar. Letter F is displayed on the large oil/water separator, marked with Tag F-003 at the P & ID in Figure 3.3.

Figure G.10: Technical room, E=Large centrifugal pump, F=Large oil/water separator, G=Air tank at 5bar